

Performance of Rehabilitated URM Shear Walls: Flexural Behavior of Piers

by

**Shaun Franklin
Jaret Lynch
Daniel Abrams**

**Department of Civil Engineering
University of Illinois at Urbana-Champaign
Urbana, Illinois**

December 2001

Acknowledgments

The research investigation summarized in this report was funded by the National Science Foundation through the Mid-America Earthquake Center.

The laboratory work was done by Shaun Franklin and Jaret Lynch during their graduate study toward Masters of Science degrees. The research was supervised by the Principal Investigator, Professor Daniel P. Abrams. Gratitude is extended to Omer Erbay for his assistance during the tests and John Nichols for their assistance in the data reduction and report revisions.

Appreciation is given to the machine shop and laboratory staff of the Civil Engineering Department at the University of Illinois at Urbana-Champaign, for the fabrication of the test structure and specimens. Thanks are also given to Grzegorz Banas for his assistance with the instrumentation and operation of the actuators.

Table of Contents	Page
Chapter 1. Introduction	1
1.1 Background	1
1.2 Objective and Scope of Research Project	2
1.3 In-plane Behavior of URM Walls	3
1.3.1 Flexural vs. Shear Mechanisms	3
1.3.2 Stiffness, Cracking, and Lateral Capacity of Piers	4
1.3.3 FEMA 356 and URM Piers	5
1.3.3.1 Linear Static Procedure for URM Piers	6
1.3.3.2 Nonlinear Static Procedure for URM Piers	8
Chapter 2. Experimental Program	10
2.1 Description of Test Piers	10
2.1.1 Overall Configuration	10
2.1.2 Non-Rehabilitated Test Piers	11
2.1.3 Fiber Reinforced Polymer Test Pier	12
2.1.4 Shotcrete Test Pier	13
2.1.5 Surface Coating Test Pier	14
2.1.6 Center Core Test Piers	14
2.2 Testing Procedures	15
2.3 Loading System	15
2.4 Masonry Materials	16
2.5 Instrumentation	16
Chapter 3. Experimental Results	27
3.1 Overview	27
3.2 Visually Observed Behavior	27
3.2.1 Non-Rehabilitated Test Pier with Medium Axial Force (Specimen 1F)	27
3.2.2 Non-Rehabilitated Test Pier with Light Axial Force (Specimen 2F)	28
3.2.3 Fiber Reinforced Polymer Test Pier (Specimen 3F)	28
3.2.4 Shotcrete Test Pier (Specimen 4F)	29
3.2.5 Surface Coating Test Pier (Specimen 5F)	29
3.2.6 Non-Rehabilitated Test Pier with Heavy Axial Force (Specimen 6F)	30
3.2.7 Center Core Test Pier with Light Reinforcement (Specimen 7F)	30
3.2.8 Center Core Test Pier with Moderate Reinforcement (Specimen 8F)	31
3.3 Measured Lateral Force Versus Drift Relationships	31
3.4 Alternative Modeling Parameters and Acceptance Criteria According to FEMA 356	32
3.4.1 Idealized Lateral-Force-Deformation Pushover Curve	32
3.4.2 Acceptance Criteria	33
3.5 Initial Lateral Stiffness	34
3.6 Strength	34
3.7 Shear Stress Versus Shear Strain Relationships	34
3.8 Net Flexural Tensile Stress at Cracking	36
3.9 Crack Opening Profile	36
Chapter 4. Interpretations of Observed Behavior	49
4.1 Introduction	49
4.2 Yield Strength Estimates vs. Measured Yield Strengths	49
4.3 Stiffness Estimates vs. Measured Initial Lateral Stiffness	50
4.4 Estimated mQ_{CE} vs. Measured mQ_{CE}	50
4.5 Comparisons of Rehabilitation Methods	51
4.5.1 Strength, Q_{CE}	51
4.5.2 Stiffness, k	51
4.5.3 Ductility Ratio, m	51

4.5.4	Ductility Ratio x Strength, mQ_{CE}	52
4.5.5	Energy Dissipation	52
4.5.6	Damage.....	53
Chapter 5.	Summary and Conclusions	60
5.1	Summary	60
5.1.1	Objectives of the Study.....	60
5.1.2	Summary of Experimental Work.....	60
5.2	Conclusions	61
5.2.1	Behavior of Non-rehabilitated Piers	61
5.2.2	Behavior of Rehabilitated Piers	62
5.3	Future Research.....	64
References	64
Appendix A.	General Form of Appendices.....	A.1
Appendix B.	Material Properties	B.1
Appendix C.	Measured Behavior for Specimen 1F (Non-Rehabilitated Pier with Medium Axial Force).....	C.1
Appendix D.	Measured Behavior for Specimen 2F (Non-Rehabilitated Pier with Light Axial Force).....	D.1
Appendix E.	Measured Behavior for Specimen 3F (Fiber Reinforced Polymer Rehabilitated Pier).....	E.1
Appendix F.	Measured Behavior for Specimen 4F (Shotcrete Rehabilitated Pier).....	F.1
Appendix G.	Measured Behavior for Specimen 5F (Surface Coating Rehabilitated Pier)	G.1
Appendix H.	Measured Behavior for Specimen 6F (Non-Rehabilitated Pier with Heavy Axial Force)	H.1
Appendix I.	Measured Behavior for Specimen 7F (Center Core Rehabilitated Pier with Light Reinforcement).....	I.1
Appendix J.	Measured Behavior for Specimen 8F (Center Core Rehabilitated Pier with Moderate Reinforcement).....	J.1

List of Figures	Page
Figure 1-1. m Factor Representation.....	9
Figure 1-2. Idealized Force-Deflection Relation for URM Walls.....	9
Figure 2-1 Test Pier and Loading Rig.....	19
Figure 2-2 Shaun beside Test Pier.....	19
Figure 2-3 Modeling of Piers for Test.....	20
Figure 2-4 Testing Setup.....	21
Figure 2-5. Specimen Loading and Dimensions.....	22
Figure 2-6. Specimen 3F FRP Placement.....	22
Figure 2-7. Specimen 4F Rebar Placement.....	23
Figure 2-8. Fabrication of Specimen with Shotcrete.....	23
Figure 2-9. Ferro-Cement Application.....	24
Figure 2-10 Center-Core Placement.....	24
Figure 2-11 Drilling of Cores and Placement of Epoxy-Grout.....	25
Figure 2-12 Sample Loading History.....	26
Figure 3-1 Damage Photos of Non-rehabilitated pier with medium (42psi) vertical stress (1F).....	39
Figure 3-2 Damage Photos of Non-rehabilitated pier with light (25psi) vertical stress (2F).....	40
Figure 3-3 Damage Photos Of Non-Rehabilitated Specimen With Heavy (85 Psi) Axial Stress (6F).....	41
Figure 3-4 Damage Photos Of Non-Rehabilitated Specimen With 120 Psi Axial Stress (6Fb).....	42
Figure 3-5 Damage Photos of FRP Specimen (3F).....	43
Figure 3-6 Damage Photos of Shotcrete Rehabilitated Pier (4F).....	44
Figure 3-7 Specimen 5F, 2.0% Drift.....	45
Figure 3-8 Damage Photos of Center-Core Rehabilitated Pier with #3 Rebar (7F).....	46
Figure 3-9 Damage Photos of Center-Core Rehabilitated Pier with #5 Rebar (8F).....	47
Figure 3-10 Measured Shear Modulus With Respect to Drift.....	48
Figure 4-1 Strength comparison.....	55
Figure 4-2 Initial stiffness comparison.....	55
Figure 4-3 Comparison of Estimated to Measured mQ_{CE} (LS performance level).....	56
Figure 4-4 Measured strength of rehabilitated piers.....	57
Figure 4-5 Measured initial stiffness of rehabilitated piers.....	57
Figure 4-6 Measured ductility ratio of rehabilitated piers.....	57
Figure 4-7 Measured LS capacity of rehabilitated piers.....	57
Figure 4-8. Force-deflection comparison for rehabilitated specimens.....	58
Figure 4-9. Damage photos at the end of testing.....	59

Chapter 1. INTRODUCTION

1.1 Background

The masonry structures built in the late nineteenth and early twentieth centuries were designed with empirical equations derived from construction practice (Heyman, 1995). Many of these structures are still standing today, which attests to the soundness of the design with respect to gravity loads. However, many of these buildings are unreinforced and have not yet been subjected to intense lateral wind or earthquake loads (Epperson and Abrams, 1989). Throughout eastern and mid-America there exists a large inventory of unreinforced masonry (URM) buildings that pose a great hazard in the case of an infrequent but large seismic event. The earthquakes of 1999 in Turkey and Taiwan, and 2000 in India, served as a reminder to the vulnerability of URM structures and the need for sound evaluation and rehabilitation techniques (Hays, *et al.*, 1999).

Seismic performance of these structures is largely dependent on the strength and behavior of in-plane shear walls. The lateral load capacity of URM shear walls is often limited by modern design codes (MSJC, 1999) to the onset of flexural cracking. However recent research has indicated that URM walls can resist considerable lateral force after the formation of the first crack and still behave in an elastic manner while resisting loads larger than those that caused initial cracking (Abrams, 1992 and Magenes, 1997). URM walls have been proven to be ductile elements capable of dissipating energy through rocking or bed-joint sliding, and thus design codes may be overly conservative in evaluating the capacity of these components.

The leading document available today to guide an engineer on the seismic rehabilitation of URM walls is FEMA 356. This document titled “*Prestandard and Commentary for the Seismic Rehabilitation of Buildings*” was released in December of 2000 by the Federal Emergency Management Agency (FEMA), as part of the National Earthquake Hazards Reduction Program (NEHRP). This document provides methods, using the concepts of performance based design, for the analysis and rehabilitation of buildings made of masonry, concrete, steel, timber or any combination of these materials.

Performance based design allows the engineer, and building owner, to jointly specify the desired building performance level for a particular earthquake magnitude, evaluate the capacity of the structural components to determine if they meet performance objectives, and design rehabilitations for the components if they do not meet the objectives.

Performance levels are based largely on the amount of damage that would be incurred. Damage to a structural component is often considered to be a function of lateral displacements. Unlike design codes, where the acceptability of a component is determined by its strength, in FEMA 356 component acceptability is determined by the amount of damage which is expected to occur at a particular lateral deflection or drift. Numerical coefficients relating drifts to damage were deduced from laboratory tests available at the time. Further research is needed to validate and reduce the uncertainty in this data, particularly for the case of rehabilitated components such as URM shear walls.

1.2 Objective and Scope of Research Project

The objective of this research project was to investigate the performance of URM piers subjected to in-plane loading. Eight URM piers were constructed and tested by applying cycles of in-plane displacement. The test piers had a high height-to-width aspect ratio to permit a study focused on the flexural mechanisms and instabilities that lead to failure. Three of the piers were non-rehabilitated to enable a direct comparison of their performance to the performance as estimated by FEMA 356. The non-rehabilitated specimens were each subjected to a different amount of vertical force, representative of additional stories bearing on the piers being tested. The remaining five specimens were rehabilitated using modern techniques to investigate the resulting modifications to wall behavior and acceptability of the rehabilitation techniques.

The experimental study parameters of interest include lateral strength, stiffness, and deformation capacity. In particular, the testing of the flexural walls was directed toward answering the following questions:

1. Are the lateral strength and deformation capacity of a URM wall dominated by flexure as estimated by FEMA 356?
2. How does wall behavior change with an increase in axial compressive force?
3. How are flexural mechanisms for slender masonry walls affected by different rehabilitation interventions?
4. What drift is permissible for URM walls governed by rocking behavior?
5. How does the FEMA 356 estimated behavior compare to the measured behavior of the rehabilitated piers?

1.3 In-plane Behavior of URM Walls

1.3.1 Flexural vs. Shear Mechanisms

The behavior of URM walls under in-plane loads can generally be divided into two categories, shear and flexure. Whether a wall is dominated by shear behavior or flexural behavior is largely dependent on the aspect ratio and the vertical axial compressive force. For slender walls (L/h less than 1.0) with relatively light axial stress, behavior is usually dominated by flexure and a limiting mechanism of either rocking or toe-crushing. For stocky walls (L/h greater than 1.5) with moderate to heavy axial stress, shear usually dominates behavior and leads to failure through bed joint sliding or diagonal tension (Magenes, 1997). Within these categories, limiting mechanisms of rocking and bed joint sliding are classified as “deformation controlled actions” because research has shown that large inelastic deformations are possible without a significant loss in strength. In contrast, diagonal tension and toe crushing behavior modes are known as “force controlled actions” because the ultimate failure can be abrupt with little or no subsequent deformation. This testing of the eight piers is focused on flexural behavior (i.e. rocking and toe crushing) with test piers of a single aspect ratio (L/h of 0.56).

1.3.2 Stiffness, Cracking, and Lateral Capacity of Piers

The in-plane stiffness of URM walls prior to cracking can be estimated using a common equation for homogenous materials. In this case, where the wall is cantilevered, the pier stiffness is calculated using Equation (1) (FEMA 356, Section C7.4.2.1):

$$k_{pier} = \frac{1}{\frac{h_{eff}^3}{3E_m I_g} + \frac{h_{eff}}{A_v G_m}} \quad (1)$$

where k_{pier} is the lateral stiffness, h_{eff} is the pier height to the point of lateral load, E_m is the elastic modulus, A_v is the effective shear area (assumed to be 5/6 gross area, A_g), and G_m is the shear modulus (assumed to be $0.4E_m$).

In walls or piers with light axial compressive stress, the bed joint at the wall heel will crack in tension prior to the toe crushing in compression. The lateral force at which the mortar will crack is given by the following equation (Abrams 2000):

$$H_{cr} = \frac{L^2 t}{6h} (f_a + F_{tu}) \quad (2)$$

where H_{cr} is the lateral load to cause cracking, L is the length of the pier, t is the thickness of the wall, h is the height to the applied load, f_a is the applied axial compressive stress, and F_{tu} is the flexural tensile strength of the masonry normal to the bed joint.

After flexural cracking has occurred, the ultimate limit state is rocking of the pier or crushing of the masonry in the toe region depending on the aspect ratio and axial load. Under light axial loads the pier will usually rock with a lateral strength given by (FEMA 356, Section 7.4.2.2.1):

$$H_{rock} = 0.9\alpha f_a A_g \left(\frac{L}{h} \right) \quad (3)$$

where α is a factor to account for boundary conditions (0.5 for cantilevered and 1.0 for fixed-fixed), and A_g is the gross cross sectional area. Under moderate to heavy axial stresses toe crushing can occur and the lateral capacity is given by (FEMA 356, Section 7.4.2.2.2):

$$H_{tc} = \alpha f_a A_g \left(\frac{L}{h} \right) \left(1 - \frac{f_a}{0.7 f'_m} \right) \quad (4)$$

where f'_m is the ultimate masonry compressive strength. Clearly these two equations (3) and (4) are very similar. The main difference is the last term in equation (4) that reduces the capacity depending on the amount of applied axial stress relative to the compressive strength. As the relative amount of axial stress increases so does the likelihood of toe crushing. The level of axial stress that would result in equal toe crushing and rocking strengths can be found by setting the equations equal to one another and solving for f_a . Following this process it is shown that, in theory for any wall with axial stress greater than 7% of the ultimate stress, f'_m , toe crushing will govern the behavior before rocking.

1.3.3 FEMA 356 and URM Piers

As stated in Section 1.1, FEMA 356 is based on the concept of performance based design. Three performance levels are defined and used as discrete points to guide a rehabilitation design based on the expected performance of a building (Section 2.8.3 of FEMA 356). Performance levels are based on the amount of damage to both the structural and non-structural elements. The three defined levels for primary structural elements are Collapse Prevention (CP), Life Safety (LS), and Immediate Occupancy (IO). With regard to masonry the performance levels are roughly defined as:

- Collapse Prevention- extensive cracks, dislodgment of units, noticeable offsets
- Life Safety- Extensive cracks, no dislodgment of units, significant reserve capacity
- Immediate Occupancy- only minor cracks

The *Guidelines* (FEMA 356) provide a linear static procedure (LSP) and a nonlinear static procedure (NSP) for determining the acceptability of URM walls as a function of these performance levels. A basic description of these procedures follows in this subchapter. However, a thorough explanation of these procedures is beyond the scope of this report, so the interested reader is referred to Chapters 3 and 7 of the *Guidelines*.

1.3.3.1 Linear Static Procedure for URM Piers

The linear static procedure provides a framework for determining the acceptability of components that are modeled elastically. Two procedures are given within this framework depending on whether the limiting mechanism is a deformation or force-controlled action.

As previously stated, piers or slender walls are generally limited by rocking or toe crushing mechanisms. Rocking is considered a deformation-controlled action and thus is assumed to have the capacity to deform inelastically without failure. Therefore acceptance of piers governed rocking ($H_{rock} < H_{tc}$) is given by the following equation for deformation controlled actions

$$m\kappa Q_{CE} \geq Q_{UD} \quad (5)$$

where m is a component demand modifier to account for the expected ductility of the deformation, κ is a knowledge factor, Q_{CE} is the expected strength of the component

(given by Equation 1-3), and Q_{UD} is design force due to earthquake and gravity loads. The interrelationship of these variables (assuming $\kappa=1$) is illustrated in Figure 1-1.

Where Δ_Y is the yield displacement, Δ_{IO} is the displacement for Immediate Occupancy, Δ_{LS} is the displacement for Life Safety, Δ_{CP} is the displacement for Collapse Prevention, and Δ_{UD} is the actual and model displacement for the component under design force Q_{UD} . FEMA 356 Section 7.4.2.3 defines m factors for acceptance criteria based on rocking as $1.5h/L > 1$ for IO, $3h/L > 1.5$ for LS, and $4h/L > 2$ for CP.

Equation (5) is written in terms of force quantities, however its intent is to provide an indirect measure of deflections that a component should experience (FEMA 356, Section C3.4.2.1.1).

Piers governed by toe crushing ($H_{rock} > H_{tc}$) are conversely considered to be force-controlled components. A different process is used for determining their acceptability because the ultimate limit state is based on stress and not deflection. This is because nonlinear deformations are not permitted for force-controlled actions (FEMA 356, Section 3.4.2.1.2). Therefore the force capacity (strength) must exceed the force demand in accordance with the following equation:

$$\kappa Q_{CL} \geq Q_{UF} \quad (6)$$

where κ is a knowledge factor, Q_{CL} is the lower bound strength of the component, and Q_{UF} is design force due to earthquake and gravity loads (note: Q_{UF} is not to be confused with Q_{UD} as they are different).

1.3.3.2 Nonlinear Static Procedure for URM Piers

The nonlinear static procedure provides direct information on lateral deflection and force demands that are related to a specific loading. The nonlinear behavior of primary masonry walls is idealized as shown in Figure 1-2.

The symbols d and e are empirically based terms to quantify the maximum displacements without collapse for primary and secondary elements respectively. The allowable drifts set by the acceptance criteria for a primary component are 0.1% drift for IO, d % drift for CP, and $0.75d$ % drift for LS. The ultimate drift level d is specified to be $0.4 h/L\%$ for primary walls governed by rocking, and the acceptance criteria are thus: 0.1% for IO, $0.3 h/L\%$ for LS, and $0.4 h/L \%$ for CP.

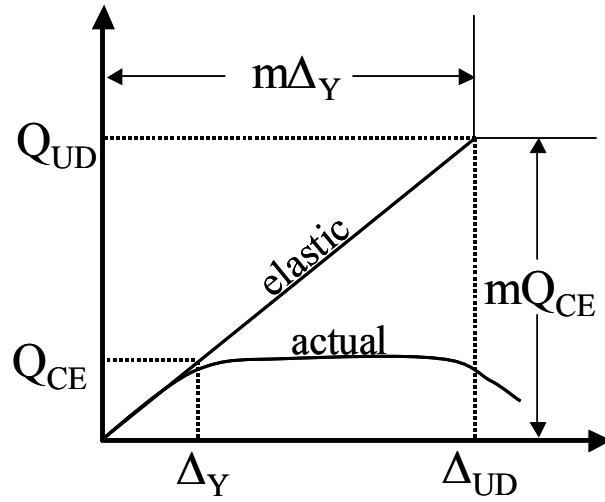
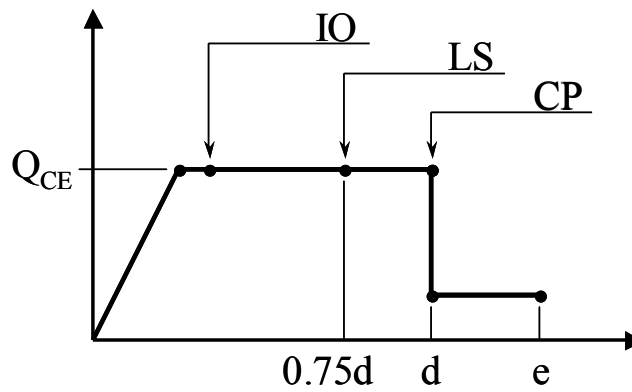
Figure 1-1. m Factor Representation

Figure 1-2. Idealized Force-Deflection Relation for URM Walls

Chapter 2. EXPERIMENTAL PROGRAM

Eight URM piers were constructed for this series of tests for the purpose of investigating the performance of rehabilitated masonry components subjected to simulated seismic loading. The full-scale test specimens as can be seen in Figure 2-1 and Figure 2-2 represent the lower half of a pier between openings in which the horizontal masonry “beams” are rigid as shown in Figure 2-3. Four of the walls were not rehabilitated. These plain walls were each tested with a different applied gravity load. This simulated a varying number of stories bearing on the pier being tested. The other piers were rehabilitated with one of four techniques described later in this chapter. All piers were subjected to a sequence of increasing drift imposed at the top of the wall to examine their performance at various levels of deflection. Figure 2-4 is a picture of the testing rig used throughout the experiment.

This chapter provides a detailed description of the test piers, a summary of the material properties, and an overview of the testing program and instrumentation.

2.1 Description of Test Piers

2.1.1 Overall Configuration

Each of the eight piers consisted of an inverted “T” built of clay masonry units. The masonry materials and dimensions of the pier, as shown in Figure 2-5, were the same for all of the piers. All walls were two wythes thick with a collar joint filled by mortar. Bricks were laid in an American Bond pattern (25 courses total) with a header row every five courses and 3/8” struck bed joints. Rehabilitations were performed on five of these “plain” walls.

The bottom of the pier being tested was constrained against in-plane rotation and translation. The top of the pier was permitted to rotate and translate freely in all directions. A reinforced concrete loading beam was mortared to the top of the pier to assist in the application of displacements.

2.1.2 Non-Rehabilitated Test Piers

Specimens 1F, 2F and 6F were tested as non-rehabilitated piers. Specimen 1F was a virgin unreinforced masonry specimen. The testing of 1F produced damage in the wall, but the limiting mode was rocking and thus damage was concentrated at one bed joint across the base of the pier. The only visible damage was a crack through the bed joint, and two cracked bricks that could be easily repaired. The wall was repaired and used as Specimen 2F.

The test wall was repaired by remortaring the bed joint and replacing the damaged bricks. The damaged bricks were removed by drilling and the new bricks were soaked prior to placement as done in initial construction. The crack had developed along the entire bed joint of course eight and could be repaired by temporarily lifting the top section of the wall. The top section of the wall was suspended by the overhead crane (courses 8 through 25 plus top beam). The bottom bed joint was cleaned by chiseling out all of the existing mortar and blowing the joint with compressed air. Then the top of course seven was wetted with water and a layer of mortar (Type N) approximately 5/8" thick was placed. The top section of the wall was then lowered into the wet mortar squeezing out the excess until a 3/8" joint was achieved. The wall was supported at this height until the mortar was cured. This repaired specimen was now tested as Specimen 2F.

The wall damage incurred by testing of 2F was slight and concentrated, with a crack through the entire bed-joint of course nine and minor cracking in the toe bricks. So this wall was used again for Specimen 3F that was rehabilitated using a Fiber Reinforced Polymer (FRP) rehabilitation.

Specimen 6F was a virgin unreinforced masonry wall, that was constructed to the same standards as Specimen 1F. After testing 6F, Specimen 6Fb was tested using the same wall as 6F with no repairs. The purpose for this will be explained in the next chapter.

2.1.3 Fiber Reinforced Polymer Test Pier

Specimen 3F was rehabilitated using strips of 27oz. Tyfo uni-directional glass fabric laminated to the surface with epoxy. This rehabilitation technique has been evaluated by the Army Civil Engineering Research Laboratory (CERL) on stocky walls, but not on walls this slender. In collaboration with engineers from CERL, the amount and location of FRP strips were designed as shown in Figure 2-6.

Strips A, B, and D were placed on both sides of the wall as shown and strip C wrapped around the wall in one continuous piece to confine the toe region. Strips A and B were both 10" wide and extended the full height of the wall but were not anchored into the concrete foundation pad or top beam. Strips C and D were 7 3/4" and 11" wide respectively.

The FRP was applied to the wall without any additional repairs to the damage incurred in the testing of 2F. This was a reasonable lower bound approach because the only visible damage was a crack through the bed joint of course nine and minor cracking of a brick in the toe region.

The surface was prepared for the FRP application by washing off all loose particles and then filling all major voids. The CERL engineers and the FRP manufacturer advised that it was not necessary to produce a continuously smooth surface for bonding. As a result, the mortar joints were not filled in the preparation process. It was only necessary to fill major voids to accommodate the varying dimensions of the reclaimed brick. This was accomplished by filling each void with epoxy thickened by fumed silica to a putty consistency. The rest of the wall, which was to be laminated, was painted with epoxy 3 hours prior to application to seal the pores. The fabric was applied and it was monitored for six hours to ensure that the brick did not absorb too much of the epoxy, which would weaken the bond. Excessive absorption of the epoxy was visible where air bubbles were pulled into the FRP fabric. This was remedied by injecting additional epoxy through the FRP fabric with a syringe thus resaturating the material.

2.1.4 Shotcrete Test Pier

Specimen 4F was a virgin pier of the same dimensions as all other specimens except that it was rehabilitated with 4" thick reinforced concrete on one side of the specimen to model the effects of a shotcrete overlay. The amount and placement of the reinforcement was based on the minimums recommended in the Rutherford Chekene report "Development of Procedures to Enhance the Performance of Rehabilitated URM Buildings" [15]. All of the reinforcement was #3 Grade 60 rebar and was placed 2" from the wall surface as shown in Figure 2-7.

The rebar and concrete were anchored the wall with 1/4" all-thread steel rods. The rods were cemented into 4" deep holes drilled in the mortar joints at the locations shown by the circles in Figure 2-9. A 2 1/4" fender washer was connected to the end of the all-thread rods to disperse bearing stress on the concrete as shown on the left in Figure 2-8.

The concrete was not sprayed onto the surface as would be done in practice but was poured through a formwork that was built around the wall as shown on the right in Figure 2-8. Twelve-inch cylinders that were cast at the time of specimen rehabilitation were tested after 28 days and had an average compressive strength of 5150 psi with a standard deviation of 40 psi.

In most practical applications, the shotcrete rehabilitation would be used to enhance the in-plane shear capacity through shear transfer across the interface between the masonry and concrete surfaces. Due to the application process, the additional concrete carries negligible or no axial load. To represent this load transfer, the vertical and horizontal loads are applied at the center of the unrehabilitated side of the pier, at the same load point as the other specimens.

2.1.5 Surface Coating Test Pier

Specimen 5F was similar to 4F in that it had a reinforced concrete coating, however in 5F the coating was only ½” thick and was reinforced with steel hardware cloth. This rehabilitation technique is commonly referred to as “ferro-cement overlay” and it was also designed according to the minimum guidelines set forth in the Rutherford Chekene report [15]. The steel hardware cloth was 19 gage wire (0.04” diameter) with a ½” grid spacing. Five wire segments were cut from the cloth and tested to determine the ultimate tension strength. This was found to be 57 ksi with a standard deviation of 2 ksi. The wire cloth was suspended ¼” from the walls surface using all-thread steel rods anchored in the bed joints, identical to the anchoring of rods in Specimen 4F. The 1000 psi cement coating was made of a 1-to-3 volume ratio of Portland cement and sand with water added until a workable consistency was achieved. This coating material was then troweled on the surface, passing the coating through the cloth as is shown in Figure 2-9.

2.1.6 Center Core Test Piers

The last two specimens utilized the Center Core technique. Two cores were drilled in each wall. The cores had a diameter of 3-inches and were placed 21-7/8” apart and centered in the wall as shown in Figure 2-10. The cores started at the top of the wall and stopped one course up from the bottom of the wall. A single rebar was placed in each cavity. #3 grade 60 rebar was used for specimen 7F, and #5 grade 60 rebar was used for specimen 8F. An epoxy-sand grout was then poured into the cavities and allowed to cure, as shown in Figure 2-11. Test cylinders of the epoxy-sand grout resulted in an axial compressive strength of 12.42 ksi +/- 0.26 ksi with a Young’s modulus of 897 ksi +/- 42 ksi.

2.2 Testing Procedures

Each test pier was subjected to a sequence of drifts of progressively increasing amplitude as shown in Figure 2-12. Measured response was examined as the testing progressed to discern variations in strength, stiffness, and damage at each drift level. Location of cracks and crushing of bricks were noted and photographed as testing proceeded.

2.3 Loading System

A custom loading system was constructed for this experiment (introduced earlier as Figure 2-4). The test piers were anchored to a reinforced concrete foundation pad using tie-downs. The foundation pad was 17' by 7' in plan and 1' thick. It was attached to the laboratory strong floor by twelve (1.375" diameter) Dywidag steel bars. A reinforced concrete beam was mortared to the top of the test pier. This beam was 84" by 26" in plan and 18" tall and was displaced horizontally to the prescribed drift level by two 110-kip servo-hydraulic actuators connected to the centerline of the beam. The south actuator was driven in displacement control, while the north actuator was driven in force control in accordance with the measured forces of the south actuator. This setup of the horizontal actuators prevented torque from forming about the vertical axis of the wall, since equal lateral forces were applied to both sides of the loading beam. A 25-kip servo-hydraulic actuator attached vertically to the center of the loading beam provided a realistic gravity force distribution to the top of the test pier. Axial forces were held constant throughout the test by operating the vertical actuator in a force-controlled mode. Axial force came from four sources: the vertical actuator, the weight of the lateral actuators on the beam (875 lbs each), the weight of the concrete beam (2.5 kips), and the weight of the masonry pier (900 lbs).

2.4 Masonry Materials

The brick and mortar for the walls was chosen to simulate older masonry structures in the Midwest. A pink Chicago common brick obtained from Colonial Brick Co. in Chicago was used for all test walls. These bricks were reclaimed from buildings built in the Midwest and thus were not imitations but the actual brick used in early twentieth century construction. These bricks were subjected to a series of compression tests that gave the average strength of 4050 psi with a standard deviation of 280 psi. The bricks were solid with relatively consistent dimensions of 7.8" long, 3.6" wide, and 2.3" tall. Bricks were soaked in water for thirty minutes prior to placement because of the high initial rate of absorption.

Type N cement mortar (1 part Portland Cement, 1 part lime, 6 parts sand) was chosen to replicate typical mortars used in the older masonry structures.

Five prisms were built at the same time as the construction of Specimen 1F and five more prisms were built when specimen 4F was constructed. These prisms were then tested in a universal compression machine according to ASTM C1314-97 after 28 days of curing. The average prism strength was determined to be 1140 psi with a standard deviation of 200 psi. The Young's Modulus was determined from the prism tests to be 640 ksi with a standard deviation of 300 ksi.

2.5 Instrumentation

Horizontal and vertical loads applied to the test pier were measured using the internal load cell of each of the three actuators. The horizontal in-plane displacement at the top of the wall was measured relative to the laboratory floor using a temposonic displacement transducer. In addition to the overall lateral displacement of the wall specimen, it was desirable to measure displacements within the wall that could later be related to strains. The arrangement of LVDTs changed slightly from test to test, but the typical arrangement is given in Table 2-1. The displacement transducers were mounted

to the wall using epoxy and small threaded rods embedded into the wall's surface. The displacement transducers forming an "X" in the upper portion of the wall were chosen to measure shear deformations in this portion of the wall.

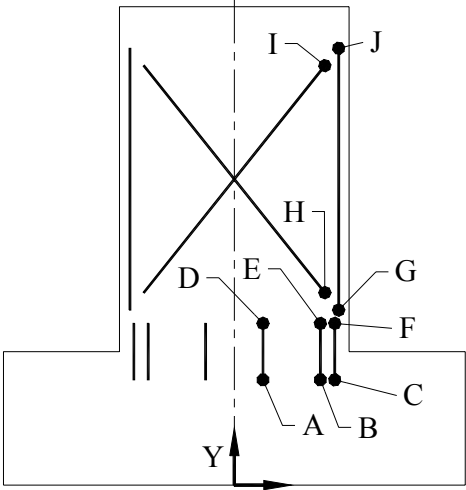
Shear strain was calculated using the following geometric relation:

$$\gamma = \frac{\delta 9 + \delta 10 - \delta 1 \sin(\theta) + \delta 8 \sin(\theta)}{2h_s \cos(\theta)} \quad (7)$$

where γ is average shear strain and $\delta 10$ (\) and $\delta 9$ (/) are the measured deformations of the diagonal LVDTs with the transducer orientation shown in parenthesis and elongation positive for $\delta 10$ and contraction positive for $\delta 9$. In addition, $\delta 1$ and $\delta 8$ are the deformations of the left and right vertical LVDTs respectively with contraction positive for $\delta 1$ and $\delta 8$. Theta is the angle of elevation of the diagonal transducers with respect the horizontal plane, and h_s is the initial height of the verticals (Abrams and Shah, 1992).

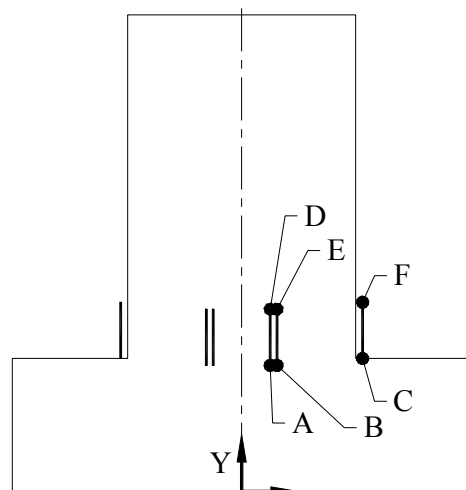
Multiple displacement transducers spanned the bed-joint where flexural cracking was expected to develop. These instruments provided a detailed record of the initiation of flexural cracking as well as the crack width across the face of the wall at different levels of drift.

Table 2-1 Displacement Transducer Mounting Locations



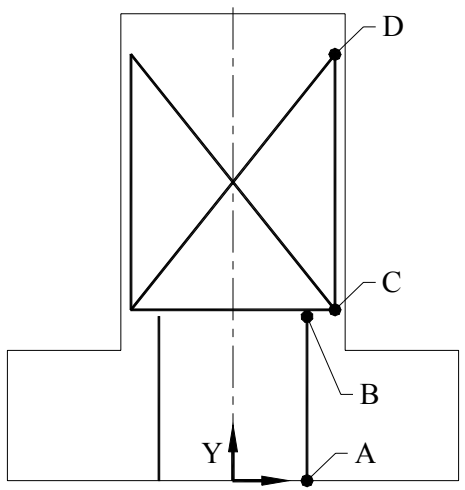
Origin (0,0) X Y

TYPICAL



Origin (0,0) X Y

FRP SPECIMEN (3F)



Origin (0,0) X Y

CENTER-CORE SPECIMENS (7F,8F)

Coordinates of Transducer Control Points (Sym. About Y-axis)										
All measurements in inches (x,y)	A	B	C	D	E	F	G	H	I	J
TYPICAL	(5.6,17.8)	(14,17.8)	(15.8,17.8)	(5.6,25.9)	(14,25.9)	(15.8,25.3)	(15.6,28.9)	(13.7,28.7)	(12.9,64.5)	(15.4,64.5)
FRP	(5.6,17.8)	(7.1,17.8)	(17.3,19.3)	(5.6,31.4)	(7.1,31.4)	(17.3,29.6)				
CENTER-CORE	(11.7,0)	(11.7,23.3)	(14.7,26.1)	(14.7,64.5)						



Figure 2-1 Test Pier and Loading Rig

- Vertical Actuator
- Loading Frame
- Loading Beam
- Safety Supports
- Horizontal Actuator
- URM Test Pier
- Displacement Transducers
- Tie Downs
- Foundation Pad
- Laboratory Floor

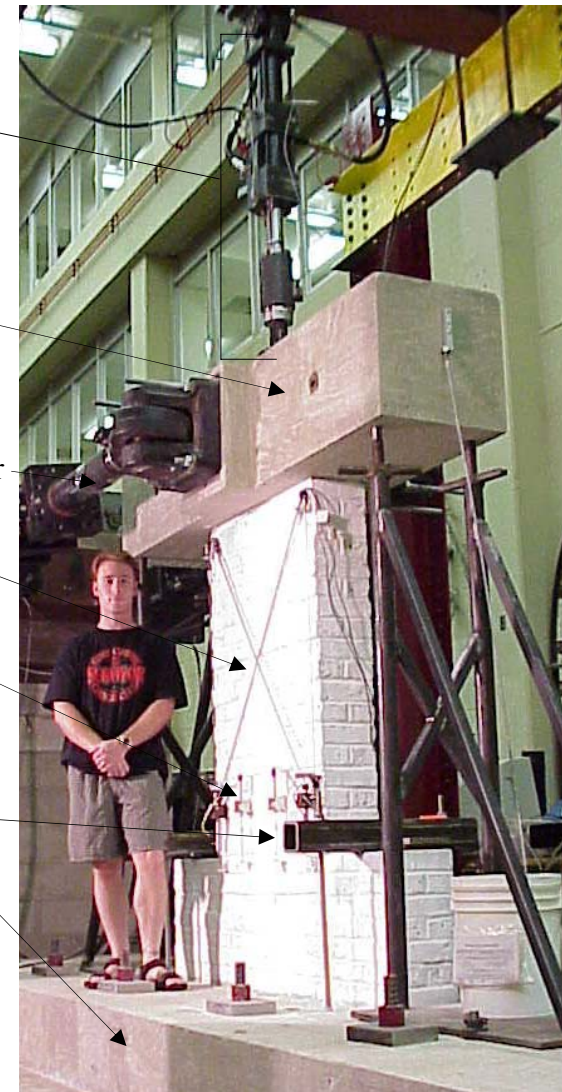
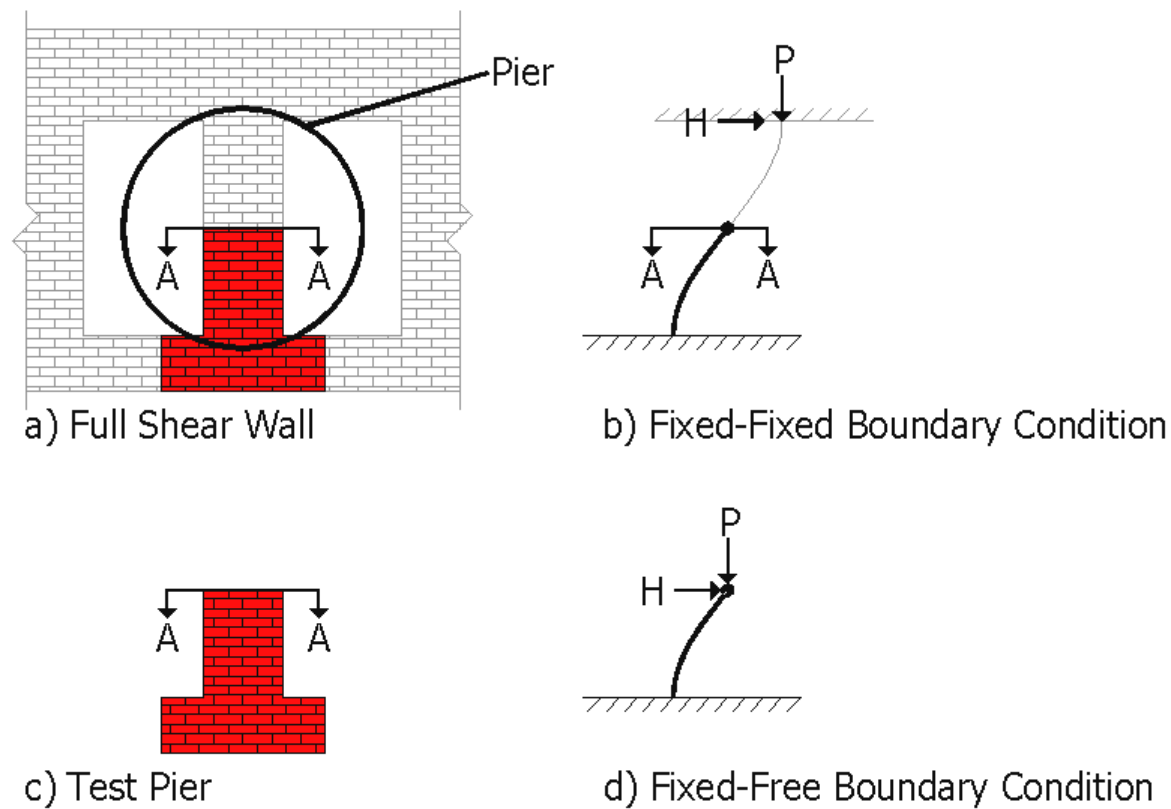


Figure 2-2 Shaun beside Test Pier

**Figure 2-3 Modeling of Piers for Test**

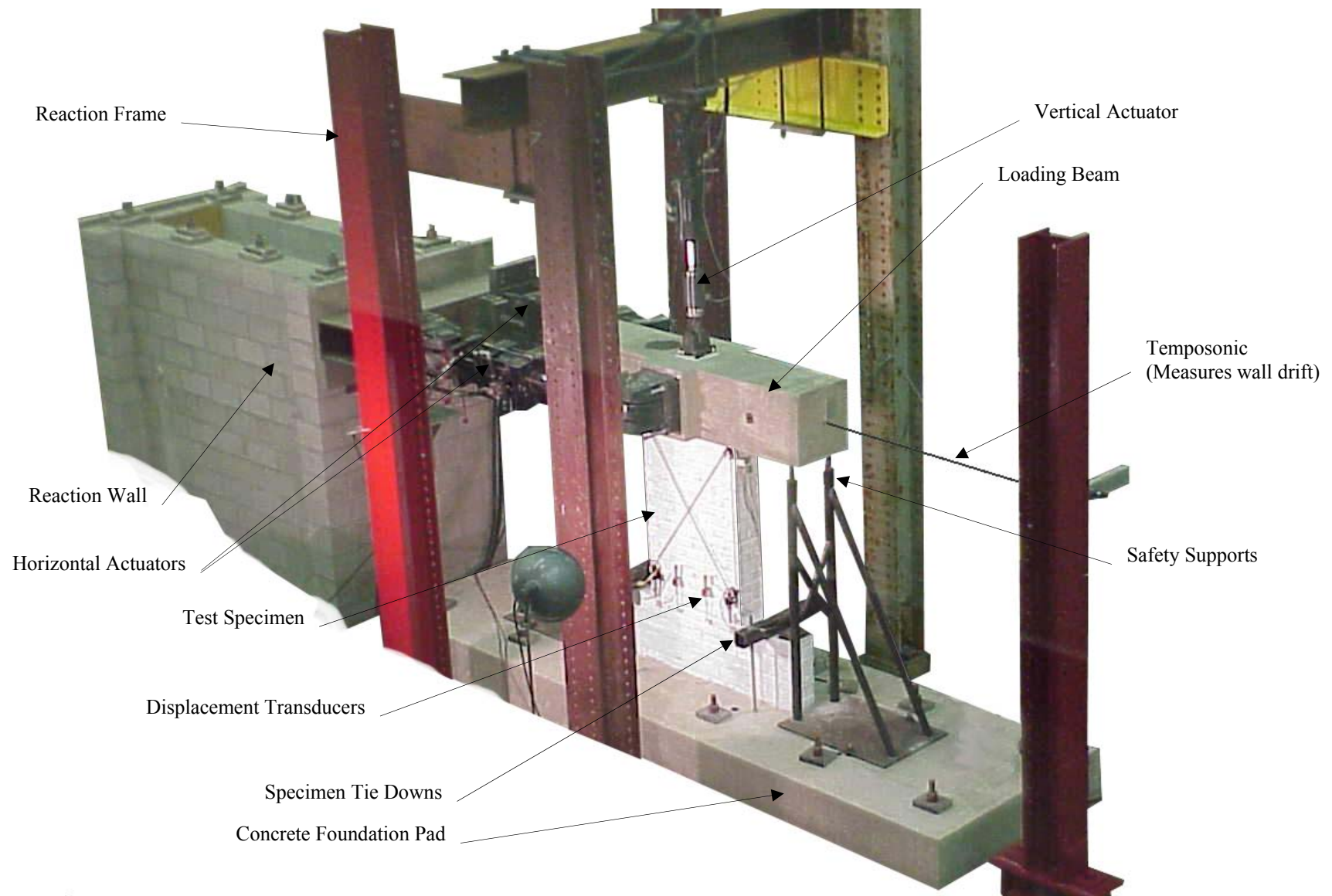


Figure 2-4 Testing Setup

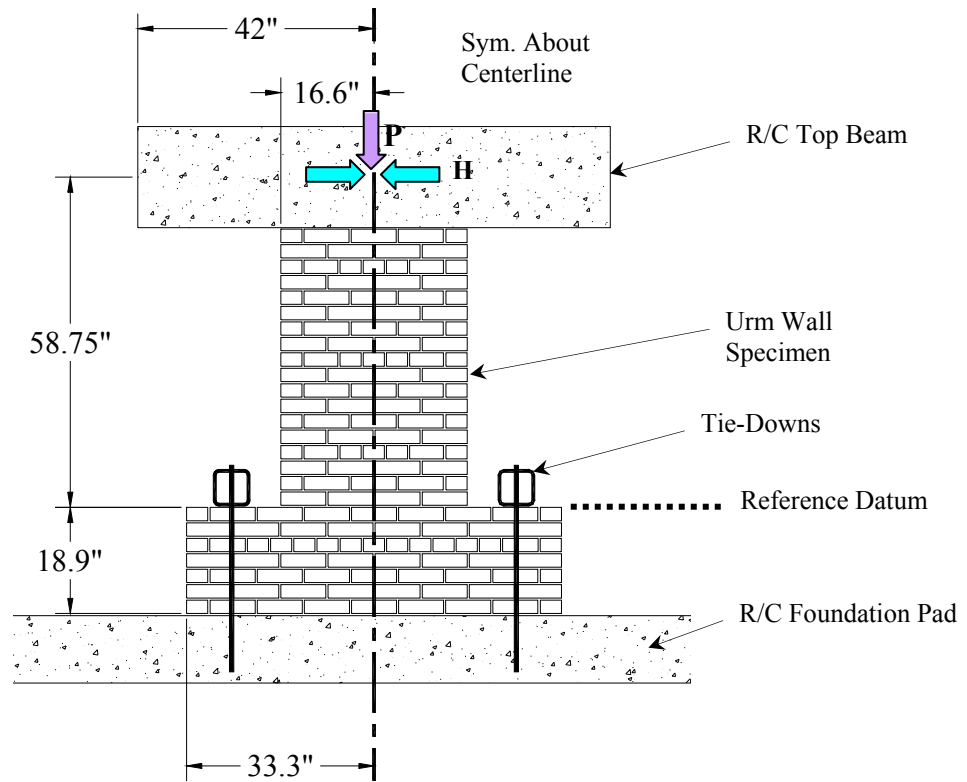


Figure 2-5. Specimen Loading and Dimensions

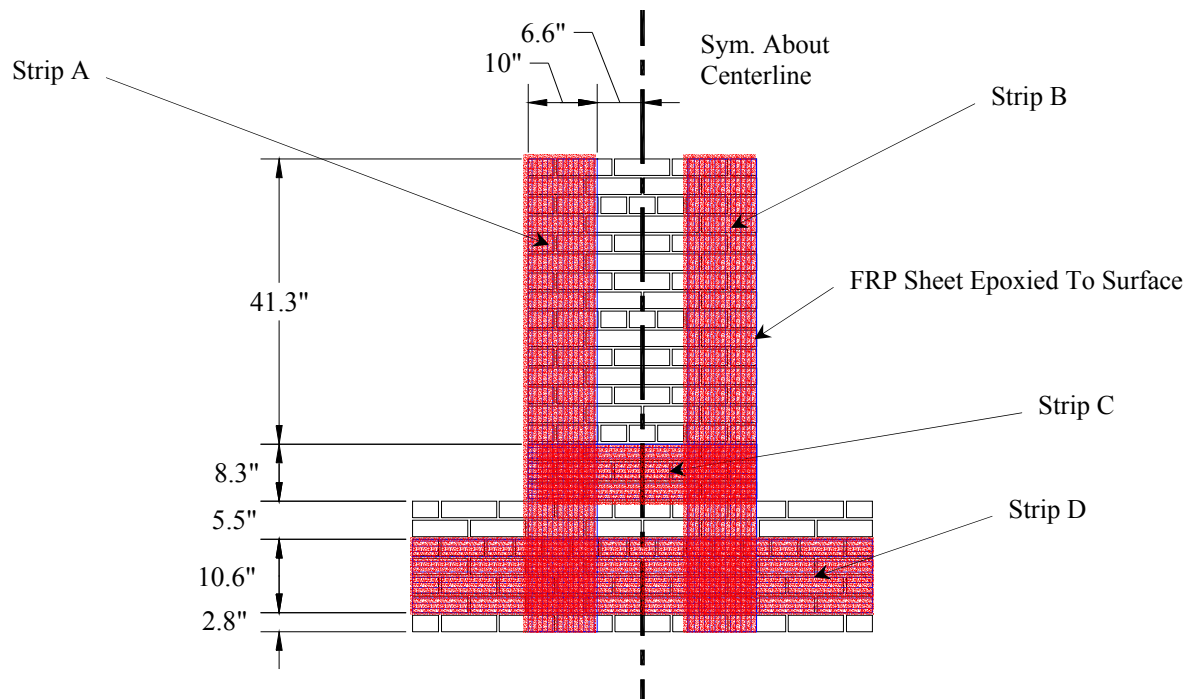


Figure 2-6. Specimen 3F FRP Placement

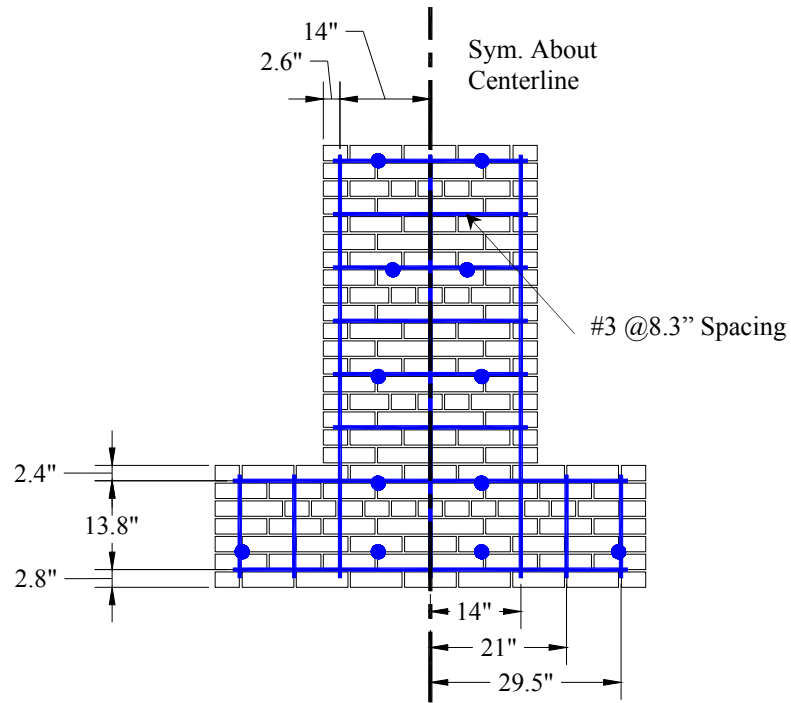


Figure 2-7. Specimen 4F Rebar Placement

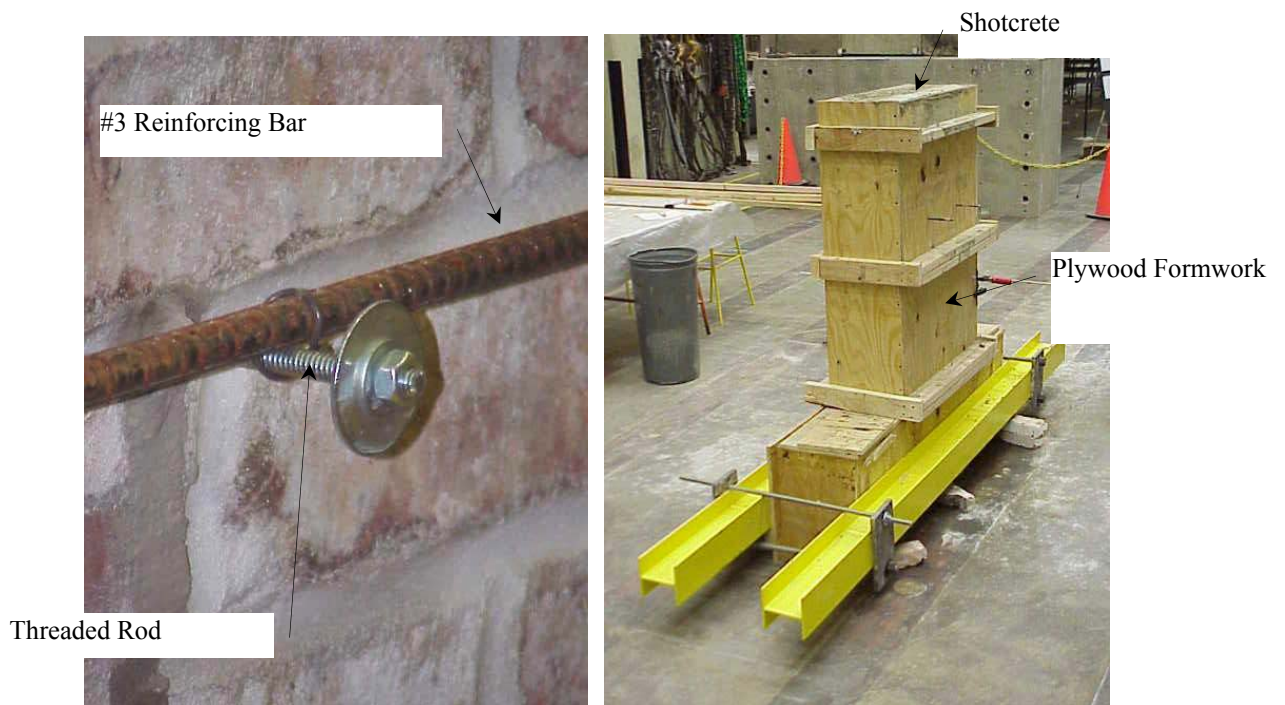


Figure 2-8. Fabrication of Specimen with Shotcrete

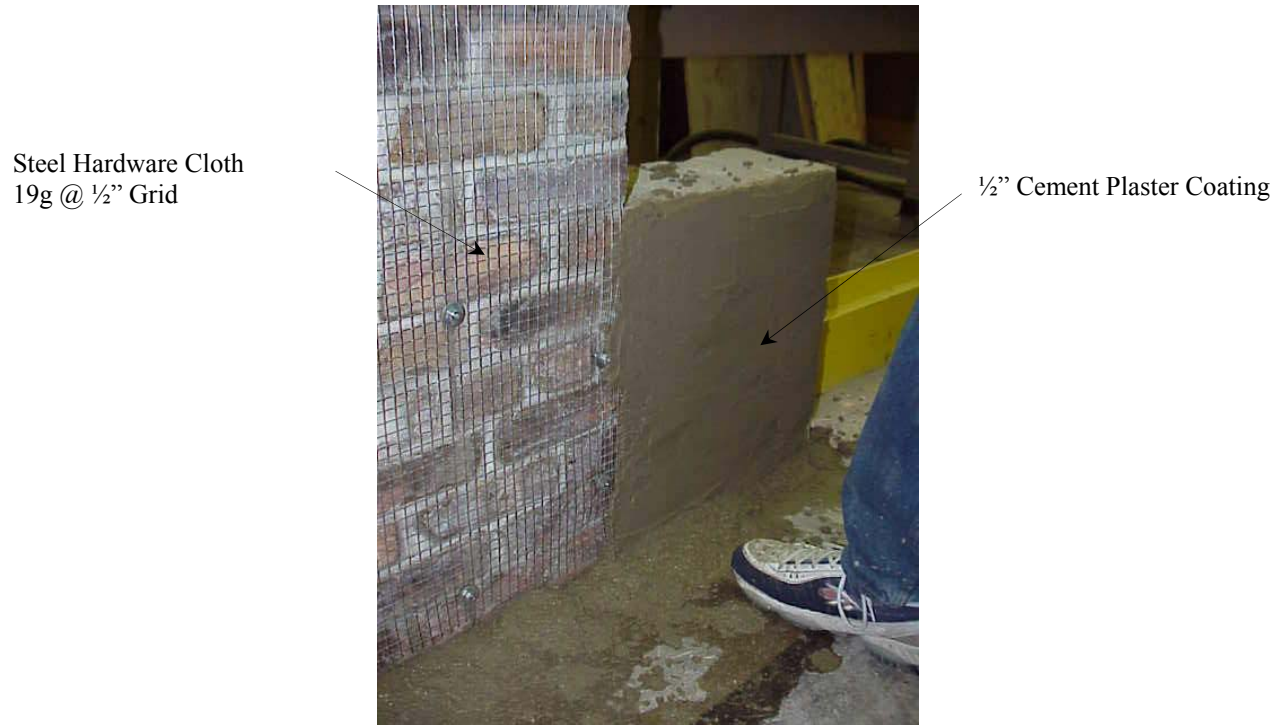
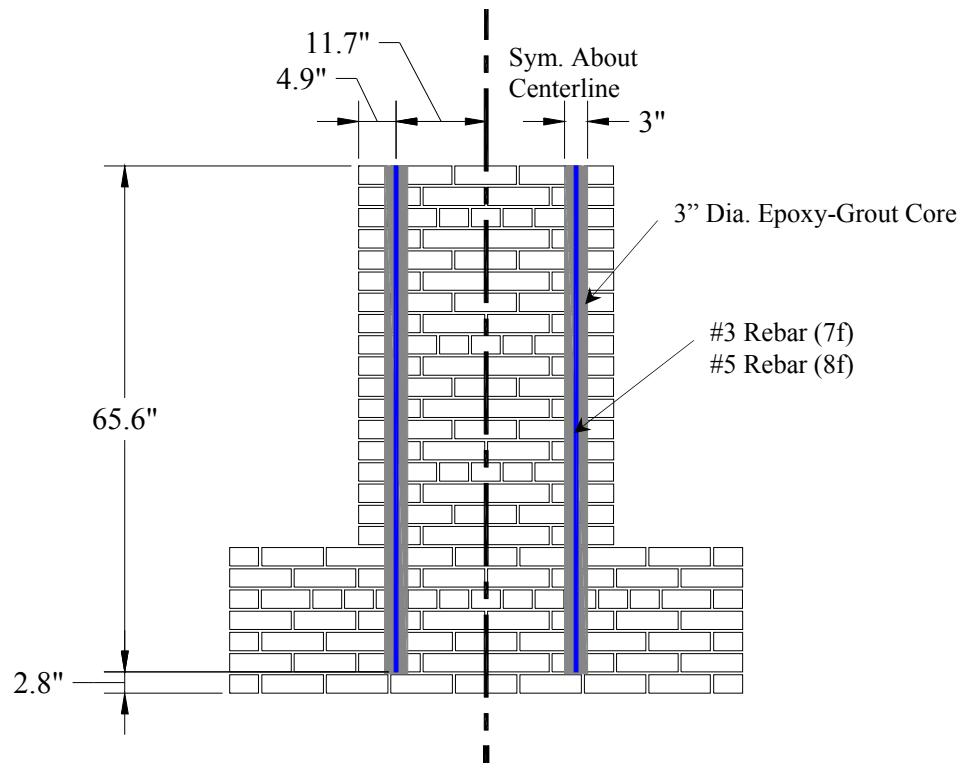
**Figure 2-9. Ferro-Cement Application****Figure 2-10 Center-Core Placement**



Figure 2-11 Drilling of Cores and Placement of Epoxy-Grout

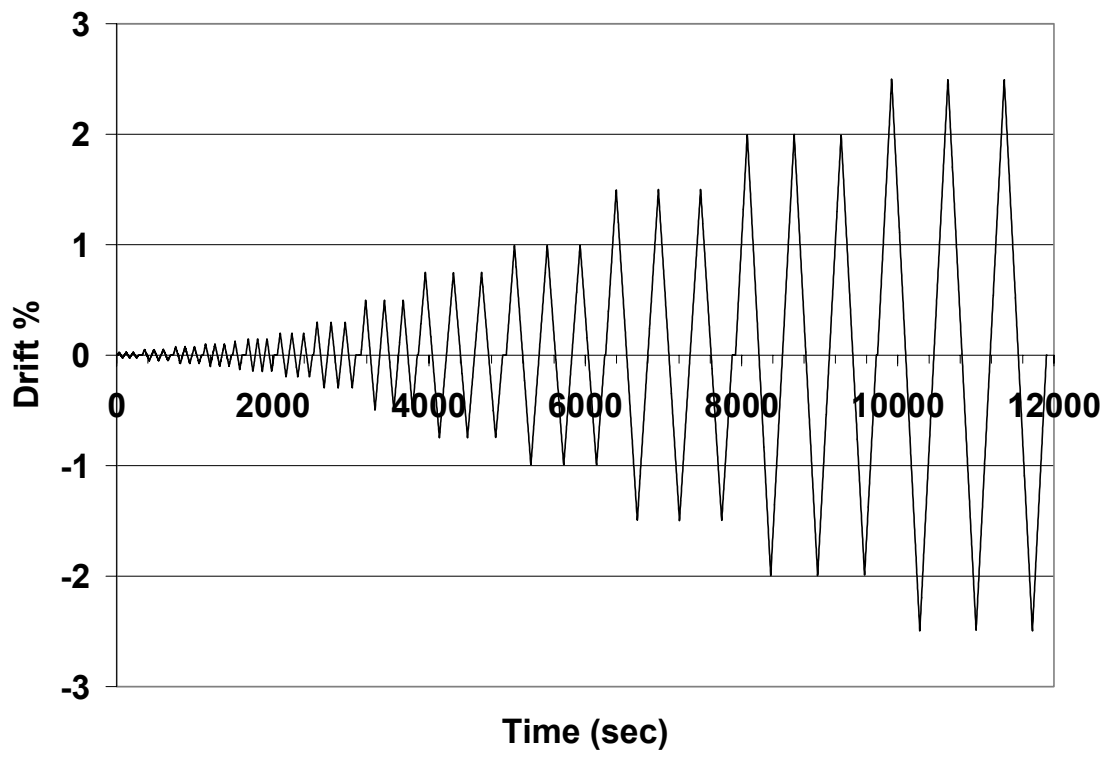


Figure 2-12 Sample Loading History

Chapter 3. EXPERIMENTAL RESULTS

3.1 Overview

As reported in Chapter 2, each test pier was subjected to a sequence of progressively increasing in-plane displacement reversals. The eight piers were subjected to peak drifts in the range of 1.5% to 2.5% in the plane of the wall. The three non-rehabilitated piers were tested with light, medium, and heavy axial force to examine variations in behavior due to changes in the applied gravity force. The rehabilitated piers were tested with medium axial force to isolate the effect of the rehabilitation.

Measurements for all test piers are given in Appendices C through J for the test piers 1F through 8F, respectively. Included in this chapter is an overview of these measurements as well as descriptions of observed behavior.

The measurements presented in this chapter provide the pieces necessary to develop linear and non-linear lateral force versus deflection relationships according to the provisions set forth in FEMA 356 Section 2.8.3.

3.2 Visually Observed Behavior

3.2.1 Non-Rehabilitated Test Pier with Medium Axial Force (Specimen 1F)

Specimen 1F was tested with a constant axial stress of 42 psi applied to the wall. Initial cracking was observed in the bed joint at the base of the pier at 0.10% drift (Figure 3-1a). The wall rocked in-plane (Figure 3-1b) with the cracks opening and then closing without any sliding or twisting until 2% drift. At 2% drift the wall began to twist about its vertical axis (Figure 3-1c) and cracking of brick in the toe section was observed in the first quarter cycle. The test was stopped at 2% drift to limit the damage to repairable levels so that the specimen could be retested as Specimen 2F.

3.2.2 Non-Rehabilitated Test Pier with Light Axial Force (Specimen 2F)

Specimen 2F was tested with a constant axial stress of 25 psi. Initial cracks in the second and third bed joints of the pier were observed at 0.05% drift. These cracks propagated through the bed joint and connected with increasing amplitudes; thus forming a continuous crack about which the wall rocked up to 2.5% drift as shown in Figure 3-2.

As described in the previous section, Specimen 2F was not an entirely new wall. The bed joint that cracked in the testing of Specimen 1F was repaired and the wall was used again for this test. The flexural cracks that formed in 2F were in the bed joints immediately above the repaired joint. This is most likely due to damage incurred within these joints during the previous test. It is interesting to note that the strength of these joints was reduced even without visible signs of damage.

3.2.3 Fiber Reinforced Polymer Test Pier (Specimen 3F)

Specimen 3F was rehabilitated with strips of FRP. All rehabilitated specimens were tested with a medium level of axial force (producing 42 psi on the cross-section of the pier). The limiting behavior mode of the specimen was delamination of the FRP. The first signs of delamination were audible “popping” sounds at 0.08% drift. Visible delamination of the four vertical strips began at 0.4% drift near the base of the pier. At 0.6% drift diagonal cracks appeared in the middle of the pier as shown in Figure 3-5a. The diagonal cracking became more extensive in the exposed bricks with all increasing amplitudes, but did not appear to propagate through the FRP to the edge of the wall.

At 1.25% drift the main vertical strip of FRP on the southeast corner (the vertical strip on the right in Figure 3-5b) fully delaminated from the base, but remained attached to the horizontal strip along the base of the wall. This horizontal strip enabled force transfer to the wall base, and prevented a loss in strength. Also at 1.25% drift it was noticed that the bed joint at the base of the wall had cracked causing the steel tie-downs to engage.

The base of the wall cracked just interior to the steel tie-downs (Figure 3-5d) and the crack propagated through the mortar toward the centerline of the wall. After successive cycles this formed a continuous u-shaped crack between the supports two courses beneath the base of the pier.

The maximum drift was 1.9% drift at which level the vertical strip on the NE corner of the wall fully delaminated causing an abrupt loss in lateral capacity.

3.2.4 Shotcrete Test Pier (Specimen 4F)

Specimen 4F was rehabilitated with 4 inches of reinforced concrete and tested with medium axial force. Cracking began in concrete at the level of the reference datum (Figure 2-5) at 0.2% drift and reached fully across the base of the pier at 0.3% drift as shown in Figure 3-6b. Cracking in the masonry began in the bed joint at the level of the reference datum at 0.3% drift as shown in Figure 3-6a. With increasing amplitudes the wall rocked about the base crack, elongating the vertical reinforcement well into the plastic range. When the cycles were reversed the vertical reinforcement did not compress to its original length, thus the wall leaned out of plane away from the shotcrete. The maximum drift was 1.5% at which point the wall was leaning three degrees out of plane and compression forces were concentrated enough on the masonry face to cause crushing as shown in Figure 3-6c.

3.2.5 Surface Coating Test Pier (Specimen 5F)

Specimen 5F was rehabilitated with a ferro-cement surface coating one-half of an inch thick that was reinforced with steel hardware cloth. The pier was tested with the same vertical force as the other rehabilitated piers. Initial cracking was heard at 0.05% drift, but it was not visible until 0.1% drift. Repeated cycles at 0.1% drift caused the hardware cloth to fracture. Once the steel reinforcement fractured, the pier rocked like the previous non-rehabilitated piers. The crack formed at the bed joint of the pier and

lengthened with increasing amplitudes until it reached across the entire width of the base at 0.2% drift. The pier continued to rock as seen in Figure 3-7 up to 2.5% drift without any signs of additional damage.

3.2.6 Non-Rehabilitated Test Pier with Heavy Axial Force (Specimen 6F)

Specimen 6F was a new URM pier with no rehabilitation that was tested under an 85psi axial stress. Unfortunately a crack formed through the second bed joint while attaching the lateral actuators, so the drift level at which cracking would begin is unknown. As expected, the wall rocked about the initial crack when loaded laterally. At 0.5% drift the head and bed joints for the bricks immediately beneath the toe cracked as shown in Figure 3-3a. The pier continued to rock in a stable manner as shown in Figure 3-3b. No further damage was observed until 2.5% drift when the toe brick in the northeast corner cracked as shown in Figure 3-3c.

To determine whether toe-crushing could be induced, Specimen 6F was tested again with 120 psi axial stress. The designation for this test was 6Fb. Since the main crack for rocking had already formed the testing began with 0.5% drift and increased to 1.5% drift. At 0.75% drift the southwest toe brick split vertically in compression as shown in Figure 3-4a.

No other damage was observed until 1.5% drift when the toe brick in the northeast corner completely and abruptly crushed causing the wall to fall out of plane as shown in Figure 3-4c.

3.2.7 Center Core Test Pier with Light Reinforcement (Specimen 7F)

The first center-core rehabilitated pier contained two #3 rebars. The vertical stress was maintained at 42 psi. The pier was tested using the same displacement history as the other tests. Visible cracking was observed at 0.15% drift in the bed joint below the

reduced-width section of the pier. The crack pattern progressed downward and toward the center of the wall with each increasing drift level, Figure 3-8a. Asymmetry was observed in the height at which the cracks crossed the center-core locations. It was discovered later that the west core did not extend down as far as was expected due to a problem during the drilling operation. The predominant behavior of the wall was rocking. The center of rotation was lower than the plain specimens and closer to the center of the pier due to the presence of the center-cores. The test was stopped at 2% drift because the top of the wall was tilting out-of-plane by approximately 1 inch, Figure 3-8b.

3.2.8 Center Core Test Pier with Moderate Reinforcement (Specimen 8F)

The second center-core rehabilitated pier was reinforced with two #5 rebar placed similarly to those of specimen 7F. The vertical stress was maintained at 42 psi for the duration of the test. The load history used was the same as all of the previous specimens. The first visible cracking was noticed at 0.15% drift. The pier rocked (Figure 3-9a) about a point similar to specimen 7F. The crack pattern was symmetrical and formed the lower half of an oval, which crossed the center-core locations approximately 3 or 4 bricks from the bottom of the specimen, Figure 3-9b. At 0.75% drift a vertical crack was observed on the back side of the wall directly in line with the East core. At 1.5% drift the wall began twisting about its vertical axis. The test was stopped at 2.5% drift because the rotation was threatening the overall stability of the pier.

3.3 Measured Lateral Force Versus Drift Relationships

Measurement of the lateral force required to impose a particular in-plane drift is essential in describing the behavior of the test piers. The base shear versus drift at the centerline of the loading beam is shown in Figure x.1 in Appendices C through J for specimens 1F through 8F, respectively.

The non-rehabilitated specimens (1F, 2F and 6F) initially behaved in a linear elastic manner. After cracking the curve softened and maintained tight hysteresis loops. Peak strength is produced at approximately 0.5% drift. The rocking strength of the pier remained constant for all subsequently larger drifts.

The rehabilitated piers displayed a wide variety of behavior. The FRP rehabilitated pier had a force-drift relationship that was smoothly decreasing in stiffness and gaining strength until there was a sudden loss of strength. The hysteresis loops indicate that the FRP specimen supplied a moderate amount of energy dissipation. The shotcrete rehabilitated pier had a force-drift relationship similar to a mildly reinforced concrete member, with an initial linear elastic region followed by yielding and large quantities of energy being dissipated as the strength increased slightly with increasing drift. The surface coating rehabilitated pier had an initial linear elastic force-drift relationship. The strength of the rehabilitated pier peaked slightly higher than that of the non-rehabilitated pier having the same axial force. However, fracture of the steel hardware cloth reduced the strength to the rocking strength of the non-rehabilitated pier. The remainder of the force-drift relationship was similar to that of a non-rehabilitated pier. The center-core rehabilitated piers also possessed an initial linear elastic region followed by softening of the force-drift relationship. However, the strength of the rocking mechanism was greater than that of a non-rehabilitated pier and the energy dissipated was moderate.

3.4 Alternative Modeling Parameters and Acceptance Criteria According to FEMA 356

3.4.1 Idealized Lateral-Force-Deformation Pushover Curve

A method for generating an idealized lateral-force-deformation pushover curve from actual test data is given in Section 2.8.3 of FEMA 356. The hysteretic curves described in the previous section are the starting point for this process. For each test pier, a backbone curve is constructed by connecting the points of the hysteretic where the first

loading curve of one deformation step intersect the last unloading curve of the previous deformation step. The backbone curve is given in Figure x.2 in Appendices C through J for Specimens 1F through 8F, respectively.

A multi-linear force-deformation curve is then fitted to the backbone curve as shown in Figure x.3 in Appendices C through J for Specimens 1F through 8F, respectively. The multi-linear approximation must conform to one of the three types given in Figure 2-3 of FEMA 356. The next step is to combine the positive and negative branches of the force-deformation relationship to form one composite curve. This is accomplished by averaging the slopes of each respective segment of the multi-linear curve, and then applying this stiffness to a region bounded by the average of the drifts of the positive and negative contributing segments. The composite force-deformation relationship is shown in Figure x.4 in Appendices C through J for Specimens 1F through 8F, respectively.

3.4.2 Acceptance Criteria

Acceptance criteria provide a standard of comparison for the structural performance of the element being designed. For deformation-controlled primary structural components, these acceptance criteria take the form of drift limits for the NSP or m-factors for the LSP.

Acceptance criteria for use with the NSP and deformation-controlled primary structural components are the drifts which cause damage to the pier in accordance to the associated structural performance level. These drifts are approximated from the composite force-deformation curve as specified in FEMA 356 Section 2.8.3.6. The LSP uses the ratio of the NSP prescribed drifts to the yield drift with a 0.75 factor in the numerator.

These acceptance criteria are shown in Figure x.5 in Appendices C through J for Specimens 1F through 8F, respectively.

3.5 Initial Lateral Stiffness

The lateral stiffness of the piers was determined from the slope of the initial segment of the composite force-deformation curve developed previously. These stiffness values are summarized in Table 3-1.

The stiffness of each of the non-rehabilitated piers was directly proportional to the axial compressive force. All of the rehabilitation methods increased the initial stiffness of the pier as compared to the non-rehabilitated pier except for the FRP rehabilitated pier. The initial stiffness is applicable for drifts less than that which causes visible cracking.

3.6 Strength

The strength of a test pier was defined according to FEMA 356 Section 2.4.4.4 to be the force corresponding to effective yielding on the composite force-deformation curve. These observed strengths are summarized in Table 3-1 and shown graphically in Figure x.4 in Appendices C through J for Specimens 1F through 8F, respectively.

3.7 Shear Stress Versus Shear Strain Relationships

As described in Section 2.5, four displacement transducers were mounted on each test pier in an arrangement to permit measurement of shear strain. By analyzing the shear strain, the shear modulus can be calculated and degradation in shear stiffness can be inferred. This discussion will include all specimens except for Specimens 3F and 2F. Specimen 3F was not instrumented with the necessary transducers to measure the shear strain, and LVDT#8 on specimen 2F did not function properly during the test.

The average shear strains for the piers were calculated using Equation (7) to relate the measured displacements of LVDTs 1, 8, 9, and 10. These strains were then plotted versus the applied shear stress to determine the amount of energy being dissipated through shear, and to determine the shear modulus. The shear stress versus strain behavior of each test pier is shown in Figure x.6 in Appendices C through J for Specimens 1F through 8F, respectively. The plots generally consisted of tight linear loops as would be expected, since no damage was observed in the region above the bed-joint crack.

The shear modulus was determined by fitting a line to the shear stress versus shear strain data using linear regression. The slope of the fitted line represents the effective shear stiffness as shown Table 3-2.

The shear modulus for Specimens 1F, 6F, and 6Fb decreased with increasing drifts, indicating that there was slight shear damage. To examine this more closely, plots were made for each specimen using the data from only four amplitudes: 0.025%, 0.5%, 1.5%, and 2.5% drift. Linear trend lines were fitted to each of these amplitudes, and the corresponding shear modulus calculated as is summarized in Table 3-2.

It can be observed that for specimens 4F and 5F the shear modulus did not decrease appreciably. Comparing the modulus at 1.5% drift to that at 0.025% drift indicates only a 2% and 6% decrease in shear stiffness for 4F and 5F respectively. However for specimen 6F there was a 20% decrease in shear stiffness over the same range. Specimen 6Fb was not tested at 0.025% drift so it can not be compared directly, but from 0.5% to 1.5% drift Specimen 6F had an 8% decrease in stiffness and 6Fb had a 15% decrease. A graphical comparison of the measured shear modulus for all five specimens is shown in Figure 3-10. The decrease in the shear modulus was greatest for the plain URM specimens and was magnified by the axial force. In the rehabilitated specimens the shear stiffness was significantly enhanced and did not deteriorate appreciably with increasing amplitudes.

3.8 Net Flexural Tensile Stress at Cracking

As previously described, the instant at which cracking is assumed to begin is when the slope decreases on the measured force-deflection envelope. In almost all cases this point of initial cracking is also visually observable. From the lateral load and vertical load at this instant of cracking the flexural tensile strength of the mortar can be deduced using the following equation.

$$f_{cr} = \frac{M}{S} - \frac{P}{A} = \frac{H_{cr}h}{S} - f_a \quad (8)$$

The calculated net flexural tension stress at cracking for each pier is listed in Table 3-1.

As previously mentioned, flexural cracks that formed in 2F were all above the repaired joint where Specimen 1F cracked. Since the wall used for 2F was the same wall used for 1F, both joints that cracked were made from the same batch of mortar, yet the data indicates the tensile strength from 2F to be almost half of that from 1F. Thus it is strongly indicated that residual damage, which was not visible, from the testing of 1F resulted in a weakened bed joint that fully cracked in 2F.

The apparent flexural tensile stress for Specimens 4F and 5F was also calculated to determine an equivalent tension capacity of the system. The tension stress calculated was not the actual tension, but rather the required tension on only the masonry cross-section to support the lateral force at cracking.

3.9 Crack Opening Profile

The openings of cracks in the lower bed joints of the pier were measured at several locations across the width of the pier (Table 2-1). Measurements were made with

displacement transducers that spanned the area where cracking was expected. The crack width profiles are plotted at three different drift levels as shown in Figures x.7 for Specimens 1F through 8F in Appendices C through J, respectively.

In general, the crack width varied linearly across the width of the pier. This is particularly true for drifts up to 0.5%. The neutral axis passes through the point at which the crack width is equal to zero. Negative crack width implies a closed crack with compressive strain existing in the masonry. Examination of the crack opening profiles demonstrates that the region of masonry required to carry the induced shear and compressive stresses is quite small. For example, the non-rehabilitated specimen with heavy axial force was able to withstand 21.4 kips of compression and 5.4 kips of shear applied to a portion of the cross-section which was 1.8 inches deep and 2-wythe thick. The resultant average shear and compressive stresses for this region were approximately 150% of the capacities estimated by the prism tests. This is due to the confinement provided by the surrounding masonry in the region immediately above and below the compression interface.

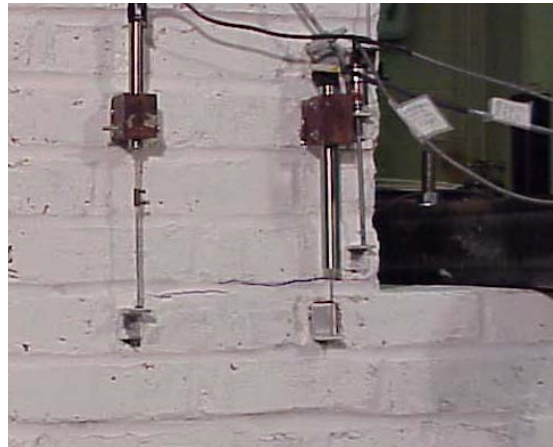
The crack width profile is also helpful in identifying the modifications to behavior produced by the rehabilitation. For example, the FRP rehabilitated pier's crack opening profile is significantly different than the other test piers. The crack geometry data indicates that the pier was not developing the typical bed joint crack observed in the other specimens. Instead, the FRP caused the cracks to be much smaller and distributed over a much larger region of the pier as compared to the non-rehabilitated walls.

Table 3-1 Summary of Experimental Results

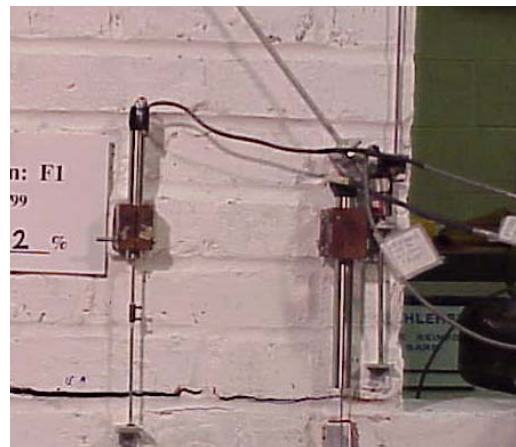
Specimen	Rehabilitation	Vertical Stress [psi]	Initial Stiffness [kips/in]	Cracking Load [kips]	Net Flexural Tensile Stress [psi]	Peak Response		
						Drift [%]	Load	
							+ [kips]	- [kips]
1F	None	42	117	2.5	63	1.5	3.3	3.4
2F	None	25	88	1.5	35	2.5	2.0	1.8
3F	FRP	42	92	N/A	N/A	1.9	11.4	9.7
4F	Shotcrete	42	238	9.3	361	1.5	10.9	10.1
5F	Surface Coating	42	179	3.9	139	2.5	4.4	3.8
6F	None	85	179	N/A	N/A	2.5	5.8	5.8
6Fb	None	120	N/A	N/A	N/A	1.5	7.7	7.7
7F	Center-Core #3	42	175	6.0	192	2.0	6.6	7.0
8F	Center-Core #5	42	176	6.6	196	2.5	6.6	8.7

Table 3-2 Summary of Shear Modulus with Respect to Drift

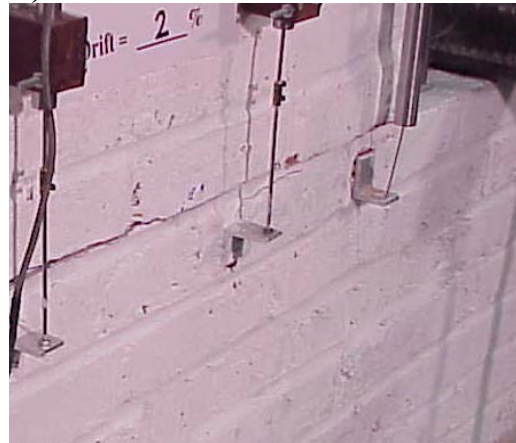
Specimen	G, Shear Modulus [ksi]			
	0.025% Drift	0.50% Drift	1.5% Drift	2.5% Drift
1F	186	184	158	N/A
4F	527	465	515	N/A
5F	281	263	265	239
6F	252	220	202	184
6Fb	N/A	236	201	N/A
7F	143	125	129	N/A
8F	178	151	152	140



a) Initial Cracking at 0.1% drift

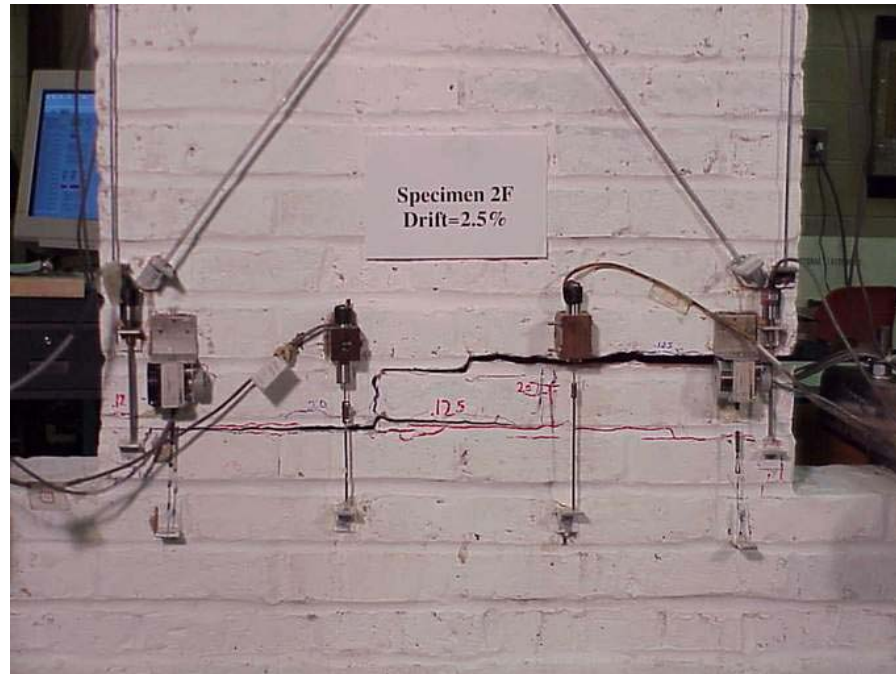


b) Rotation About Toe at 2.0 % Drift

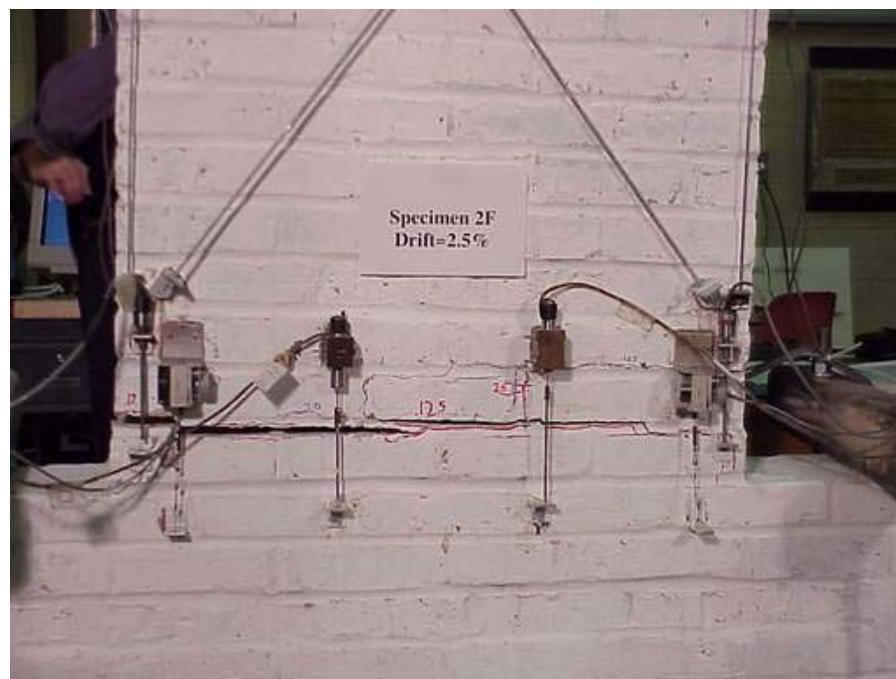


c) Rotation About Vertical Axis of at 2.0 % Drift

Figure 3-1 Damage Photos of Non-rehabilitated pier with medium (42psi) vertical stress (1F)

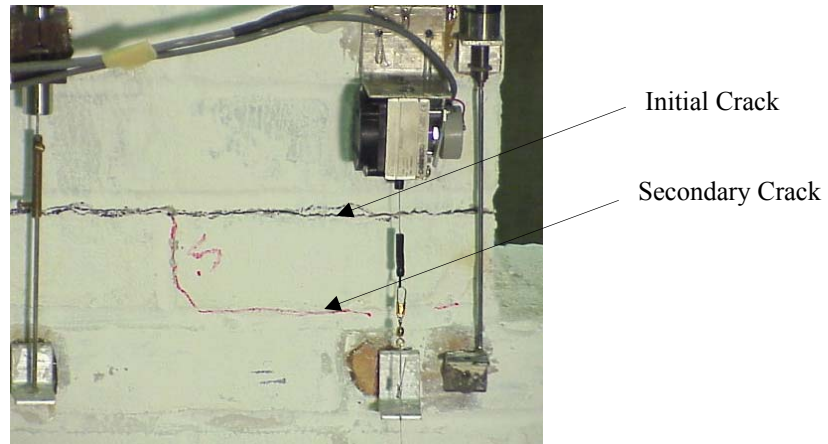


a) Positive Rotation

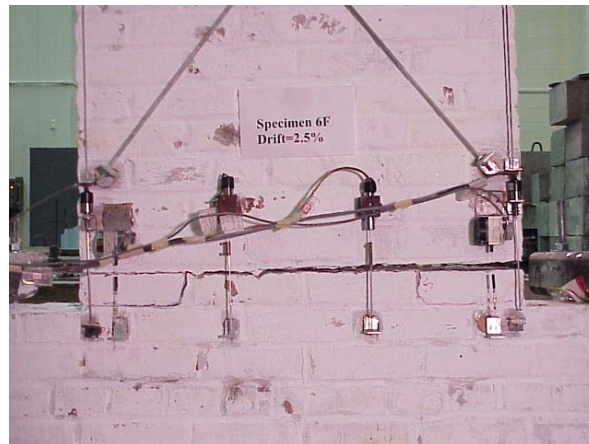


b) Negative Rotation

Figure 3-2 Damage Photos of Non-rehabilitated pier with light (25psi) vertical stress (2F)



a) Crack Formation in First Bed Joint at 0.50% Drift



b) Rocking at 2.5% Drift



c) NE Brick Cracking at 2.5% Drift

Figure 3-3 Damage Photos Of Non-Rehabilitated Specimen With Heavy (85 Psi) Axial Stress (6F)



a) SW Toe Compression Splitting

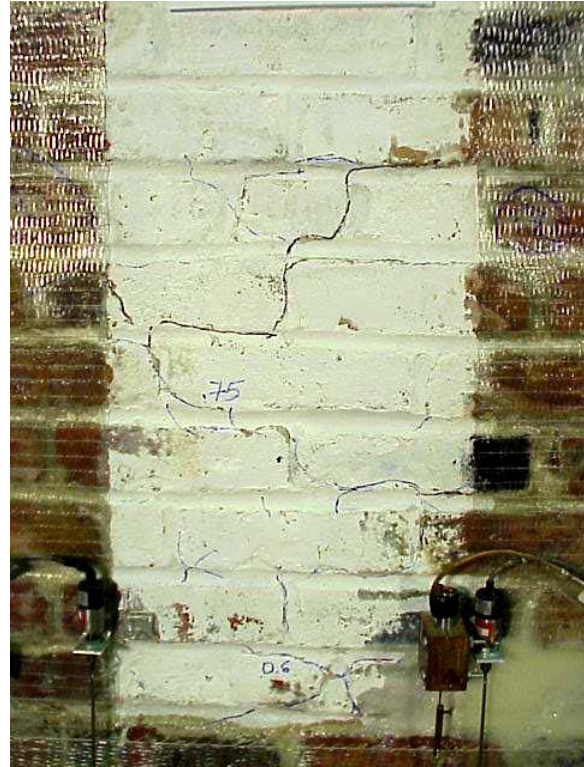


b) Toe Crushing at 1.5% Drift

Figure 3-4 Damage Photos of Non-Rehabilitated Specimen with 120 Psi Axial Stress (6Fb)



a) Onset of Diagonal Cracking



c) Diagonal Cracks at 1.25% Drift

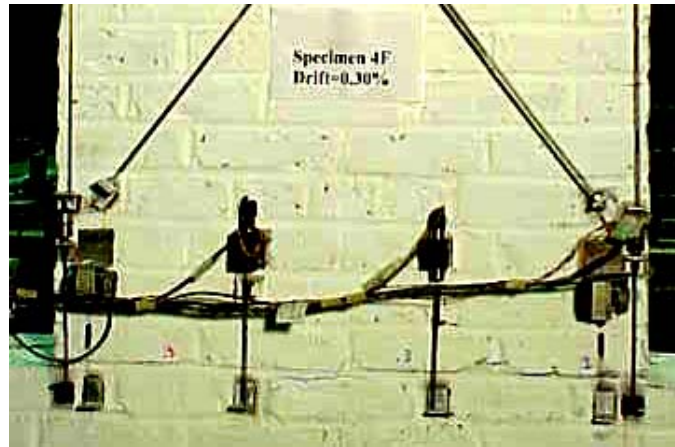


b) Delamination Pattern of SE FRP Strip

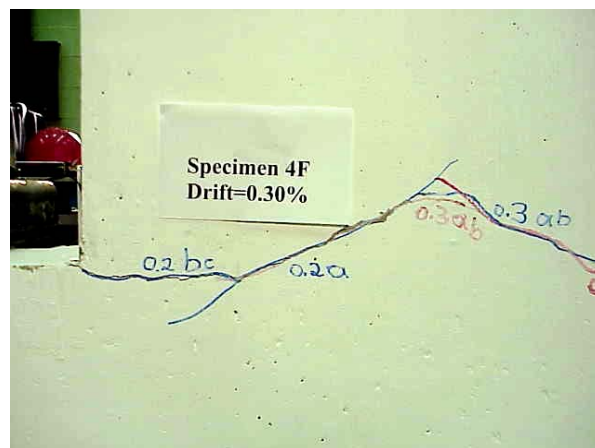


d) Cracking at Foundation Tie-down

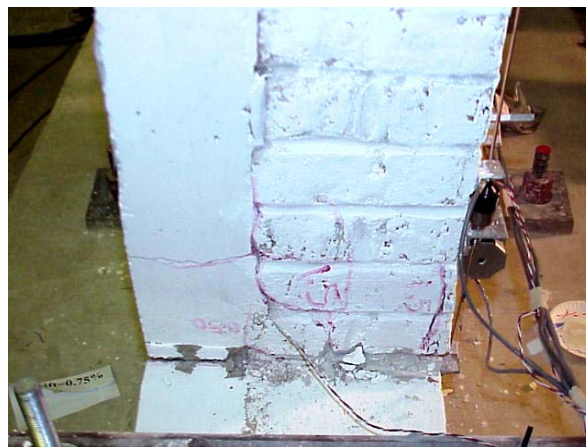
Figure 3-5 Damage Photos of FRP Specimen (3F)



a) Cracks in Masonry at 0.3% Drift



b) Cracks in Concrete at 0.3% Drift



c) Masonry Crushing

Figure 3-6 Damage Photos of Shotcrete Rehabilitated Pier (4F)

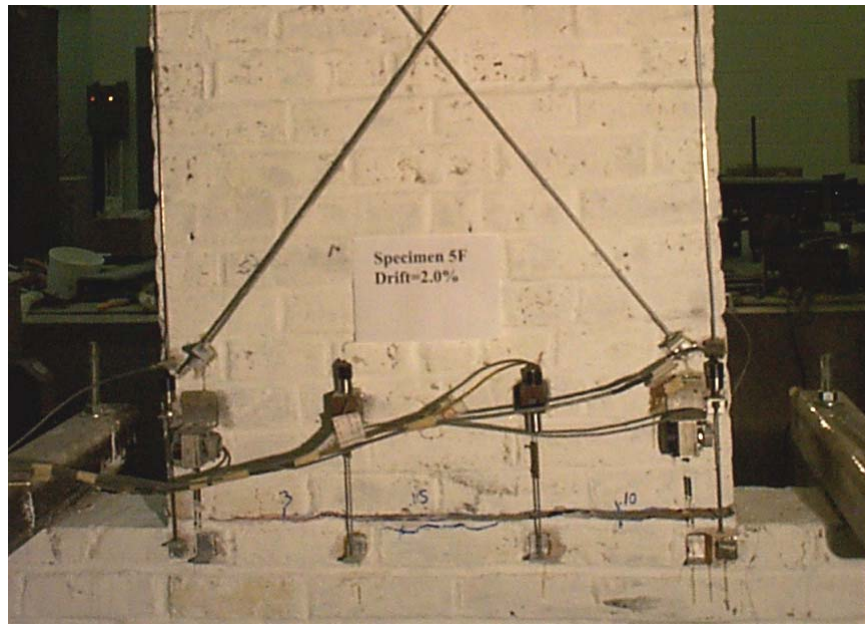
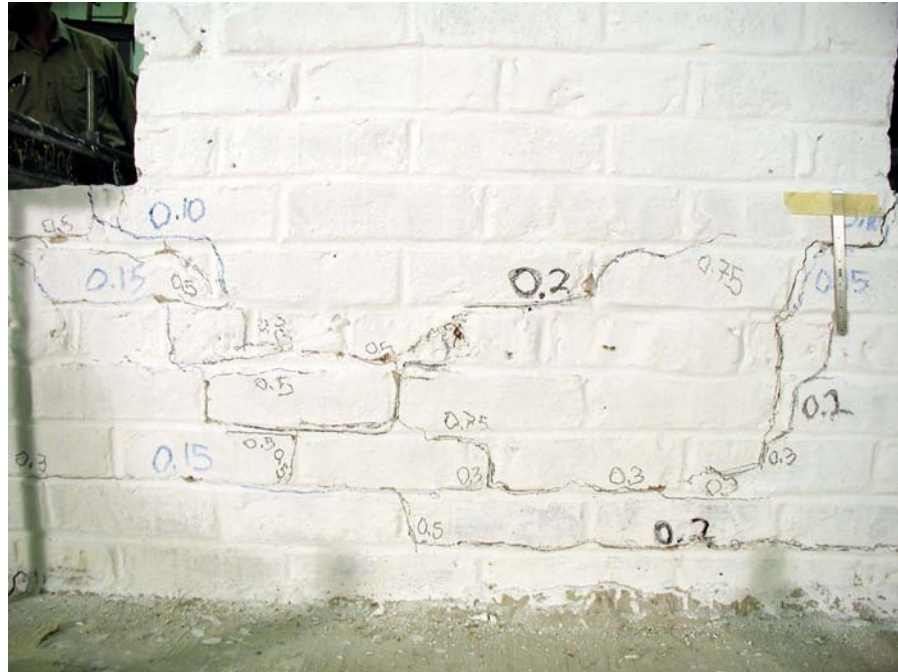


Figure 3-7 Specimen 5F, 2.0% Drift



a) Crack Pattern

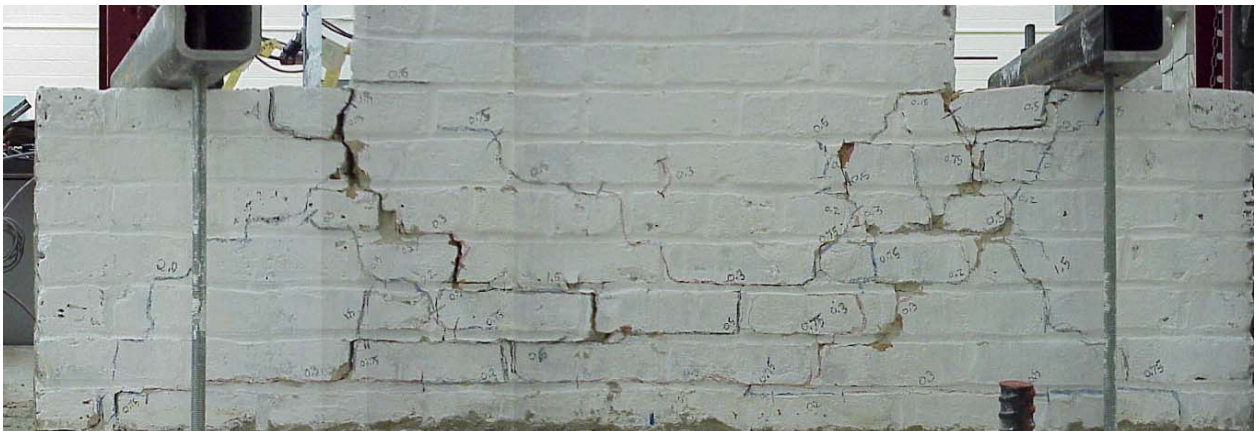


b) Out of Plane Motion

Figure 3-8 Damage Photos of Center-Core Rehabilitated Pier with #3 Rebar (7F)



a) Rocking Behavior



b) Crack Pattern

Figure 3-9 Damage Photos of Center-Core Rehabilitated Pier with #5 Rebar (8F)

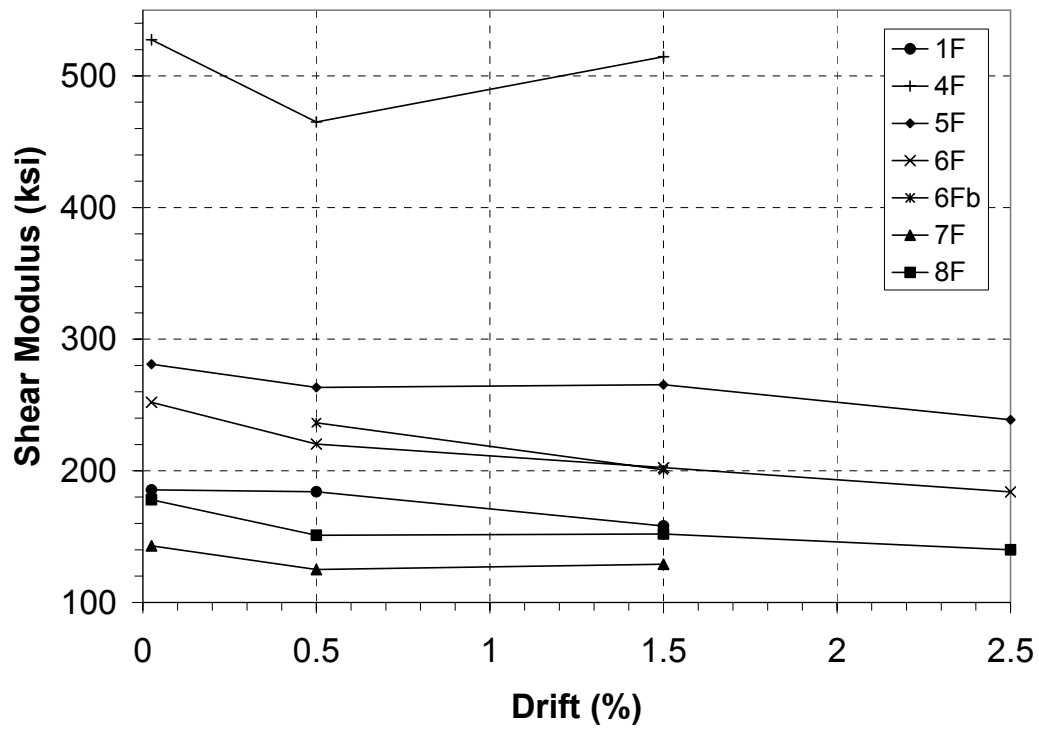


Figure 3-10 Measured Shear Modulus With Respect to Drift

Chapter 4. INTERPRETATIONS OF OBSERVED BEHAVIOR

4.1 Introduction

The URM piers tested during this investigation exhibited a wide range of behavior. The FEMA 356 *Guidelines* were used to estimate the response of each pier and to evaluate the effectiveness of different types of rehabilitations. The guidelines also set forth a method for distilling the measured response of experimental tests into force-deflection relationships used for both linear and non-linear static analyses. The comparisons below make extensive use of the experimental results contained in the previous chapter and the FEMA 356 *Guidelines*. The significant parameters describing the measured and estimated behavior of the test piers are included in Table 4-1.

4.2 Yield Strength Estimates vs. Measured Yield Strengths

The effective yield strength of a pier is the level of force at which significant deformations take place without a notable increase in the applied force. The effective yield strength of each pier was measured as described in section 3.6 of this report. Estimates of strength for the non-rehabilitated piers use the relevant rocking or toe-crushing prediction from Chapter 7 of the FEMA 356 *Guidelines*. Strength estimates for the rehabilitated piers were calculated according to the suggestions of section C7.4.1.3 and 7.4.2.2 of the *Guidelines*. A fiber analysis was used to analyze all of the rehabilitated piers since the cross-sections and material properties were varied and in non-traditional geometries. A graphical comparison of the estimated and measured strength for each pier is given in Figure 4-1. The estimated strength of the non-rehabilitated piers are approximately correct, as a result of the well-known rocking strength equation mentioned above. The strength estimates for the rehabilitated piers are consistently too high, with the exception of the Center Core rehabilitated piers. The strength estimates for Center Core are comparable to the measured strengths.

4.3 Stiffness Estimates vs. Measured Initial Lateral Stiffness

Equation 1, given in the first Chapter of this report, is used to estimate the initial stiffness of a flexural pier. The modulus of elasticity for each rehabilitation material was used to calculate a transformed cross section of equivalent masonry. Initial stiffness was measured using the slope of the first section of the composite bilinear curve (Figure x.4 in Appendices C through J for Specimens 1F through 8F, respectively). A graphical comparison of the estimated and measured initial stiffness for each pier is given in Figure 4-2. The estimated stiffness for each of the non-rehabilitated piers is approximately equal to the measured stiffness. Stiffness estimated for the rehabilitated piers are all too high. The over-estimate ranges from negligible (Center Core) to twice the measured stiffness (Shotcrete).

4.4 Estimated mQ_{CE} vs. Measured mQ_{CE}

The overall accuracy of the FEMA estimated m-factor, and mechanics based strength (Q_{CE}) and stiffness may be determined by comparison with the measured flexural behavior of the piers. Figure 4-3 shows the estimated and measured LSP capacity (mQ_{CE}) for the Life Safety Performance Objective. The initial linear portion of a pier's force-deformation relationship may be extended in a linear fashion to a point equal to the product of the product of the yield deformation, Δ_y , times the ductility factor, m . The linear static procedure, LSP, is frequently used by engineers due its simplicity and ease of implementation. Since the relationship is linear, the LSP also has the effect of increasing the yield strength, Q_{CE} , by the same ductility factor, m . More information on the LSP is given in Section 1.3 of this report. Table 4-1 contains a numerical comparison of the estimated and measured LSP capacities of each pier. A graphical construction for each pier at the Life Safety (LS) performance level is shown in Figure x.8 of Appendices C through J for Specimens 1F through 8F, respectively. These results are also summarized in Figure 4-3. Examination of Table 4-1 shows that the IO

performance level capacity is well estimated using current guidelines; however, the LS and CP performance level capacity is measured to be one to six times the estimated capacity. It should be noted that the trend of overestimating the strength and underestimating the deformation capacity has the overall effect of bringing the product of these two factors closer to the measured behavior.

4.5 Comparisons of Rehabilitation Methods

4.5.1 Strength, Q_{CE}

Figure 4-4 shows the measured strength of each of the rehabilitated piers in comparison to the non-rehabilitated pier with the same applied axial force level. All of the rehabilitation methods except surface coating are observed to increase the strength of the pier. The rehabilitated strengths are on the order of twice the non-rehabilitated pier's strength. The surface coating did not result in a significant increase in the pier's strength.

4.5.2 Stiffness, k

Figure 4-5 compares the measured initial stiffnesses for each of the rehabilitated piers in comparison to the non-rehabilitated pier. The rehabilitated stiffnesses are wide ranging, with FRP being approximately half of the control specimen and shotcrete being twice the control specimen's stiffness. Surface coating showed no appreciable change in the pier stiffness, while Center Core resulted in a slight increase in initial stiffness.

4.5.3 Ductility Ratio, m

The measured ductility ratio for each of the rehabilitated piers is given in Figure 4-6. The plain pier and surface-coating pier are seen to have the greatest deformation

capacity. This is due to the purely rocking mechanism developed in both of these specimens. Shotcrete and Center Core show a reduced deformation capacity of approximately 75% of the plain specimen. FRP has the lowest deformation capacity which is equal to 25% of the non-rehabilitated specimen.

4.5.4 Ductility Ratio x Strength, mQ_{CE}

The measured mQ_{CE} capacity of each of the rehabilitated piers is given in Figure 4-7. The combined effects of strength and ductility are evident in this representation. It is interesting to recognize that the shotcrete, surface coating and Center Core rehabilitated piers all have similar effectiveness (approximately 30% increase compared to non-rehabilitated wall). Also of note is the reduction of effectiveness with FRP. The FRP rehabilitated pier attained only 50% of the LSP capacity of the plain wall.

4.5.5 Energy Dissipation

The measured force-deflection relationships for each of the rehabilitated test piers are shown in Figure 4-8. The control specimen having no rehabilitation is included for comparison in each of the graphs. The relative amount of energy dissipation may be inferred from the area enclosed by the force-deflection curves. Energy dissipation is most often a result of damage occurring to the pier. Crushing or yielding of the masonry or the rehabilitation material results in large amounts of energy being dissipated as is evident in Figure 4-8 a and b corresponding to the FRP and shotcrete rehabilitated piers, respectively. Figure 4-8 c relates to the surface coating rehabilitated pier and shows very little energy dissipation as with the non-rehabilitated pier. Figure 4-8 d and e correspond to the Center Core rehabilitated piers and show modest amount of energy dissipation. The Center Core specimens showed significant cracking of the masonry in the anchorage zones of the cores; however, larger amounts of dissipated energy were not achieved since the steel rebar did not yield.

4.5.6 Damage

Damage to the test piers varied with each type of rehabilitation. The non-rehabilitated pier sustained the least amount of damage (Figure 4-9a). The rocking mechanism leads to damage which is confined to the critical bed-joint leaving the surrounding masonry in good condition. The bed-joint crack in the non-rehabilitated pier is almost completely closed following the testing. Damage to the FRP rehabilitated pier is much more extensive (Figure 4-9b). Cracks can be seen throughout the upper region of the pier and delamination of the FRP strips has taken place throughout the lower portion of the pier. The shotcrete rehabilitated pier also shows one primary crack at the critical section of the specimen (Figure 4-9c). This crack does not close with subsequent displacement reversals because the rebar has deformed plastically. The crack width continues to increase with each cycle until the pier leans out-of-plane toward the masonry. Such damage is permanent and would require substantial repair following an earthquake. The surface coating rehabilitated pier behaves the same as the non-rehabilitated pier. A single crack is seen to cross the entire width of the pier and close almost completely after each cycle (Figure 4-9d). The steel mesh has fractured on the reverse side and would need to be patched or replaced with new mortar applied following an earthquake. The Center core rehabilitated piers sustained to most damage (Figure 4-9e). Extensive cracking in the lower anchorage region of the pier is evidence of the change in behavior caused by the presence of the cores. These cracks close partially at the end of each cycle but are still clearly visible. The damage to the masonry was significant enough to cause small portions of the masonry to dislodge from the pier.

Table 4-1 Comparison of estimated and measured flexural behavior

Test Pier	Vertical Stress [psi]	Strength [kips]		Initial Stiffness [kips/in]		LSP						mQ _{CE} [kips]					
						m _{IO}		m _{LS}		m _{CP}		IO		LS		CP	
		Estimated	Measured	Estimated	Measured	Estimated	Measured	Estimated	Measured	Estimated	Measured	Estimated	Measured	Estimated	Measured	Estimated	Measured
Non-Rehabilitated (1F)	42	2.7	2.9	176	140	2.6	2.1	5.3	24.8	7.1	33.1	7.0	6.2	14.3	72.7	19.2	97.0
Non-Rehabilitated (2F)	25	1.6	1.8	176	100	2.6	1.2	5.3	36.9	7.1	49.2	4.2	2.2	8.5	66.1	11.4	88.1
Fiber Reinforced Polymer (3F)	42	12.6	6.9	182	71	2.1	1.8	2.8	4.6	3.8	6.2	26.5	12.4	35.3	32.0	47.9	42.6
Shotcrete (4F)	42	7.7	6.8	499	266	2.0	3.4	2.5	12.7	4.0	16.9	15.4	23.4	19.3	86.8	30.8	115.7
Surface Coating (5F)	42	4.2	3.1	197	119	2.1	1.7	2.8	24.8	3.8	33.1	8.8	5.3	11.8	77.3	16.0	103.1
Non-Rehabilitated (6F)	85	5.3	5.8	176	154	1.0	1.2	1.0	17.5	1.0	23.4	5.3	6.8	5.3	101.1	5.3	134.8
Center Core #3 (7F)	42	5.9	5.9	188	175	2.1	2.0	3.7	14.8	4.8	19.8	12.4	11.6	21.8	87.1	28.3	116.1
Center Core #5 (8F)	42	10.2	6.9	200	171	1.8	1.6	2.8	16.4	3.6	21.8	18.4	11.3	28.6	112.6	36.7	150.1

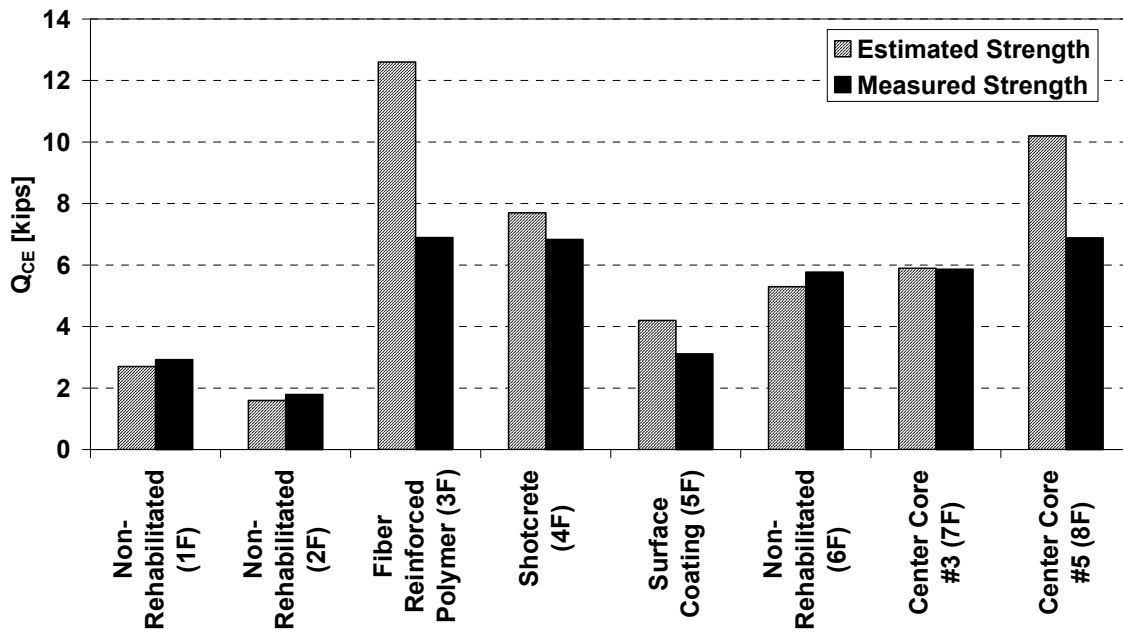


Figure 4-1 Strength comparison

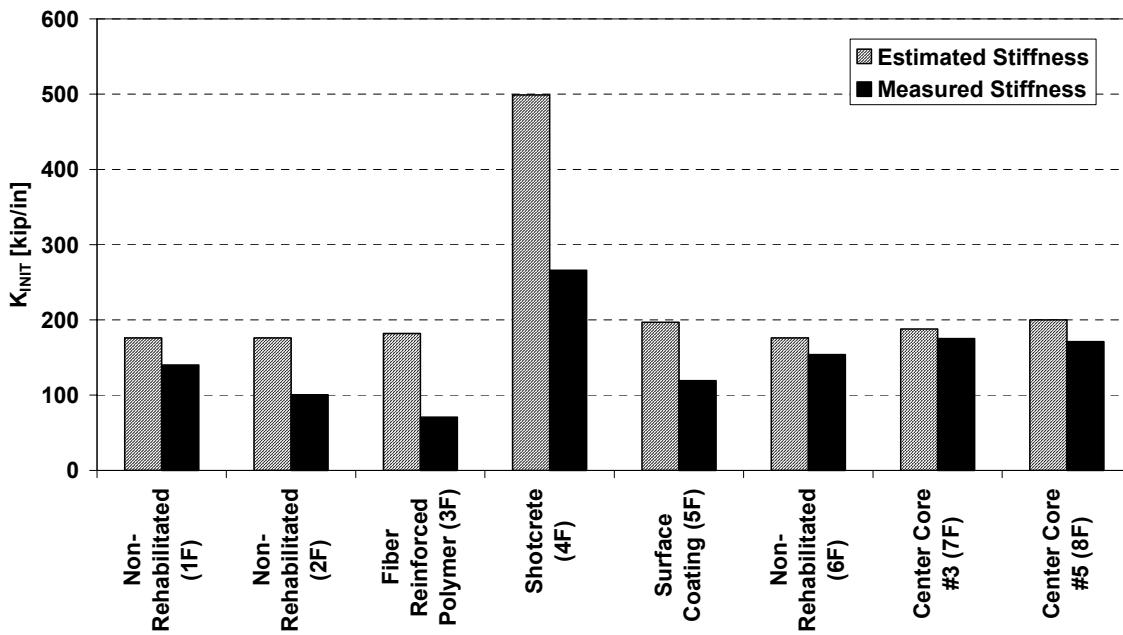


Figure 4-2 Initial stiffness comparison

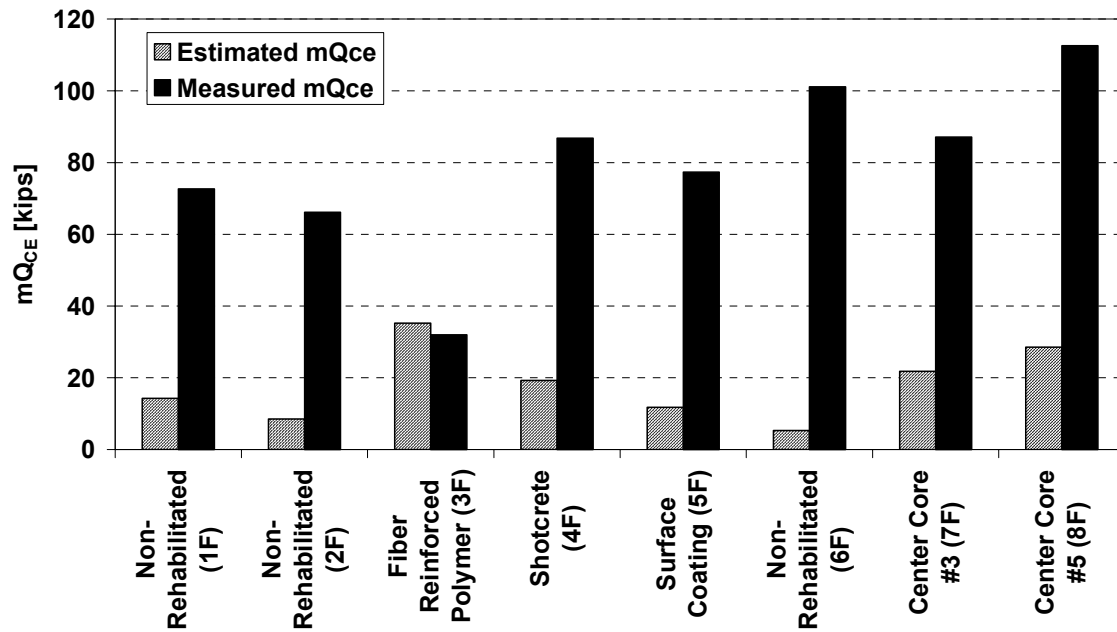


Figure 4-3 Comparison of Estimated to Measured mQ_{CE} (LS performance level)

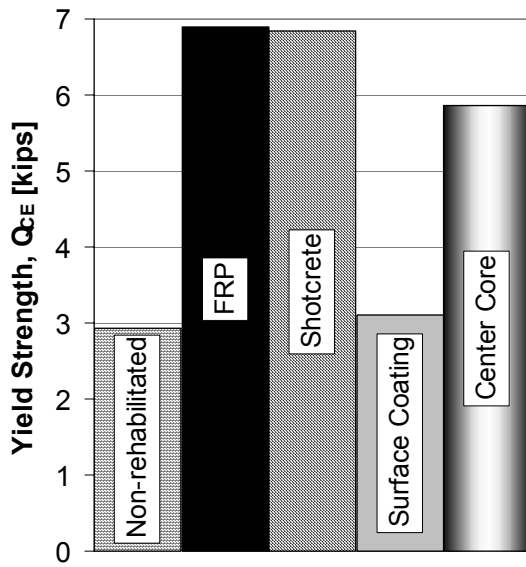


Figure 4-4 Measured strength of rehabilitated piers

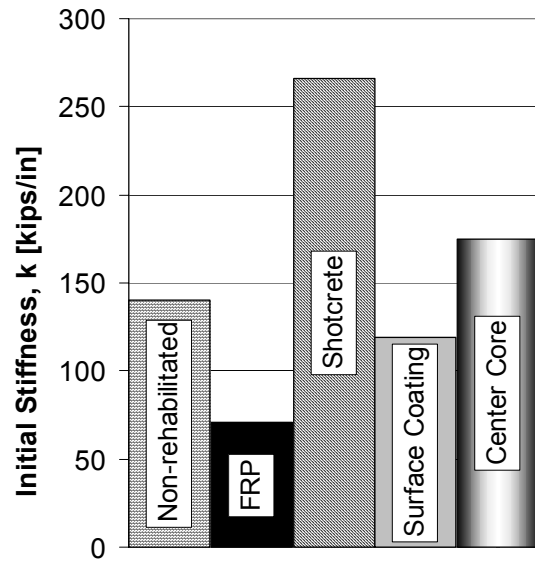


Figure 4-5 Measured initial stiffness of rehabilitated piers

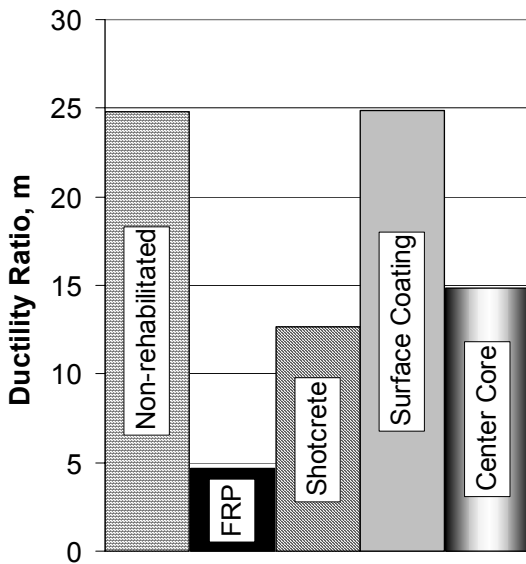


Figure 4-6 Measured ductility ratio of rehabilitated piers

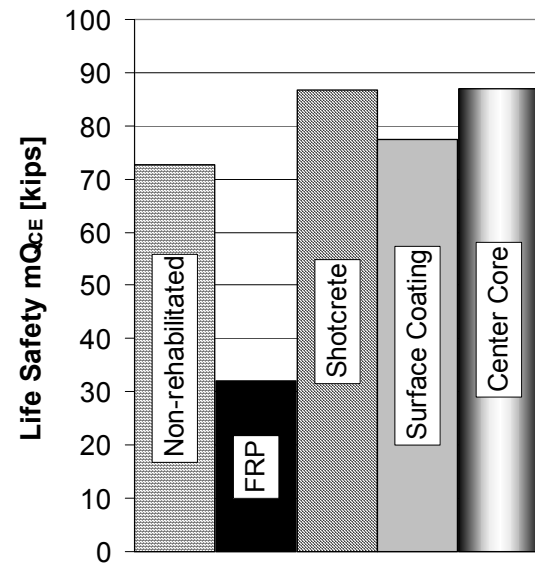
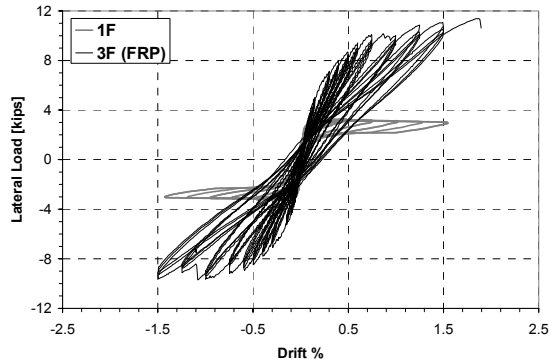
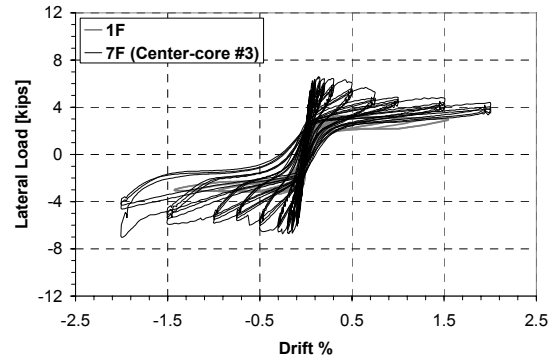


Figure 4-7 Measured mQ_{cE} of rehabilitated piers

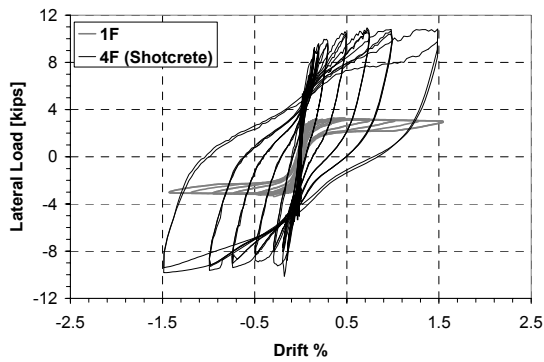
a) FRP Rehabilitated Pier



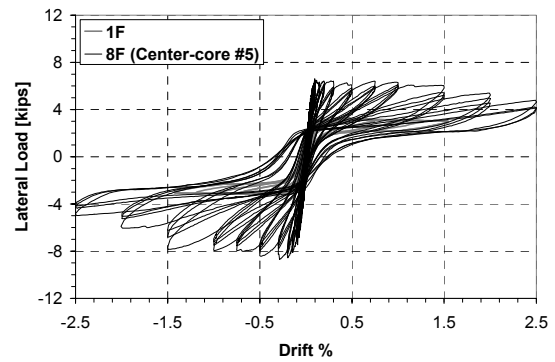
d) Center-Core #3 Rehabilitated Pier



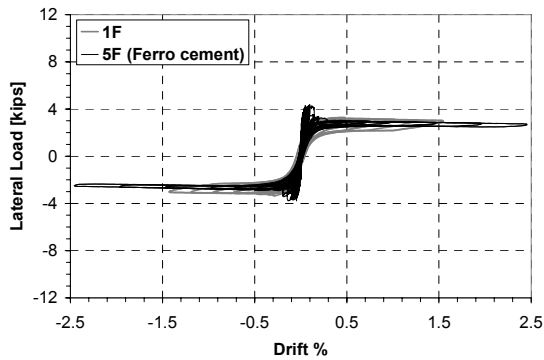
b) Shotcrete Rehabilitated Pier



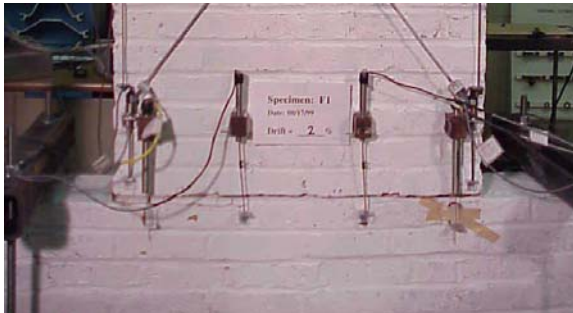
e) Center-Core #5 Rehabilitated Pier



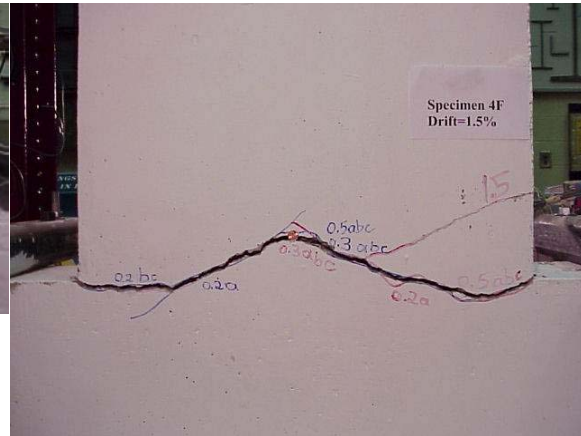
c) Surface Coating Rehabilitated Pier

**Figure 4-8. Force-deflection comparison for rehabilitated specimens**

a) Non-Rehabilitated Pier



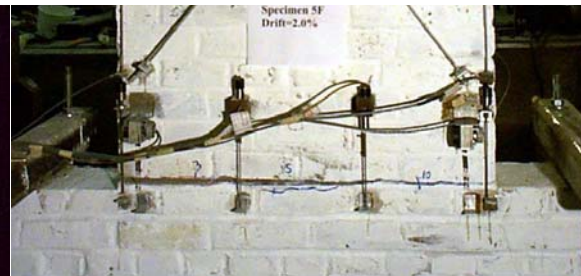
c) Shotcrete Rehabilitated Pier



b) FRP Rehabilitated Pier



d) Surface Coating Rehabilitated Pier



e) Center-Core Rehabilitated Pier



Figure 4-9. Damage photos at the end of testing

Chapter 5. SUMMARY AND CONCLUSIONS

5.1 Summary

5.1.1 Objectives of the Study

The objective of this research project was to investigate the performance of URM piers subjected to in-plane loading. More specifically, this investigation studied the changes in response for masonry piers with varying amounts of vertical applied force and different types of rehabilitations applied to the piers. Another objective of this study was to verify the methods of analysis for seismic rehabilitation of masonry structural components set forth in FEMA 356.

5.1.2 Summary of Experimental Work

Eight URM shear walls of equal dimensions and material were constructed, rehabilitated in some cases, and tested to failure by imposing predefined static reversals of lateral drift. The test specimens represented the lower half of a slender masonry pier subjected to constant vertical force from higher floors of the building. Three of the specimens were non-rehabilitated and were each tested using different axial compressive forces. This test protocol allowed a detailed investigation of the effects of axial stress on the non-linear deformation of slender URM walls. The remaining five specimens were rehabilitated using shotcrete, FRP, surface coating or Center-core. The rehabilitated specimens were all tested at the same axial stress to permit comparison of each individual rehabilitation method. The non-rehabilitated pier with the same applied axial force acted as the control specimen and basis for comparison of the effectiveness of each of the rehabilitations.

5.2 Conclusions

5.2.1 Behavior of Non-rehabilitated Piers

The three non-rehabilitated piers were tested with different levels of applied axial compressive force. The piers with light and medium levels of applied compressive force were expected to behave in a rocking fashion, while the pier tested with a heavy applied axial force was expected to exhibit toe-crushing as the limiting mechanism. The pier with heavy applied force did not toe-crush, so it was tested again at an even higher level of applied axial compressive force. The following conclusions were drawn from the measured behavior of the non-rehabilitated pier tests.

- Rocking is observed to be a stable mechanism capable of in-plane drifts of not less than 1.5 percent.
- The strength and stiffness of non-rehabilitated piers is accurately estimated using current engineering principles and FEMA 356.
- The measured deformation capacity of non-rehabilitated piers behaving in a rocking manner is much greater than that estimated by FEMA 356.
- The transition from a deformation-controlled element to a force-controlled element is conservatively estimated by FEMA 356. The pier with heavy axial force was expected to toe-crush when it actually rocked. Toe-crushing was not observed until the applied axial force was increased substantially beyond the level estimated by FEMA 356.
- Out-of-plane instabilities are more likely in piers with increased levels of axial compressive stress. Local crushing of the masonry and amplification of any out-of-plumb construction existing in the pier bring about this trend. Such instabilities are restrained in a conventional building system where walls are placed along both principal axes.
- FEMA 356 provides an accurate estimate of the IO performance level for non-rehabilitated piers. The observed damage to the piers meets the description provided by FEMA 356, and the strength and ductility ratios match well with the measured response.
- The LS and CP performance level estimates provided by FEMA 356 are overly conservative. The observed damage to the piers is not as severe as

that described by the *Guidelines*. It should be noted that FEMA 356 estimates the performance of an entire building system by the behavior of individual masonry piers. This results in the damage to a primary structural element being much less severe than the performance level assigned to the system because it is assumed that other non-structural elements will be damaged more severely.

- Damage to a rocking pier is confined to the immediate bed-joint where cracking takes place. This crack closes almost completely after the seismic excitation ceases, and little repair is necessary.

5.2.2 Behavior of Rehabilitated Piers

Four types of rehabilitation were applied to the remaining test piers. Each provided different modifications to the behavior of the non-rehabilitated pier. The rehabilitated piers included FRP, Shotcrete, Ferro-cement surface coating, and two different sizes of rebar embedded in the pier using the Center-core technique. The following conclusions were deduced from the tests of the rehabilitated masonry piers.

- The FRP rehabilitated specimen softened as the lateral force increased to a point at which the composite fully delaminated from the surface of the masonry causing an abrupt loss of capacity.
- The shotcrete rehabilitated specimen behaved as a reinforced concrete pier with no evidence of composite action with the masonry. Large amounts of energy were dissipated as the rebars yielded repeatedly. The plastic deformation of the rebar caused the pier to tilt out of plane, thus stopping the test. Shotcrete is an effective rehabilitation method because of the large deformation capacity and the energy dissipated through steel yielding.
- The surface-coating rehabilitated pier exhibited a similar force-deflection relationship to that of the plain wall with the exception of a slight increase in strength of the initial linear portion of the force-deflection curve. Once the steel hardware mesh fractured, the rocking behavior returned and provided large deformation capacity. Ferro-cement surface coating is effective at increasing the shear stiffness and possibly the strength capacity. However, its contribution to the flexural strength and energy dissipation is limited to the poor ductility of light gage wire.

- The success of the center-core technique is heavily dependent on providing adequate anchorage to the reinforced cores. Center-core provides a moderate increase in the flexural strength of the pier and moderate energy dissipating qualities. The center-core rehabilitation provided no increase in the deformation capacity of the piers. The aesthetic properties of the wall are not altered by the center-core method of rehabilitation. The Center Core rehabilitated pier benefited from the presence of the reinforcing bars; however, an embedment length of 40 bar diameters was not sufficient to anchor the core. The core proceeded to slip in its cavity such that the rebar did not yield.
- Strength and stiffness estimates for rehabilitated masonry piers may be accurately calculated if the stress-strain behaviors of the constituent materials are known.
- The deformation capacity of the rehabilitated piers (excluding FRP) is much greater than that estimated by FEMA 356.
- The strength of the rehabilitated piers is usually over-estimated by current engineering practice. This is most likely a result of inadequate nature of the sectional response used to calculate the behavior of a rocking pier with the addition of rehabilitation elements.
- FEMA 356 suggested m-factors reasonably represent actual loading conditions even though they are many times smaller than the measured ductility ratio of the piers. This is because the overestimate of the strength balances the underestimate of the ductility.
- Strength enhancements of a factor of two are noted for each of the rehabilitation methods except surface coating.
- The deformation capacity was diminished (as compared to the non-rehabilitated pier) for each of the rehabilitation methods except surface coating.
- The effectiveness of shotcrete, surface coating and Center-core rehabilitated piers all are roughly equal to that of the non-rehabilitated pier. Effectiveness is measured by the increase in the product of mQ_{CE} as compared to that of the non-rehabilitated pier.
- The best approach to rehabilitation of URM piers and walls may be to do nothing to structural elements expected to behave in a rocking mode and induce rocking if possible in other cases. If rehabilitation is necessary,

shotcrete or Center Core should be the methods of choice; however, cost versus benefits should be explored before any rehabilitation is performed.

5.3 Future Research

The plain URM specimens governed by rocking did not have the lateral capacity and energy dissipation of the shotcrete, but there was very little damage to be repaired and they were capable of larger deformations than the shotcrete. Therefore, from the perspective of performance based design, the best option may be to maintain the behavior of piers governed by rocking, or alter the aspect ratio of wider piers to induce this mechanism. Center-core is a viable rehabilitation technique, although more study is needed to examine the anchorage problems observed during this testing program.

These findings need to be corroborated with further research to justify the large m factors that were assigned to rocking piers for this project. This should preferably be tested in a structural system where the interaction of the diaphragm and the out-of-plane walls on rocking piers can be investigated.

There is a particular need to assess the effect of three directional accelerations on the permissible drift limits. In this project, the only applied force to simulate earthquake acceleration was in-plane, but the effect of simultaneous in-plane, out-of-plane and vertical accelerations needs to be investigated. The permissible in-plane drift limits could be seriously jeopardized if out-of-plane accelerations tended to rotate a rocking wall off the base or if vertical motion reduces rocking capacity. These potential problems could not be investigated in this experiment, but are crucial to the allowable deformation capacity of the in-plane walls.

REFERENCES

1. Abrams, D. P. "Strength and Behavior of Unreinforced Masonry Elements", *Proceedings of Tenth World Conference on Earthquake Engineering*, pp. 3475-3480 July 1992, Madrid.
2. Abrams, D. P., Shah, N., "Cyclic Testing of Unreinforced Masonry Walls", *Advanced Construction Technology Center*, Report No. 92-26-10, University of Illinois, Dec. 1992.
3. Abrams, D. P., "A Set of Classnotes for a Course in: Masonry Structures", The Masonry Society. 2000, Boulder.
4. Alcocer, S. M., Ruiz, J., Pineda, A., and Zepeda, J. A., "Retrofitting of Confined Masonry Walls with Welded Wire Mesh", *Proceedings of Eleventh World Conference on Earthquake Engineering*, 1996, Mexico.
5. Breiholz, D. C., "CenterCore Seismic Hazard Reduction System for URM Buildings", *Proceedings of Tenth World Conference on Earthquake Engineering*, July 1992, Madrid.
6. Calvi, G. M., Kingsely, G. R., and Magenes, G., "Testing of Masonry Structures for Seismic Assessment", *Earthquake Spectra*, Vol. 12, No. 1, pp. 145-162, Feb. 1996.
7. Ehsani, M. R., and Saadatmanesh, H., "Seismic Retrofitting of URM Walls With Fiber Components", *The Masonry Society Journal*, Vol. 14, No. 2, Dec. 1996.
8. Epperson, G. S. and Abrams, D.P., "Nondestructive Evaluation of Masonry Buildings.", *Advanced Construction Technology Center*, Report No. 89-26-03, University of Illinois, Oct. 1989.
9. FEMA 356: "Prestandard and Commentary for the Seismic Rehabilitation of Buildings", Federal Emergency Management Agency, 2000.
10. Heyman, J., *The Stone Skeleton*, Cambridge: Cambridge UP, 1995.
11. Hays, W., Chaker, A., Hunt, C., "Learning From Disaster", *Civil Engineering Magazine*, ASCE, Dec. 1999.
12. Hutchinson, D.L., Yong, P. M. F., and McKenzie, G. H. F., "Laboratory Testing of a Variety of Strengthening Solutions for Brick Masonry Wall Panels", *Proceedings of Eighth World Conference on Earthquake Engineering*, Vol. 1, pp. 575-582, 1984, San Francisco.
13. Kahn, L. F., "Shotcrete Retrofit For Unreinforced Brick Masonry", *Proceedings of Eighth World Conference on Earthquake Engineering*, Vol. 1, pp. 583-590, 1984, San Francisco.
14. Kahn, L. F., "Shotcrete Strengthening of Brick Masonry Walls", *Concrete International*, pp. 34-40, July 1984.
15. Lizundia, B., Holmes, W. T., Longstreth, M., Kren, A. (Rutherford & Chekene), and Abrams, D. P. (University of Illinois), "Development of Procedures to Enhance the Performance of Rehabilitated URM Buildings", *NIST Contract NO. 50SBN5C8622*, March 1997.
16. Magenes, G., and Calvi, G.M., "In-plane Seismic Response of Brick Masonry Walls", *Earthquake Engineering and Structural Dynamics*, Vol. 26, pp.1091-1112, 1997.
17. Masonry Standards Joint Committee (MSJC), *Code, Specifications and Commentaries*, 1999.

18. McNary W. S., and Abrams D. P., "Mechanics of Masonry in Compression", *Journal of Structural Engineering*, Vol. 111, No. 4, pp. 857-870, April 1995
19. "NEHRP Guidelines for the Seismic Rehabilitation of Buildings", *Federal Emergency Management Agency Document No. 273*, Oct. 1997, Washington D. C.,
20. "NEHRP Commentary on the Guidelines for the Seismic Rehabilitation of Buildings", *Federal Emergency Management Agency Document No. 274*, Oct. 1997, Washington D. C.
21. Nunan, W. L., Goel, S. C., and Rai, D. C., "Seismic Strengthening of Unreinforced Masonry Buildings using Steel Bars and Tendons Embedded in Ferrocement Strips", *Earthquake Hazard Mitigation Program Grant No. CMS9422010*, University of Michigan, Aug. 1996.
22. Oliveira, F. L., and Hanai, J. B., "Strengthening and Repair of Masonry Walls with Ferrocement Overlays", *Sixth International Symposium on Ferrocement*, June 1998, Ann Arbor, Michigan.
23. Reinhorn, A. M., and Madan, A., "Evaluation of TYFO W Fiber Wrap System For in-plane Strengthening of Masonry Walls", *Report NO. AMR 95-0002*, State University of New York at Buffalo, Aug. 1995.
24. Reinhorn, A., Prawel, S.P., and Jia, Z.H., "Experimental Study of Ferrocement as a Seismic Retrofit Material for Masonry Walls", *Journal of Ferrocement*, Vol. 15, No. 3, pp. 247-260, July 1985.
25. Tomazevic, M., "Recent Advances in Earthquake-Resistant Design of Masonry Buildings: European Prospective", *Proceedings of Eleventh World Conference on Earthquake Engineering*, 1996, Mexico.
26. Triantafillou, T. C., "Strengthening of Masonry Structures Using Epoxy-Bonded FRP Laminates", *Journal of Composites for Construction*, pp. 96-104, May 1998.

APPENDIX A

Index of Figure Numbers for Appendices B through J

Index of Figure Numbers for Appendices B through J

- x.1 - Hysteretic Response
- x.2 - Backbone Curve
- x.3 - Multi-Linear Force-Deformation Curve
- x.4 - Composite Force-Deformation Curve
- x.5 - Performance Level Acceptance Criteria
- x.6 - Shear Stress versus Shear Strain Response
- x.7 - Crack Width Profile
- x.8 - Comparison of Estimated to Measured LSP Behavior

APPENDIX B

Measured Material Properties

General Setup of Appendix B

Appendix B – Material Properties Data

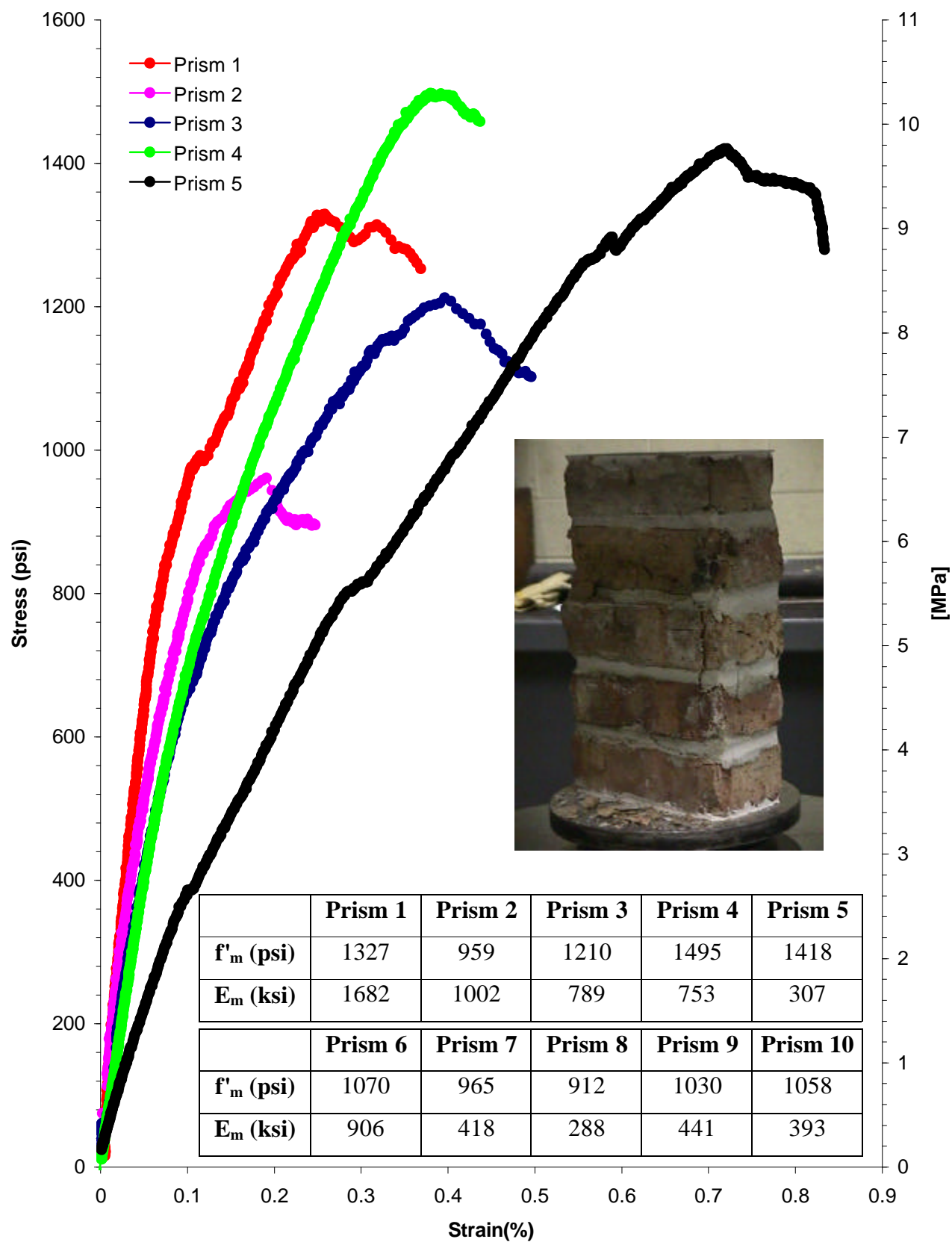
B.1 - Masonry Prism Tests

B.2 - FRP Coupon Tests

B.3 - Steel Hardware Cloth Wire Tests

B.4 - Center Core Cylinder Tests

B.5 - Material Properties Used in Analyses

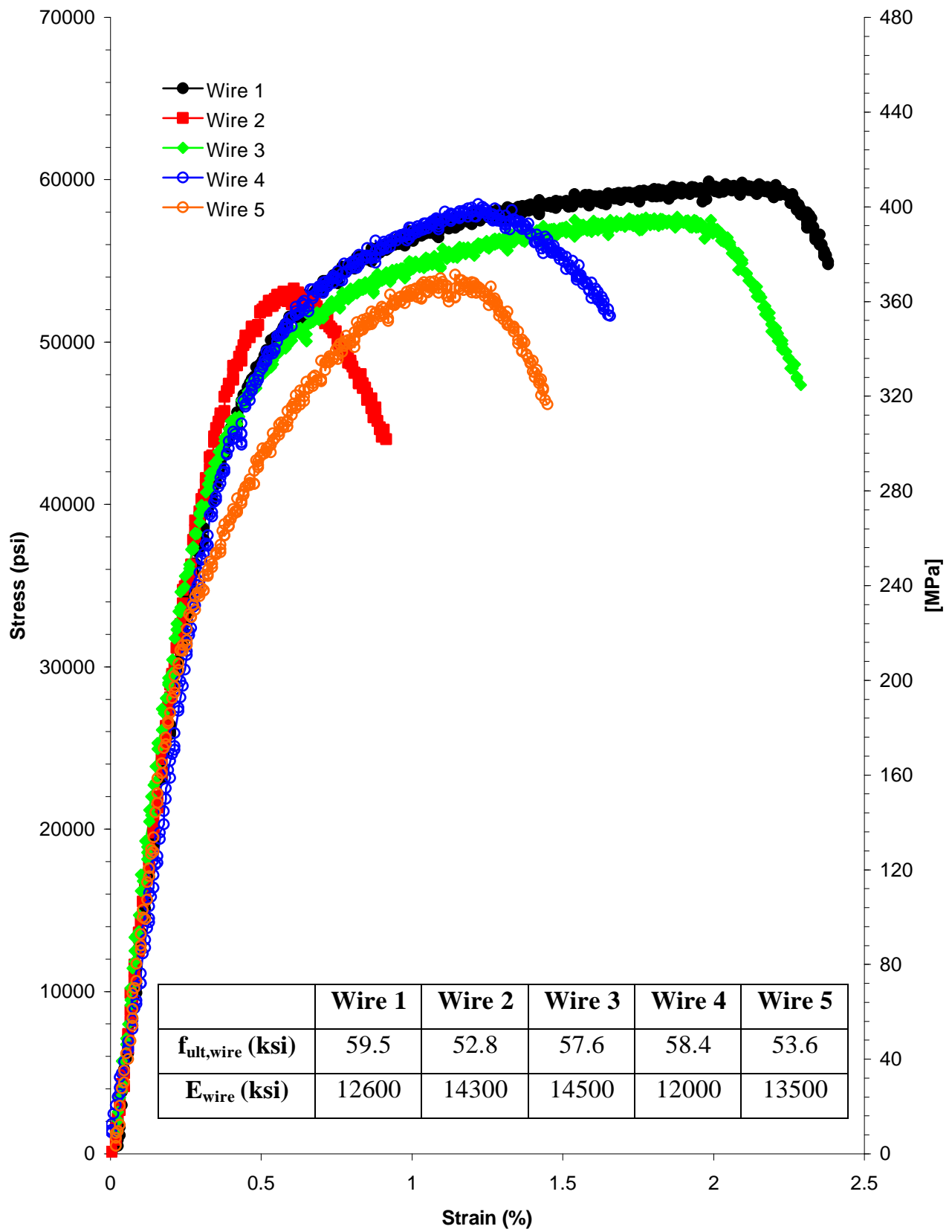


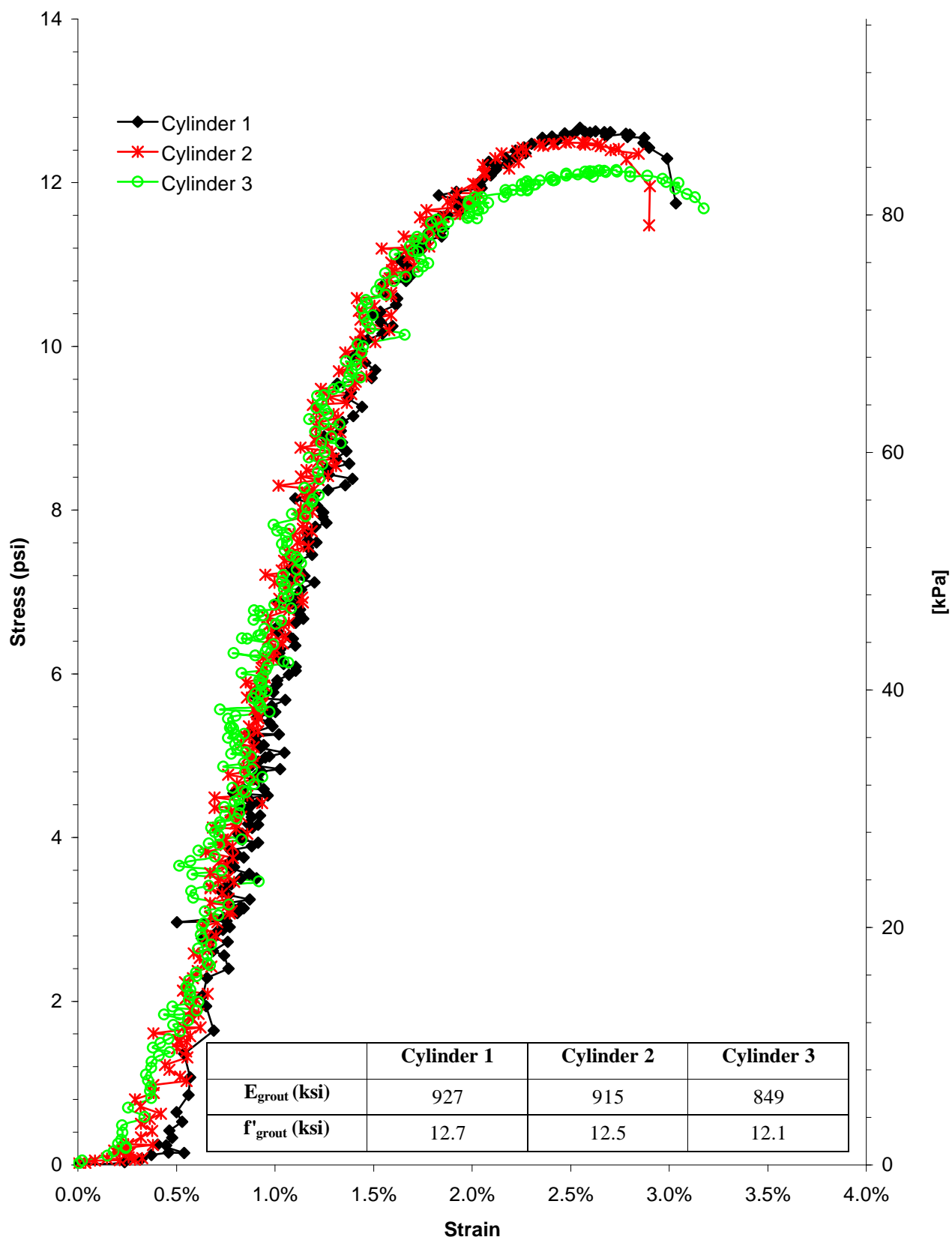
FRP Coupon Material Properties

Glass Fibers; 0 degree orientation; 1 ply		
Coupon No.	Yield Stress (psi)	Modulus of Elasticity (psi)
1	75147	1387993
2	74031	2012774
3	62490	2272027
4	43232	1578374
5	55407	1637949
Average	62061	1777823

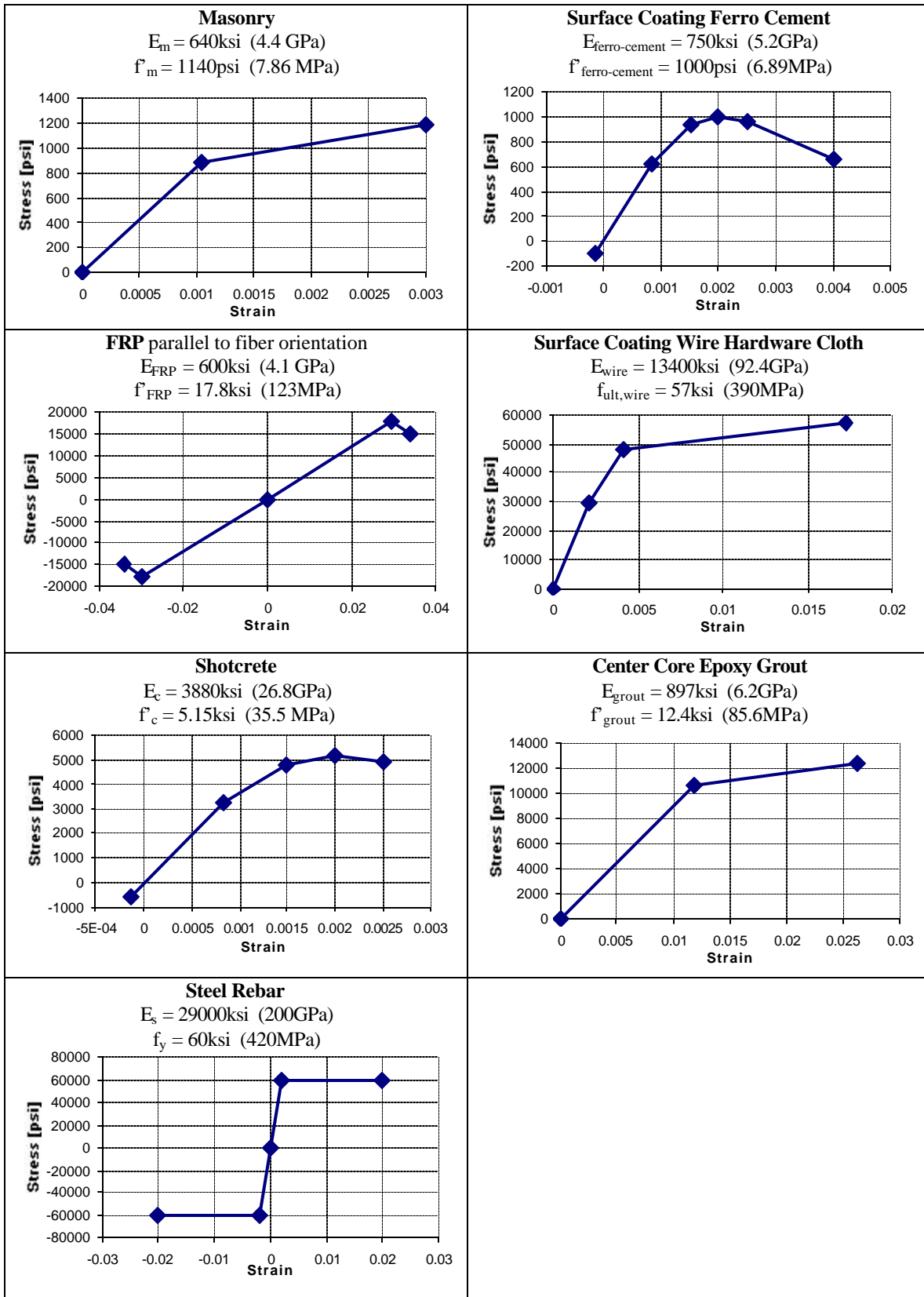
Glass Fibers; 90 degree orientation; 1 ply		
Coupon No.	Yield Stress (psi)	Modulus of Elasticity (psi)
1	3616	1054708
2	4029	920139
3	3879	1109896
4	3430	1138000
5	2111	930335
Average	3413	1030616

FRP Material Property Data





Center Core Cylinder Tests
B.4



Material Properties Used in Analyses

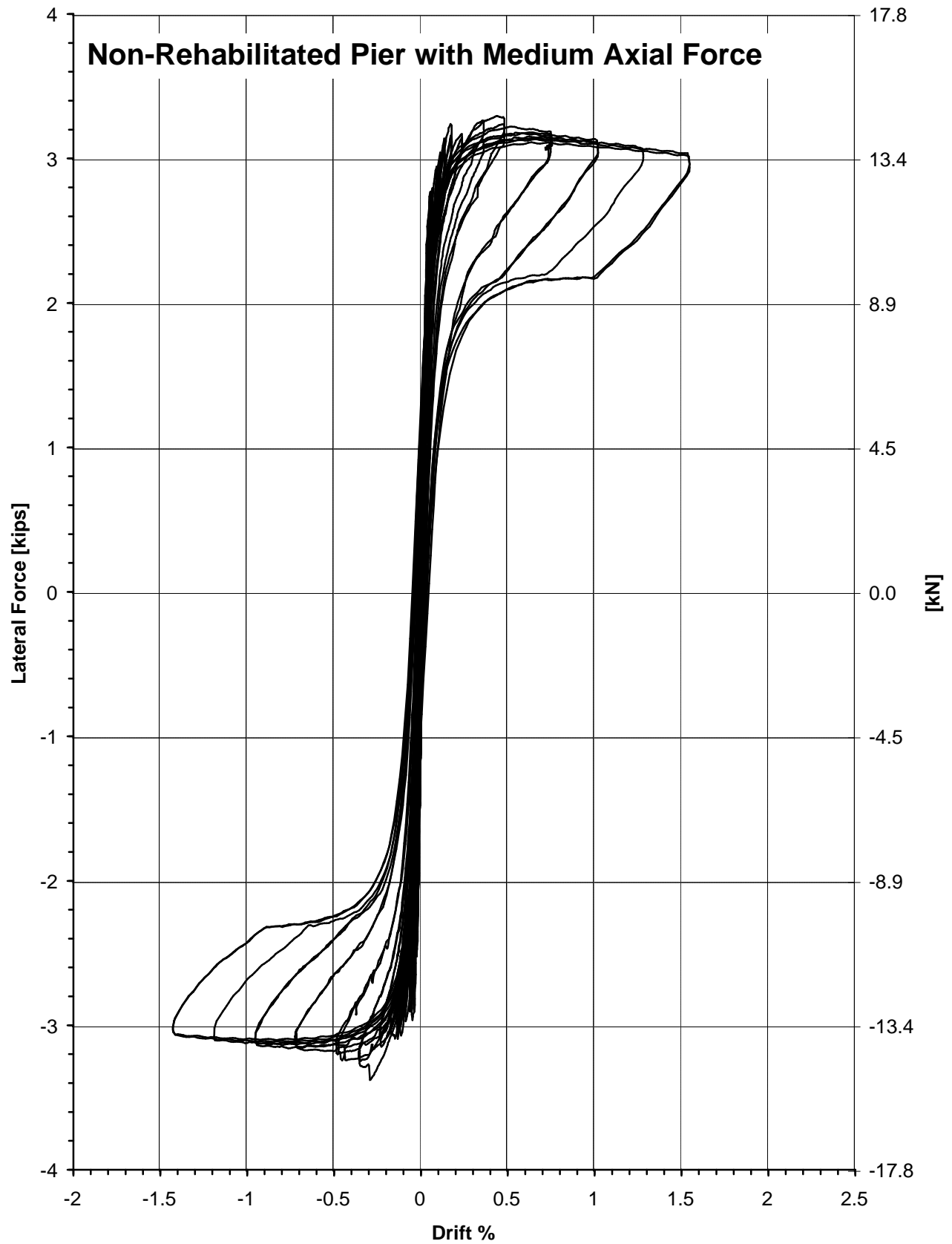


Figure C.1 - Specimen 1F, Hysteretic Response
C.1

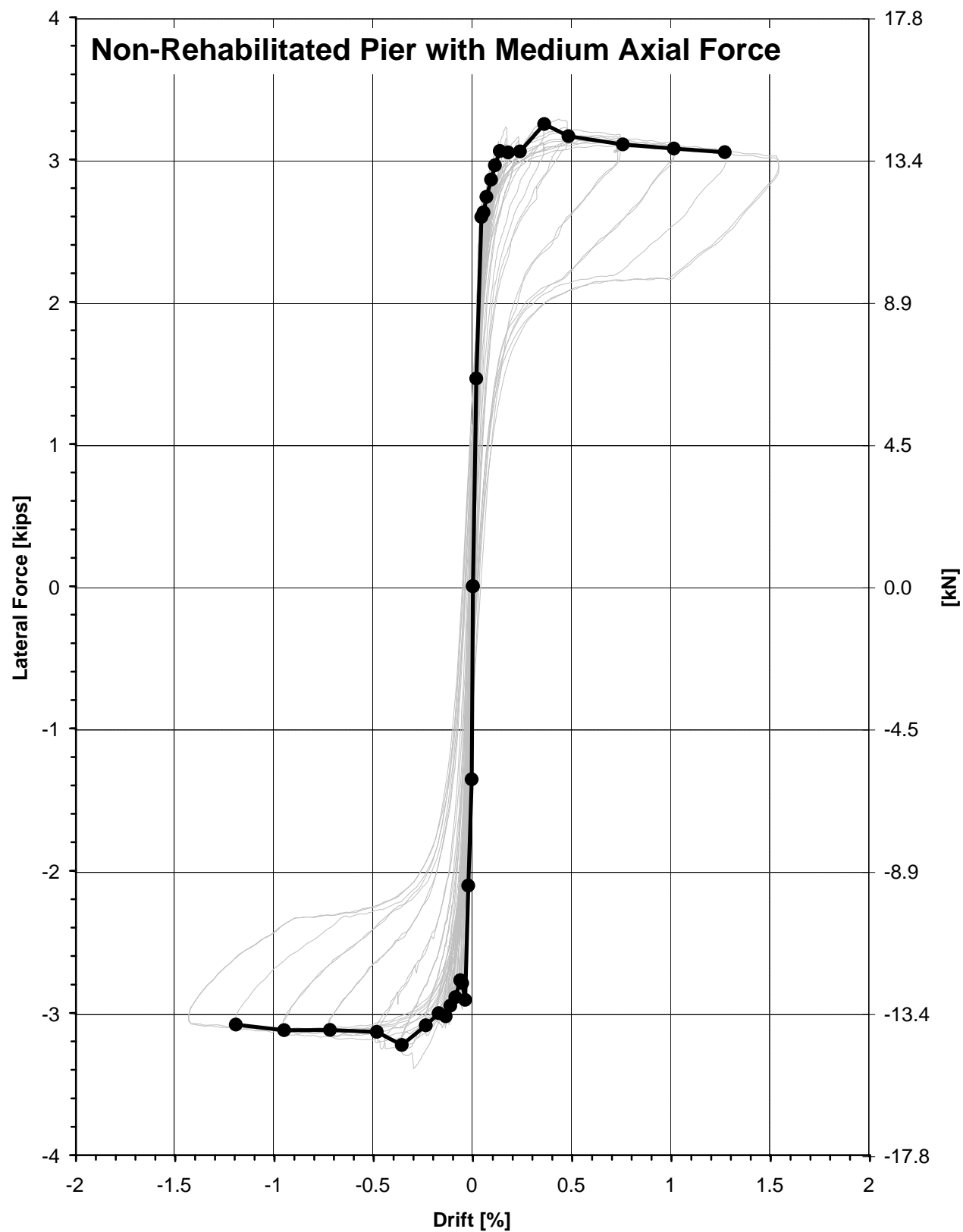


Figure C.2 - Specimen 1F, Backbone Curve
C.2

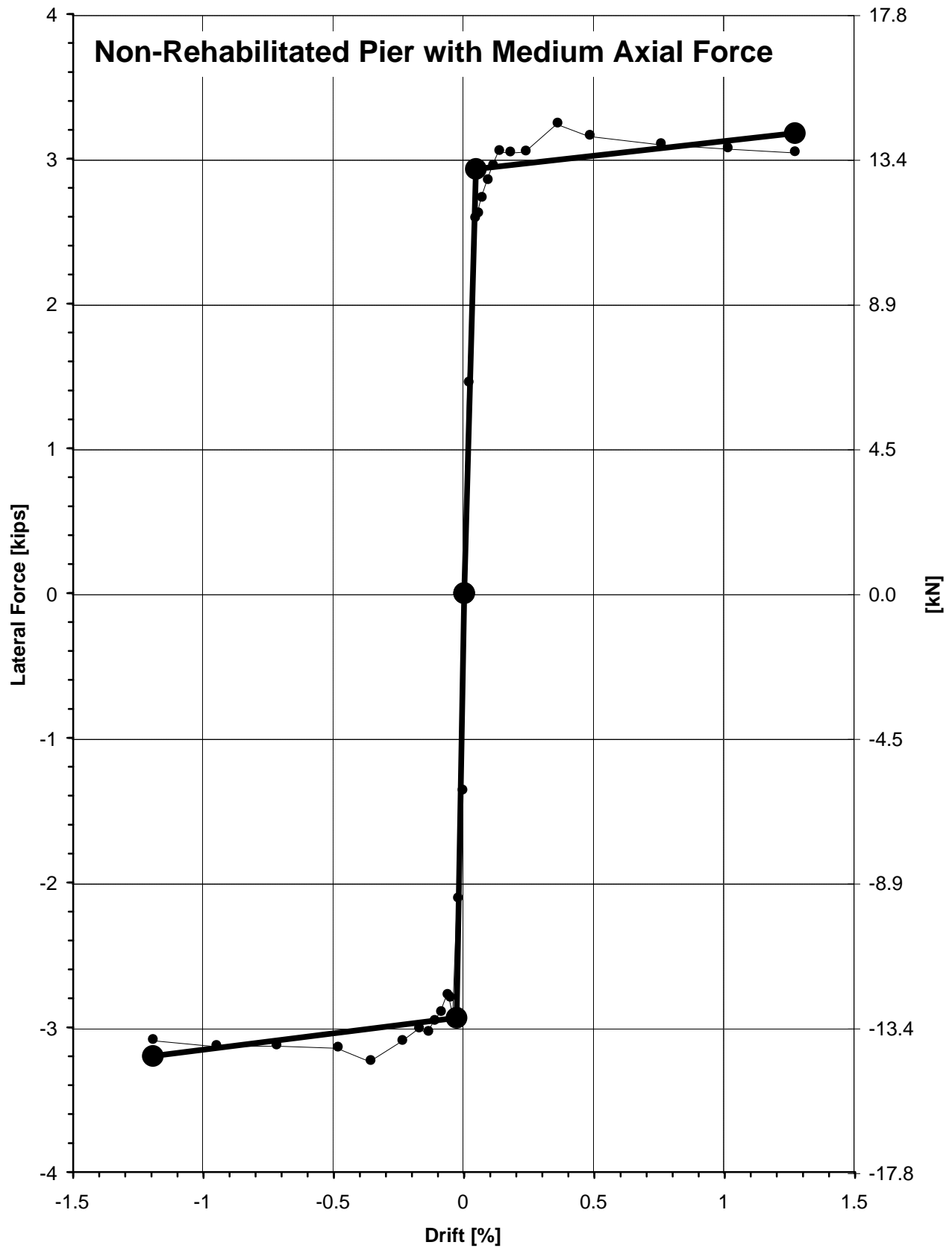


Figure C.3 - Specimen 1F, Multi-Linear Force-Deformation Curve
C.3

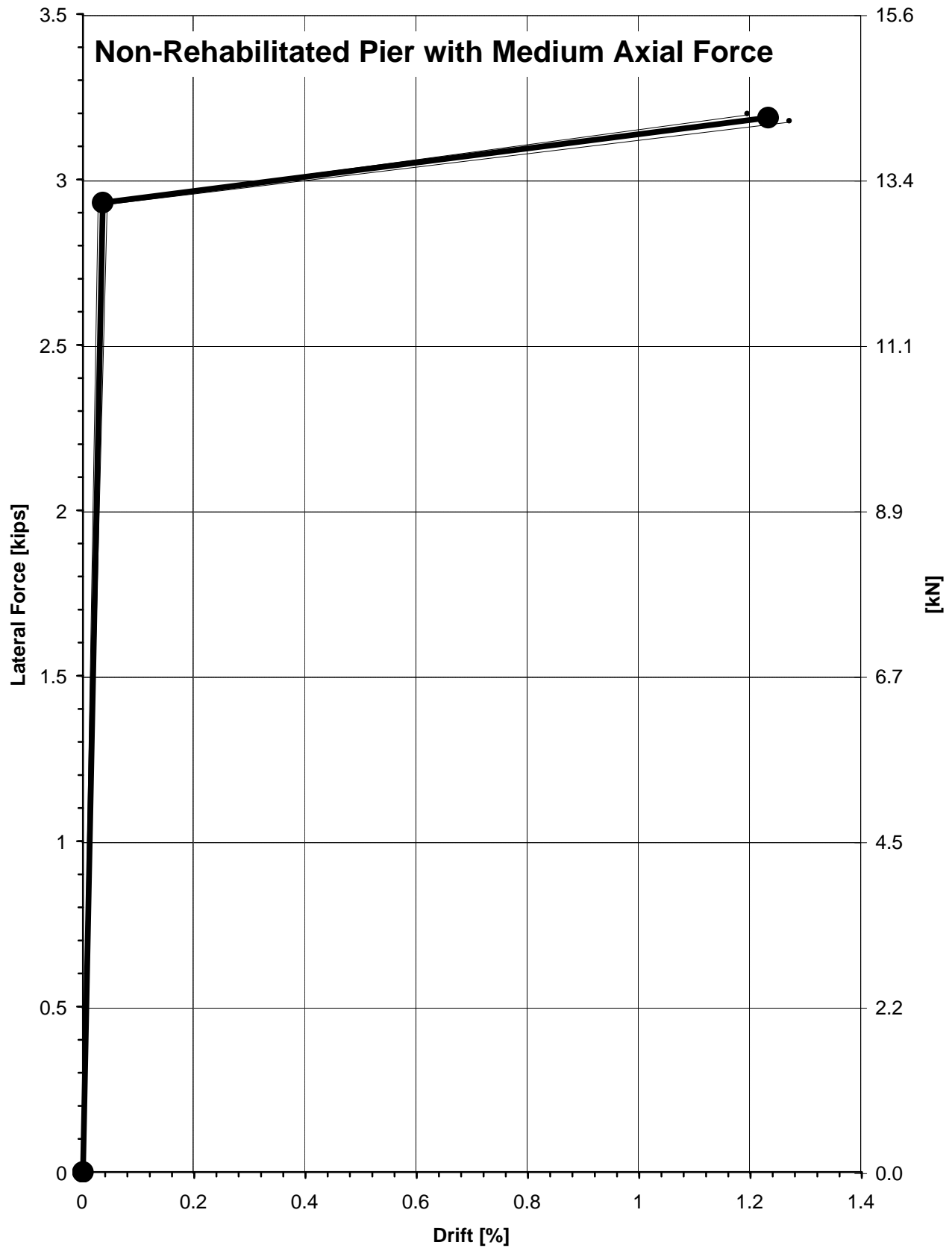


Figure C.4 - Specimen 1F, Composite Force-Deformation Curve
C.4

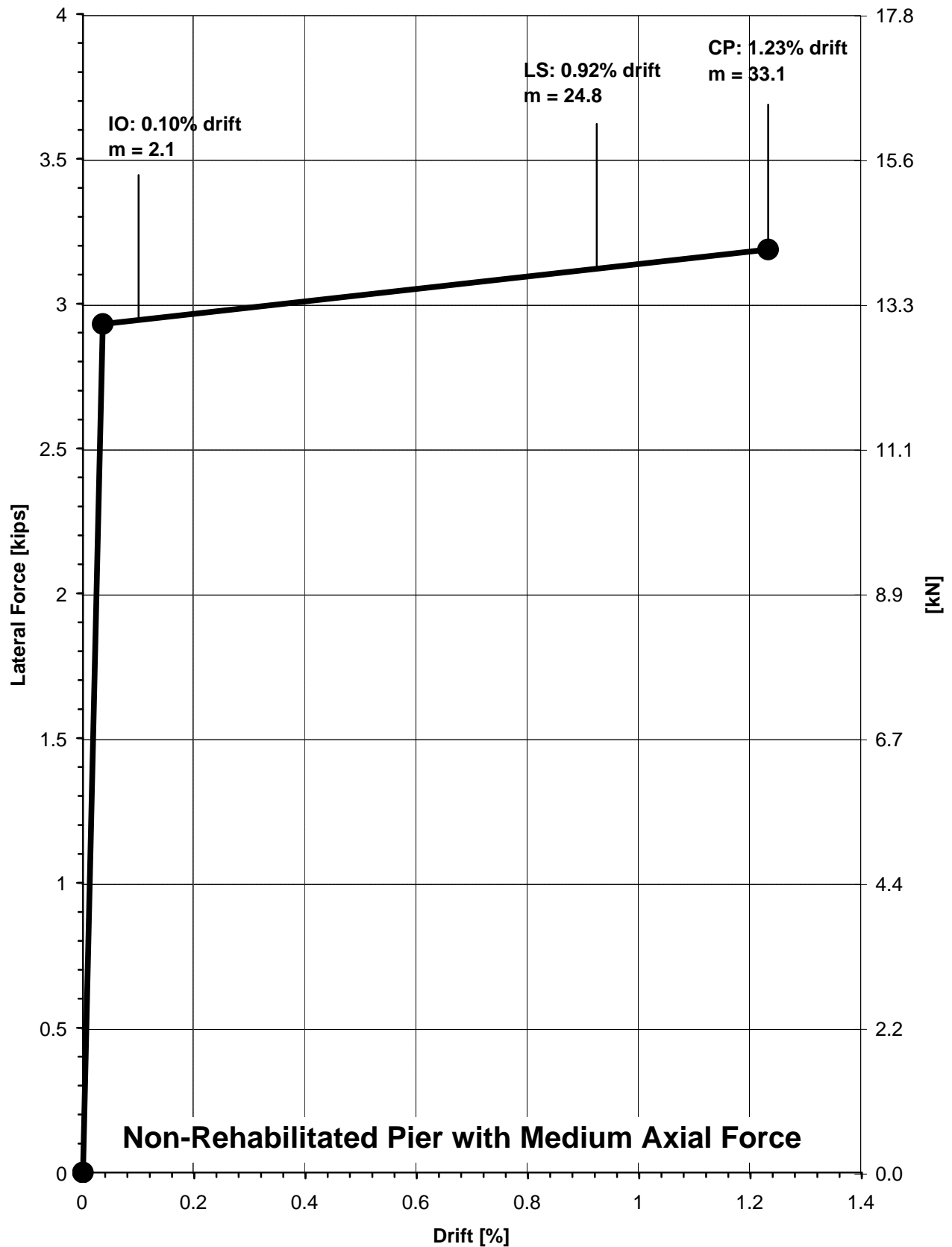


Figure C.5 - Specimen 1F, Performance Level Acceptance Criteria
C.5

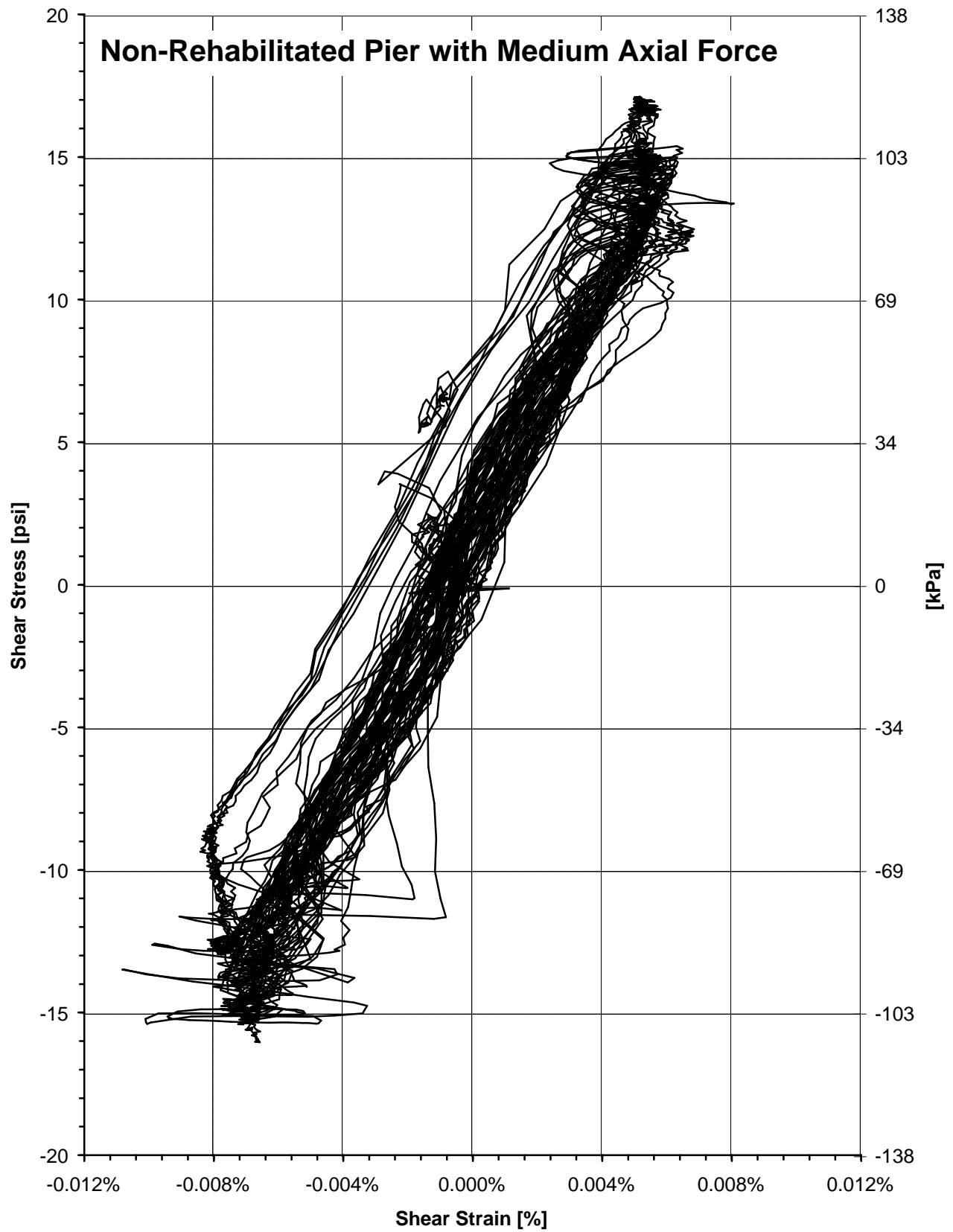


Figure C.6 - Specimen 1F, Shear Stress versus Shear Strain Response
C.6

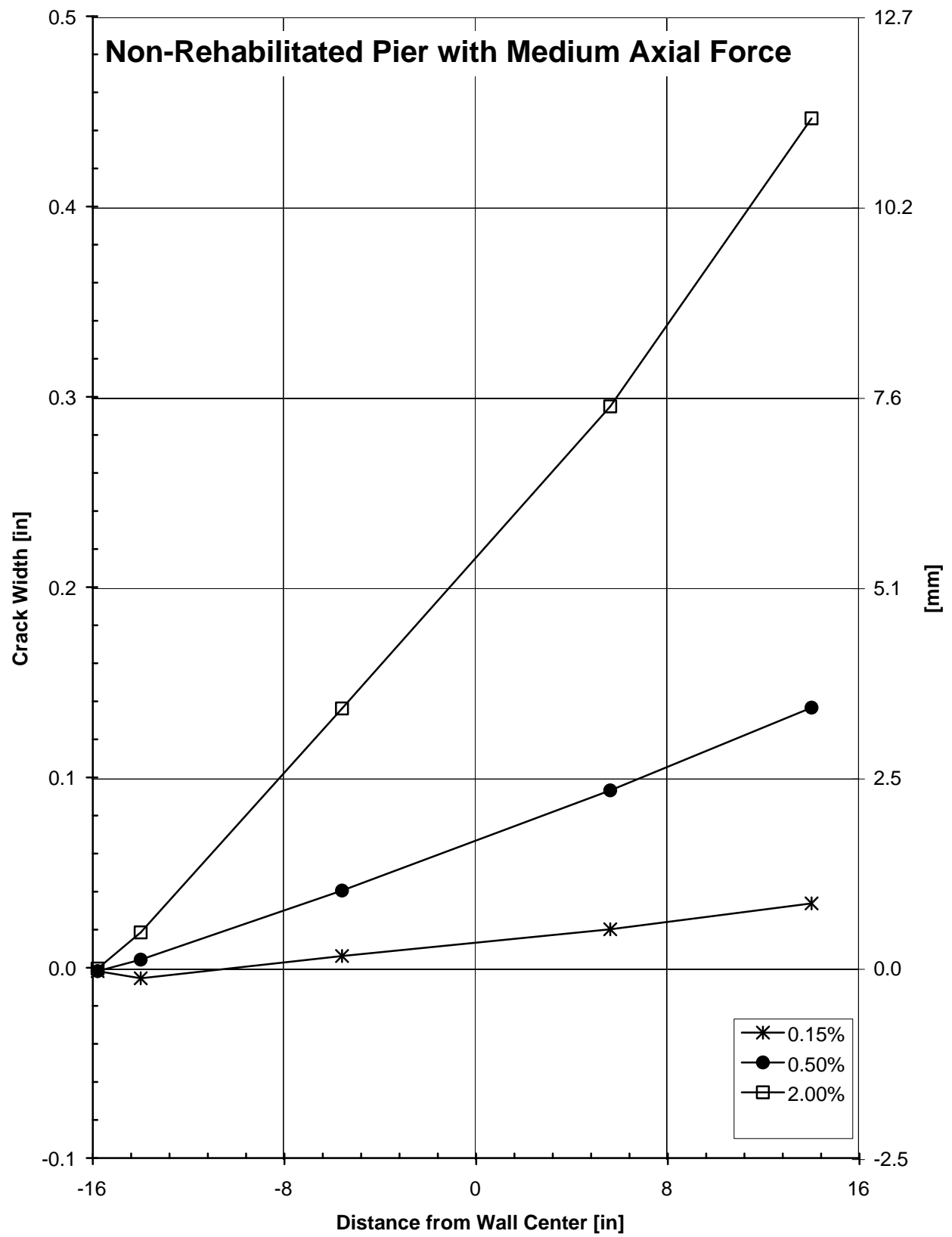


Figure C.7 - Specimen 1F, Crack Width Profile
C.7

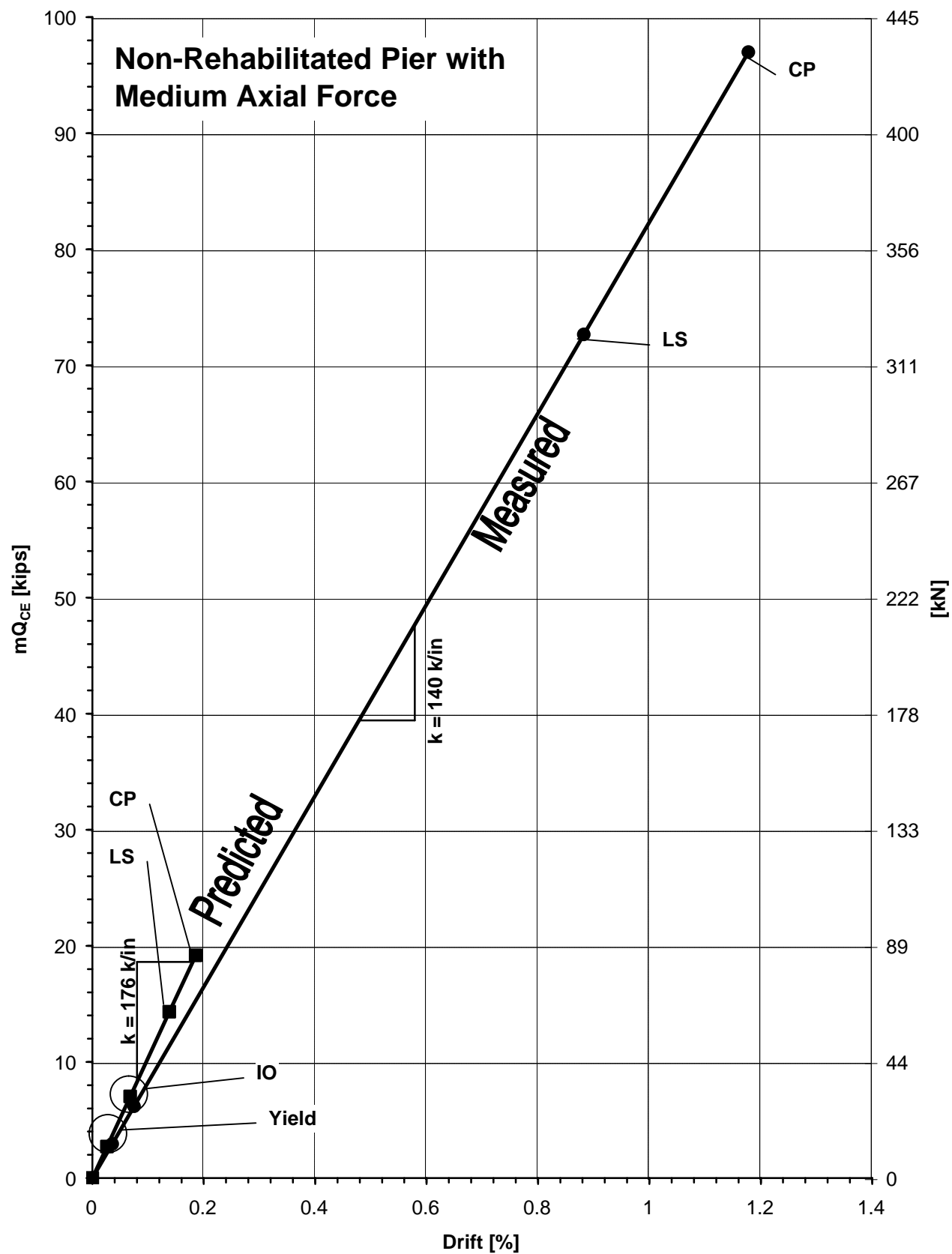


Figure C.8 - Specimen 1F, Comparison of Estimated to Measured LSP Behavior
C.8

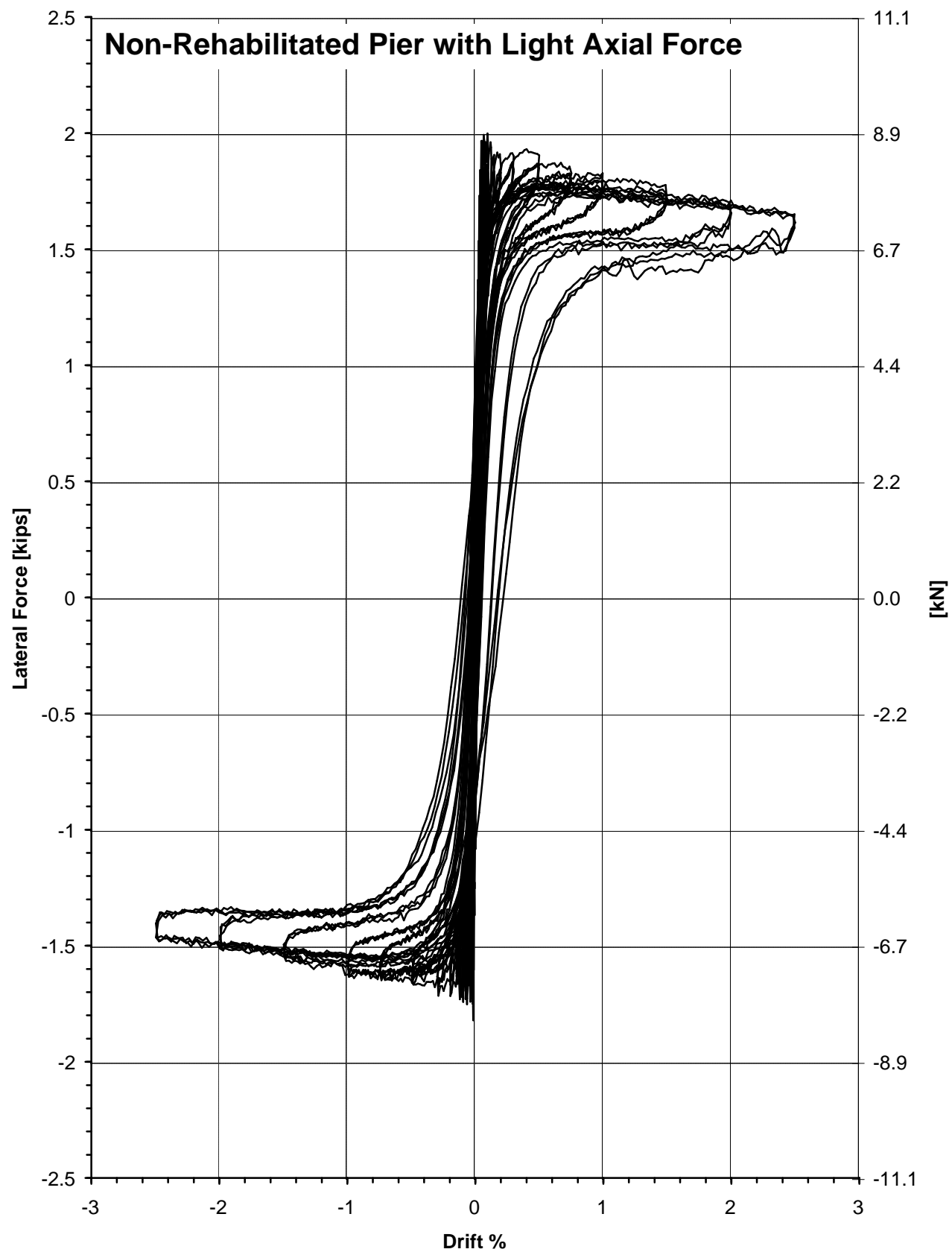


Figure D.1 - Specimen 2F, Hysteretic Response
D.1

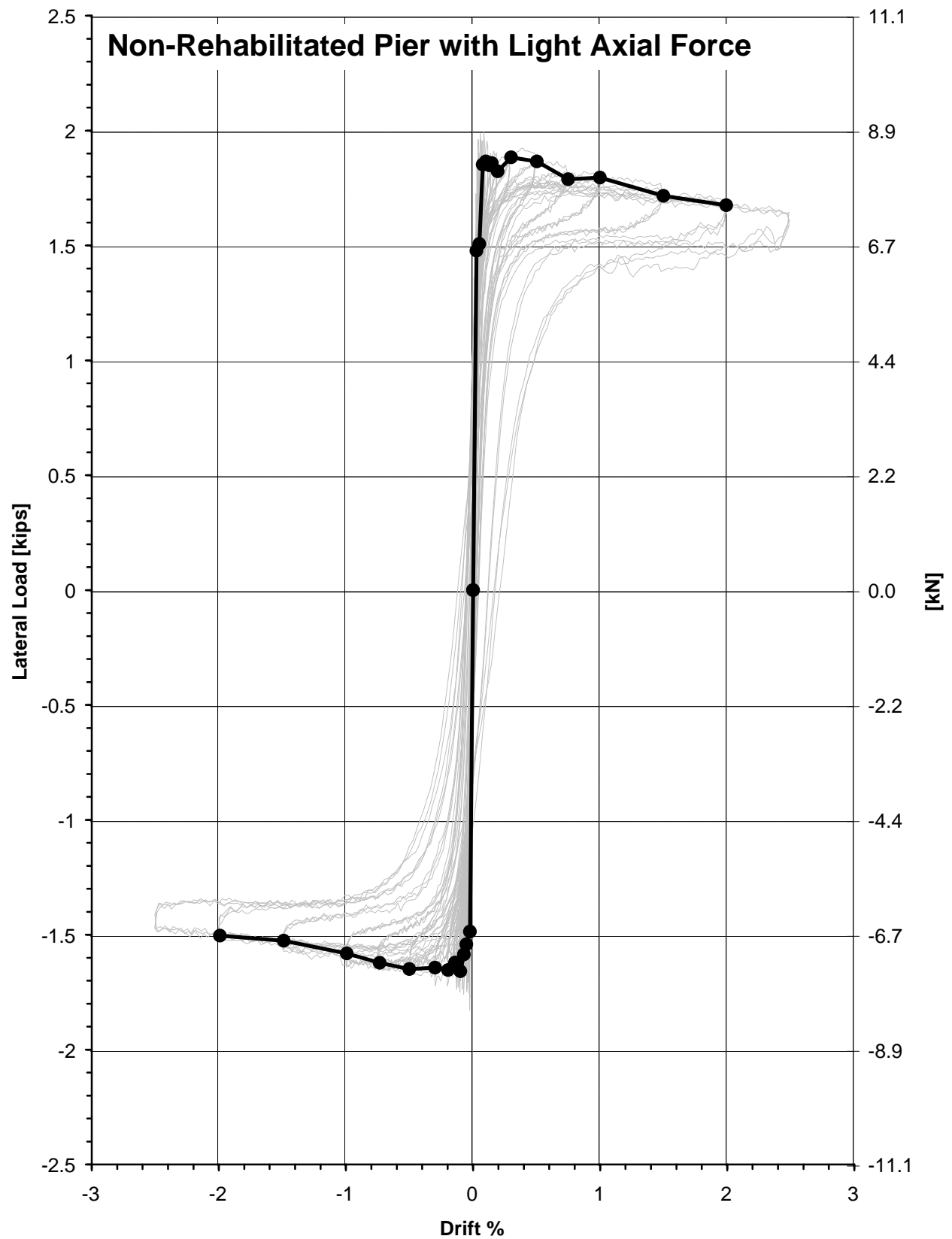


Figure D.2 - Specimen 2F, Backbone Curve
D.2

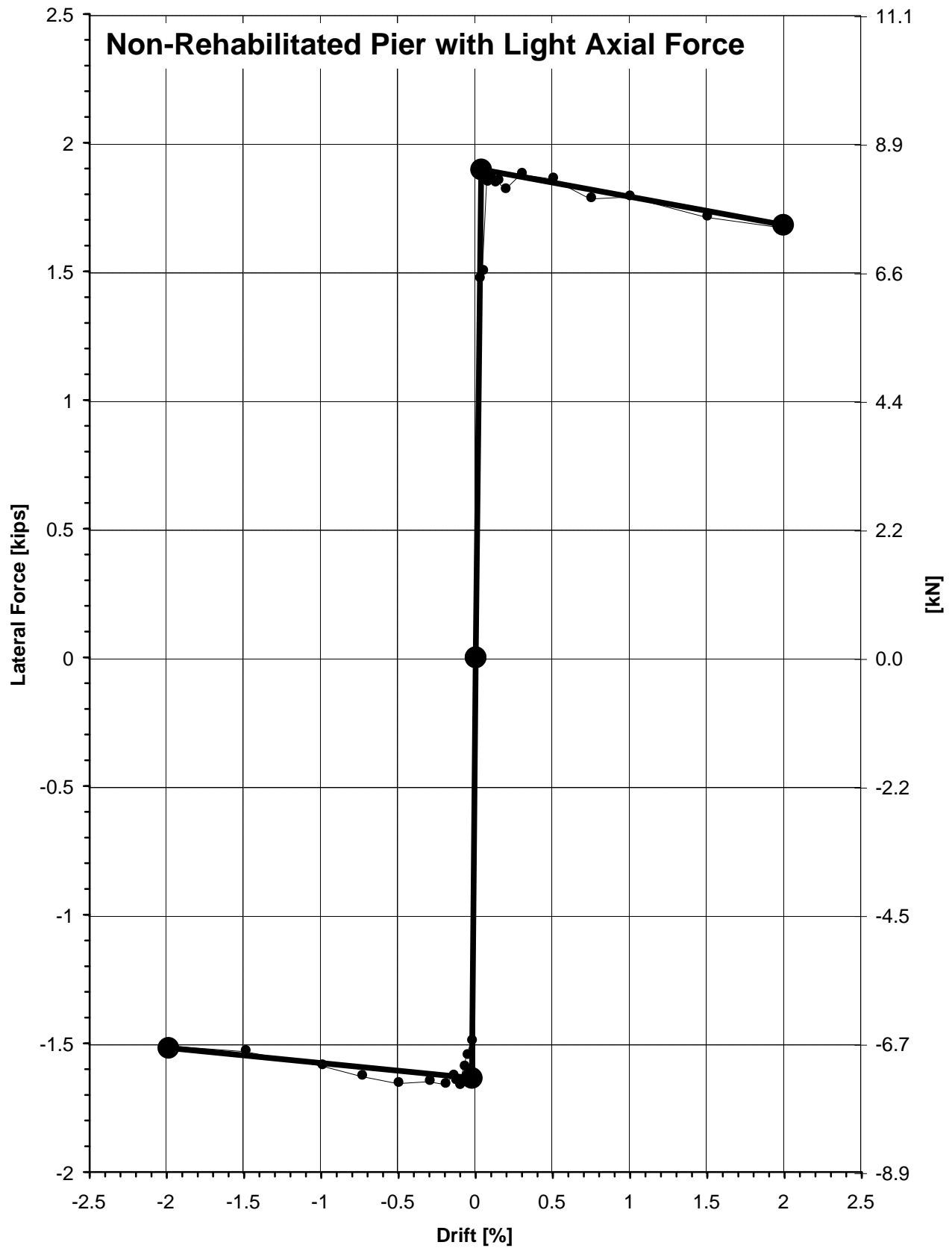


Figure D.3 - Specimen 2F, Multi-Linear Force-Deformation Curve
D.3

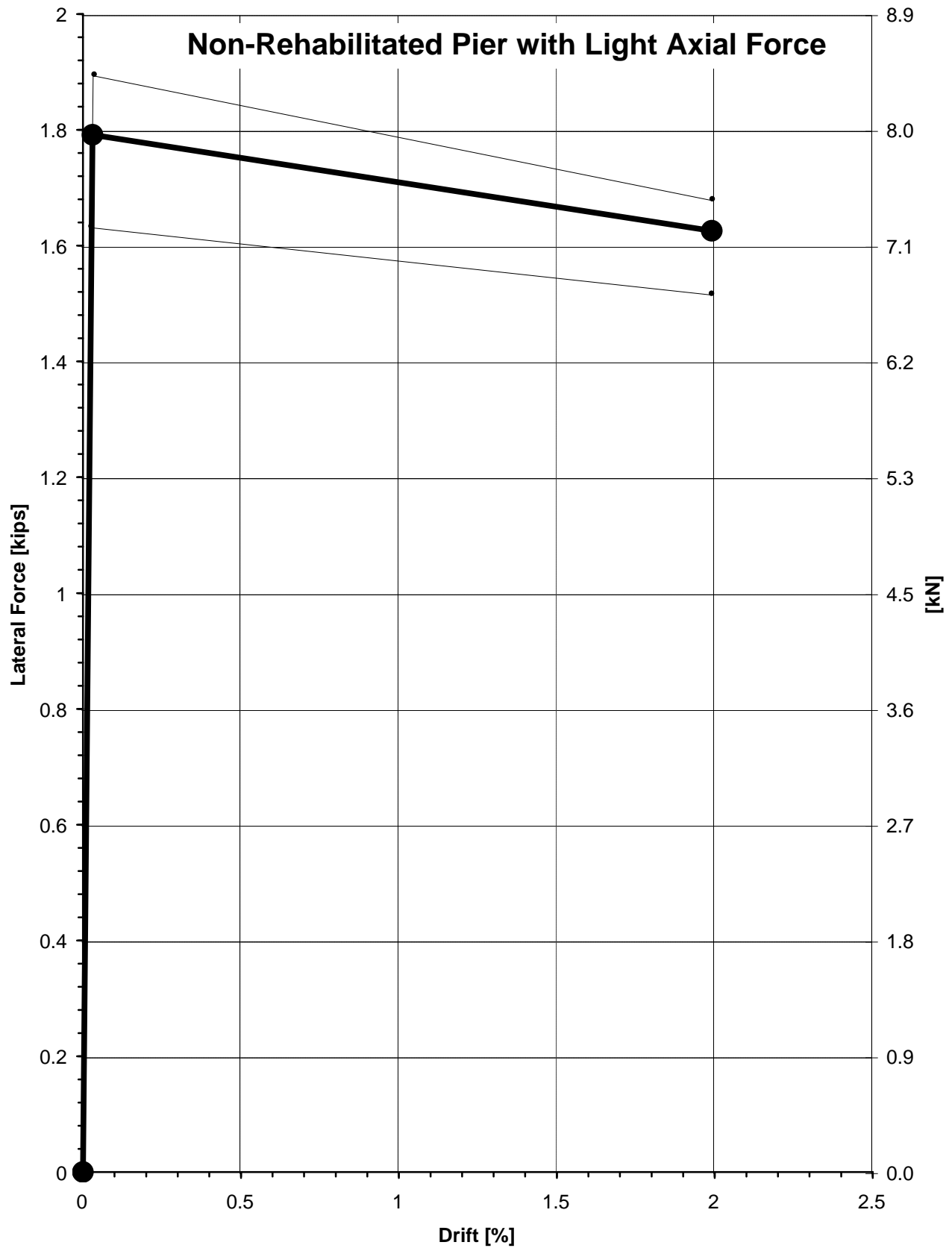


Figure D.4 - Specimen 2F, Composite Force-Deformation Curve
D.4

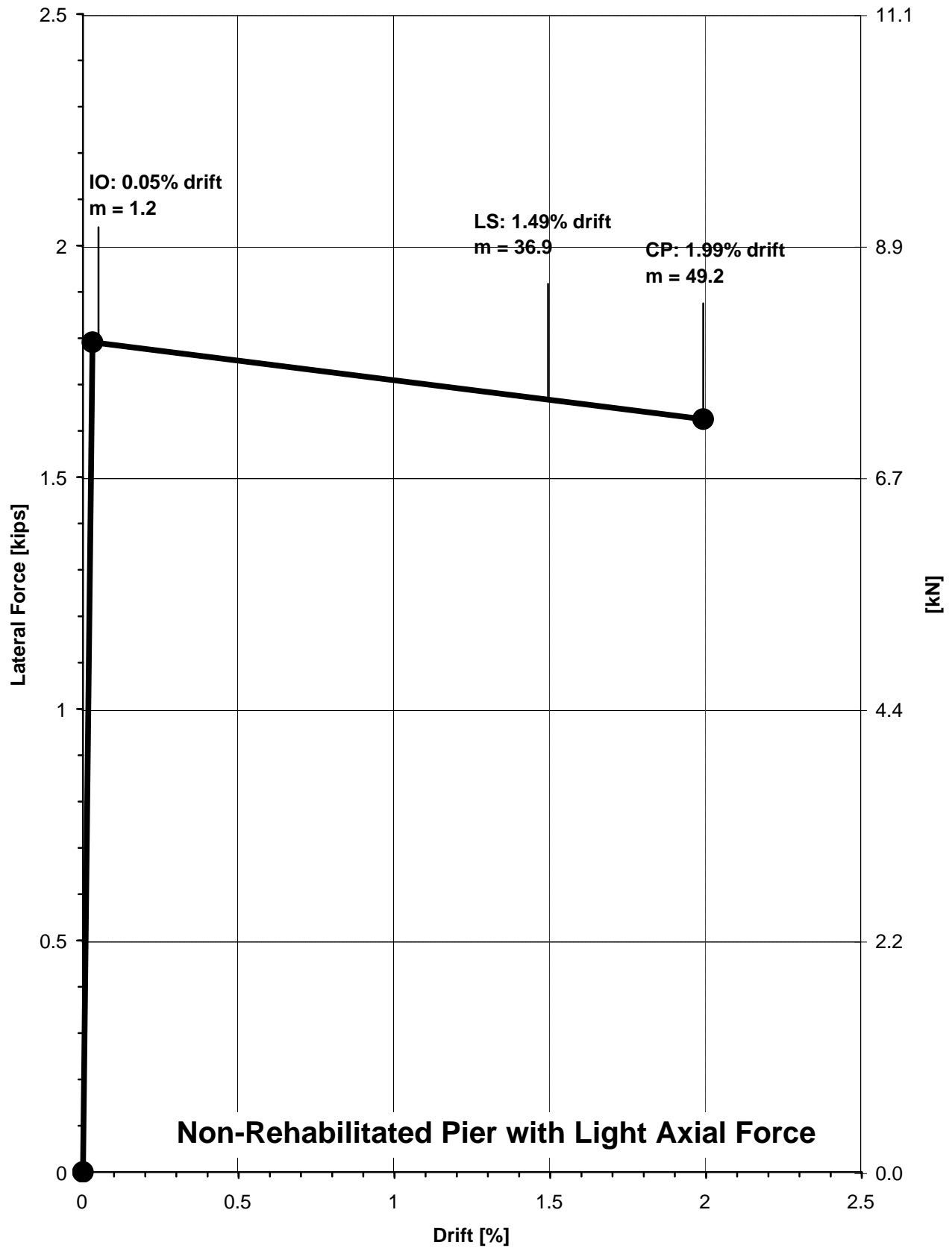


Figure D.5 - Specimen 2F, Performance Level Acceptance Criteria
D.5

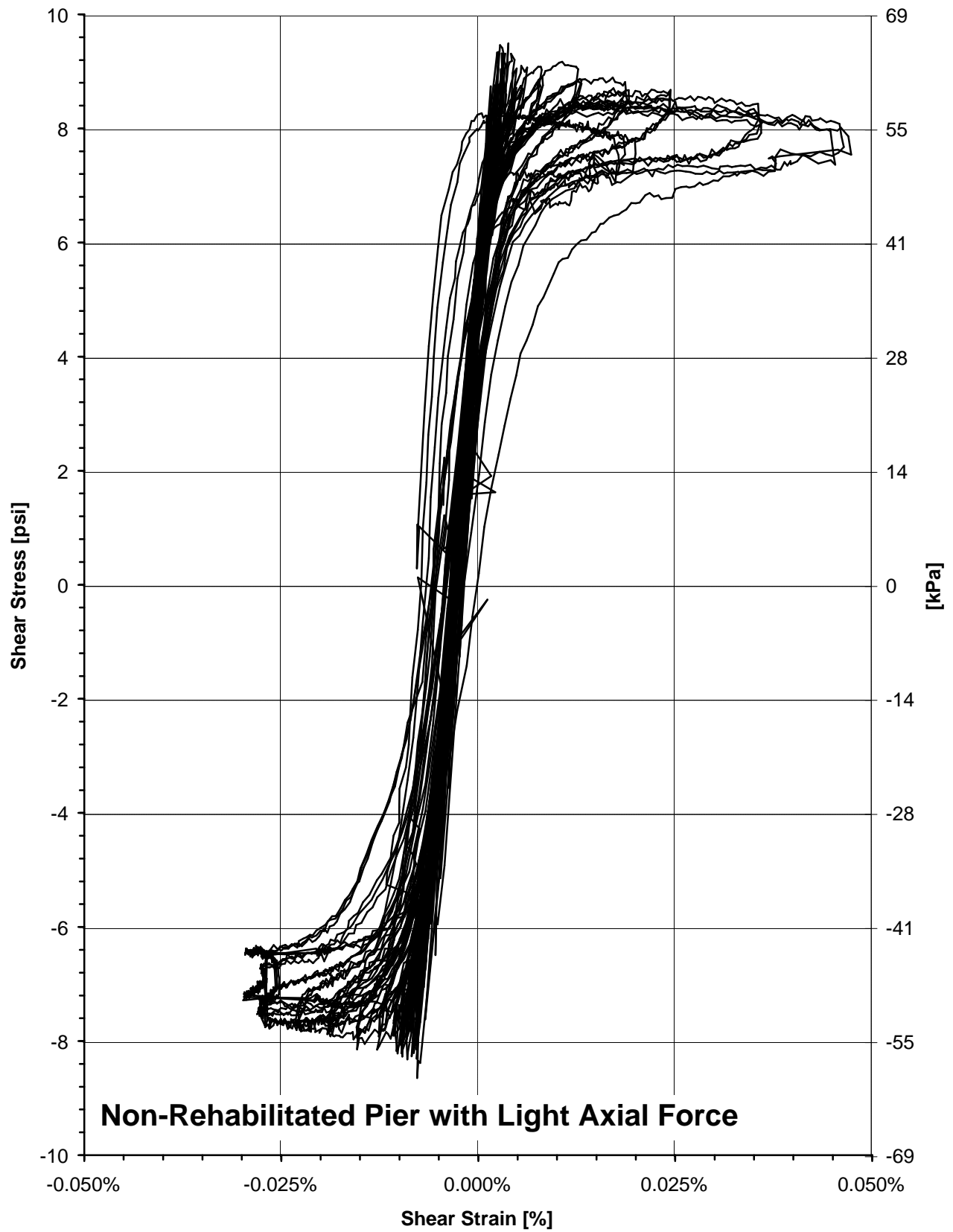


Figure D.6 - Specimen 2F, Shear Stress versus Shear Strain Response
D.6

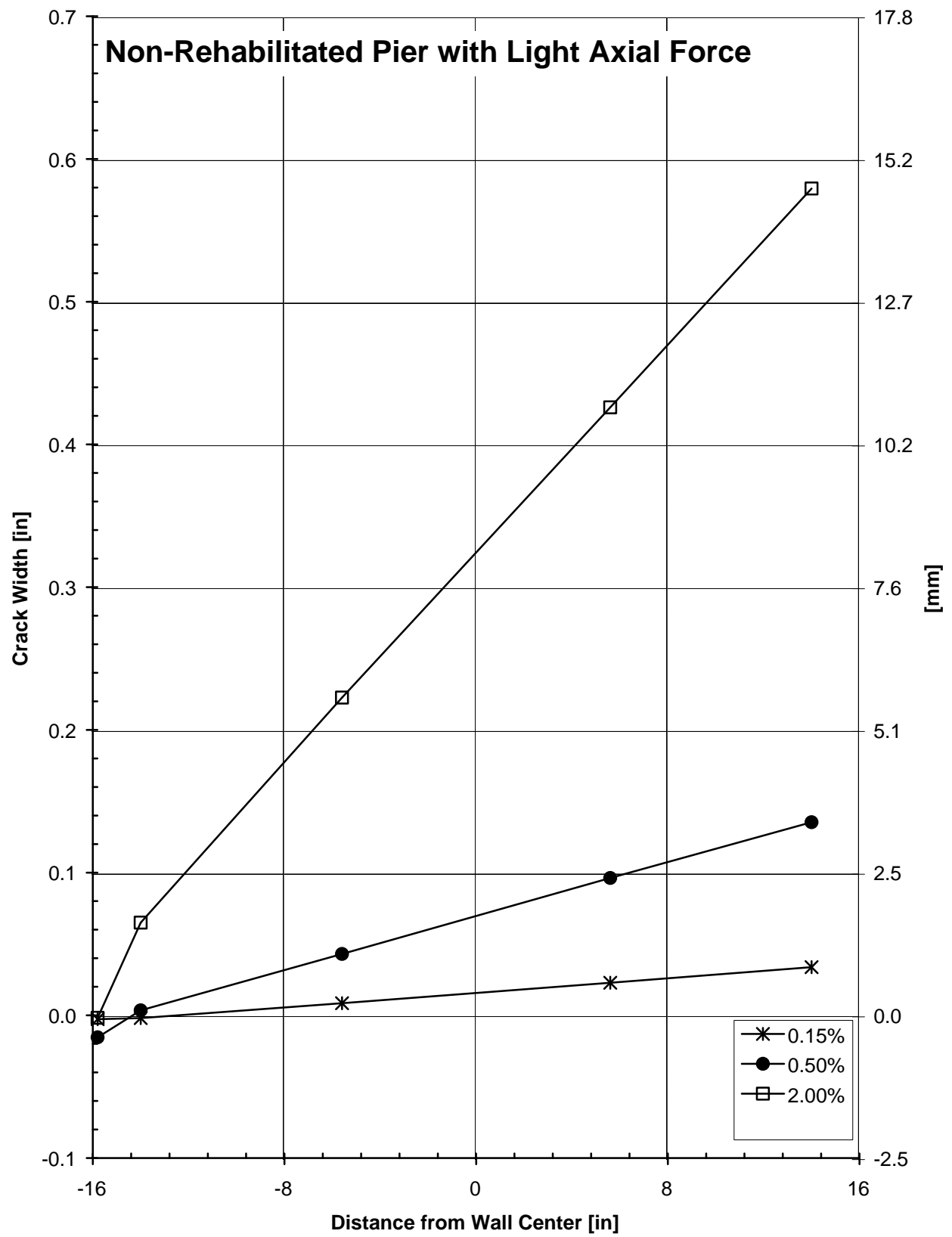


Figure D.7 - Specimen 2F, Crack Width Profile
D.7

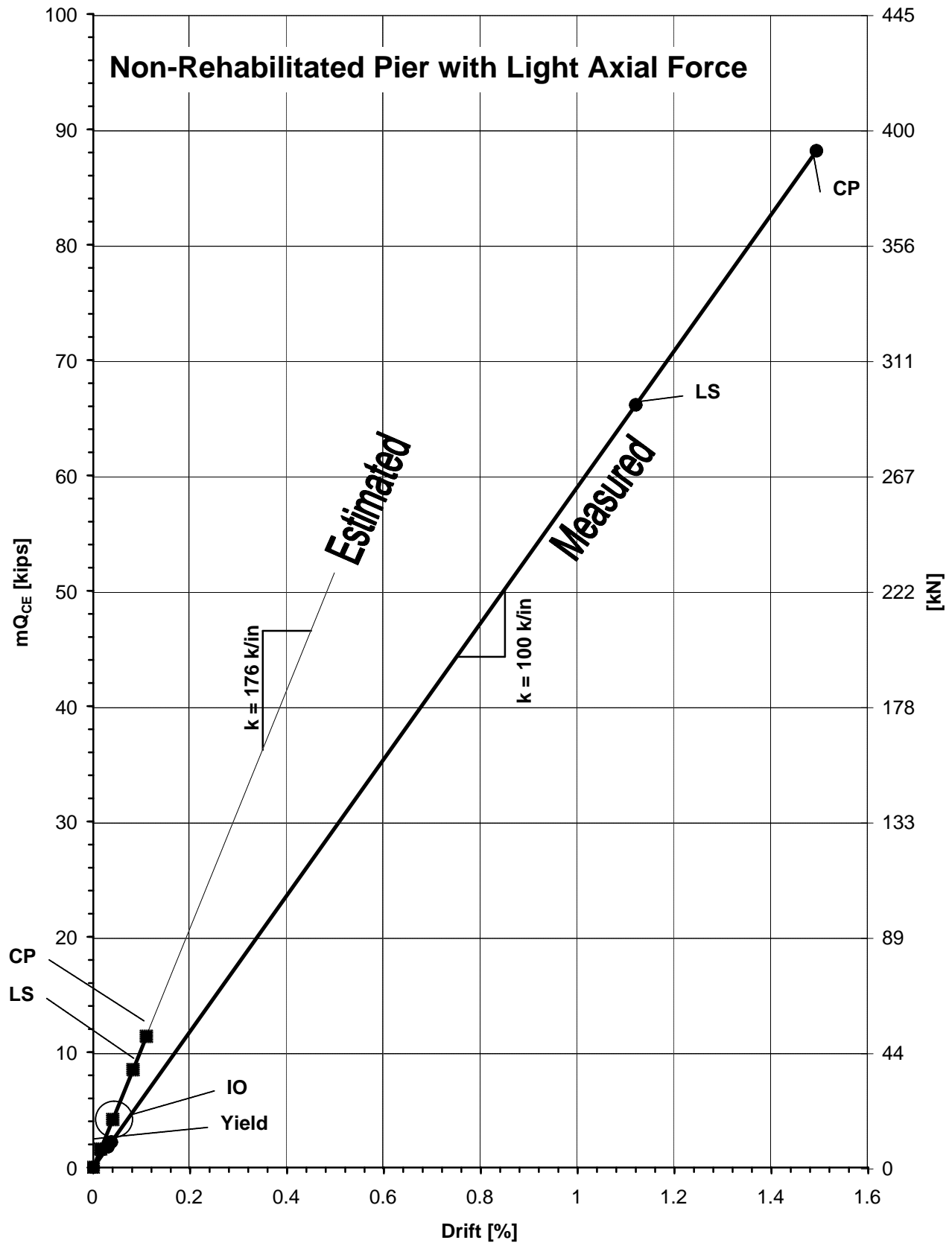


Figure D.8 - Specimen 2F, Comparison of Estimated to Measured LSP Behavior
D.8

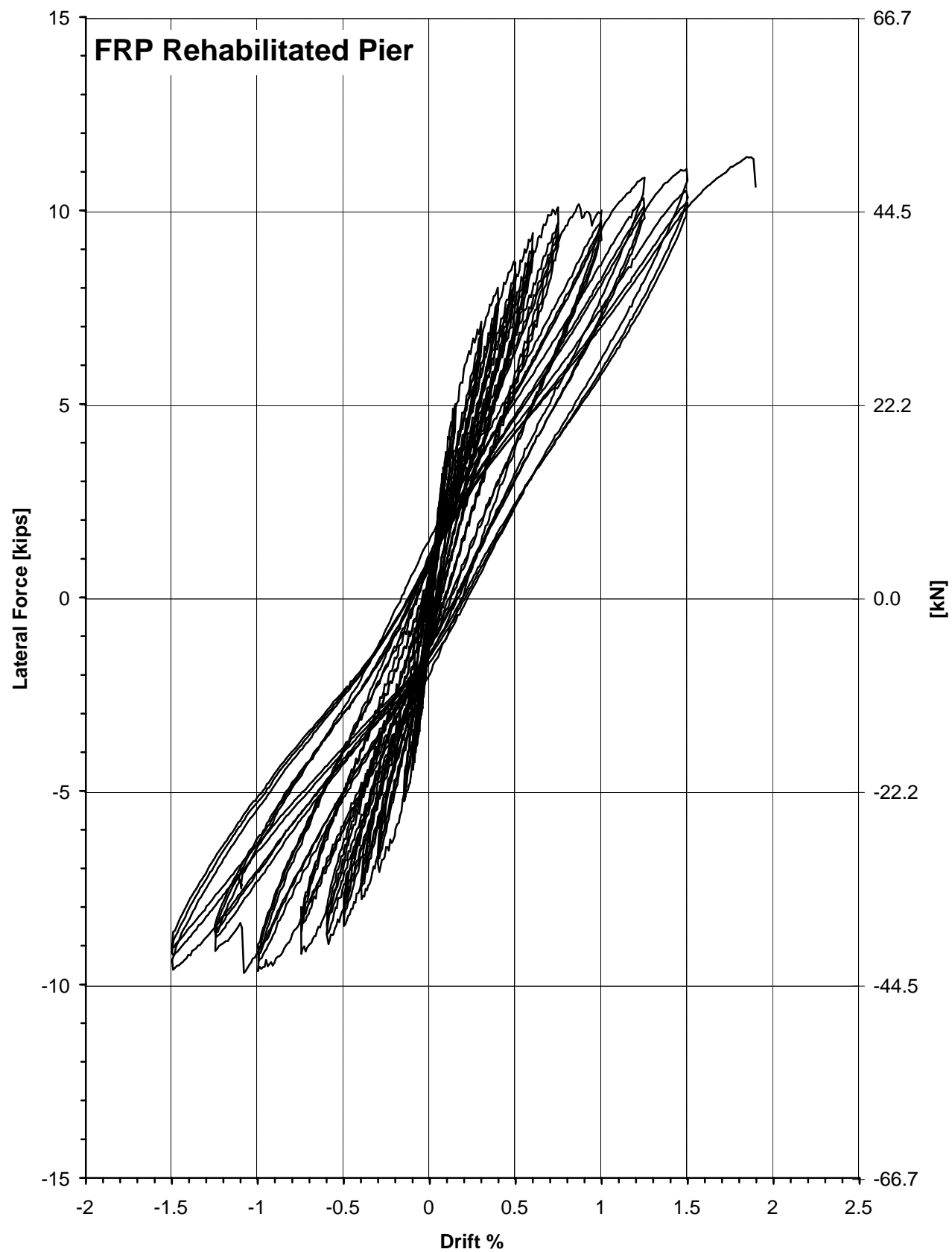


Figure E.1 - Specimen 3F, Hysteretic Response
E.1

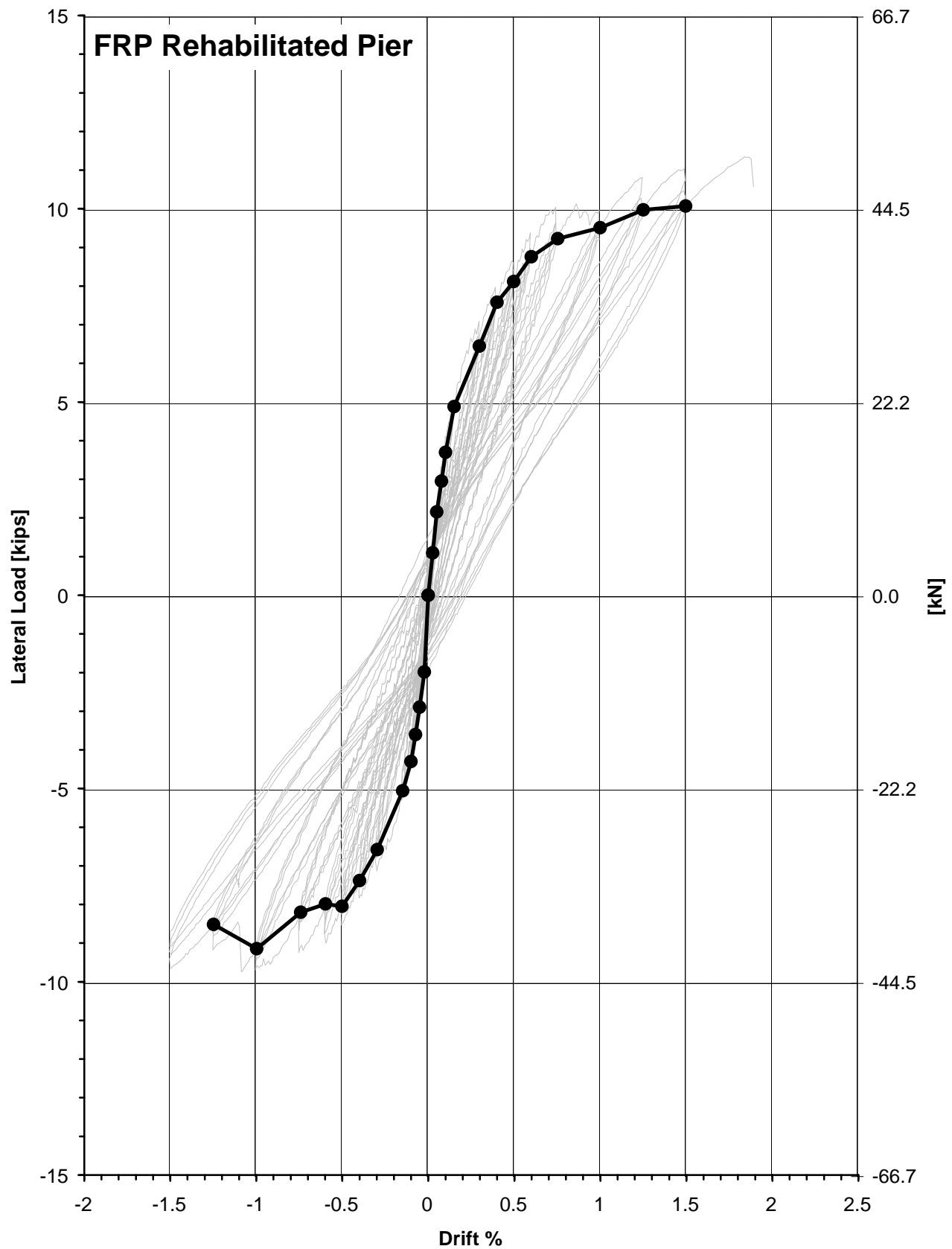


Figure E.2 - Specimen 3F, Backbone Curve
E.2

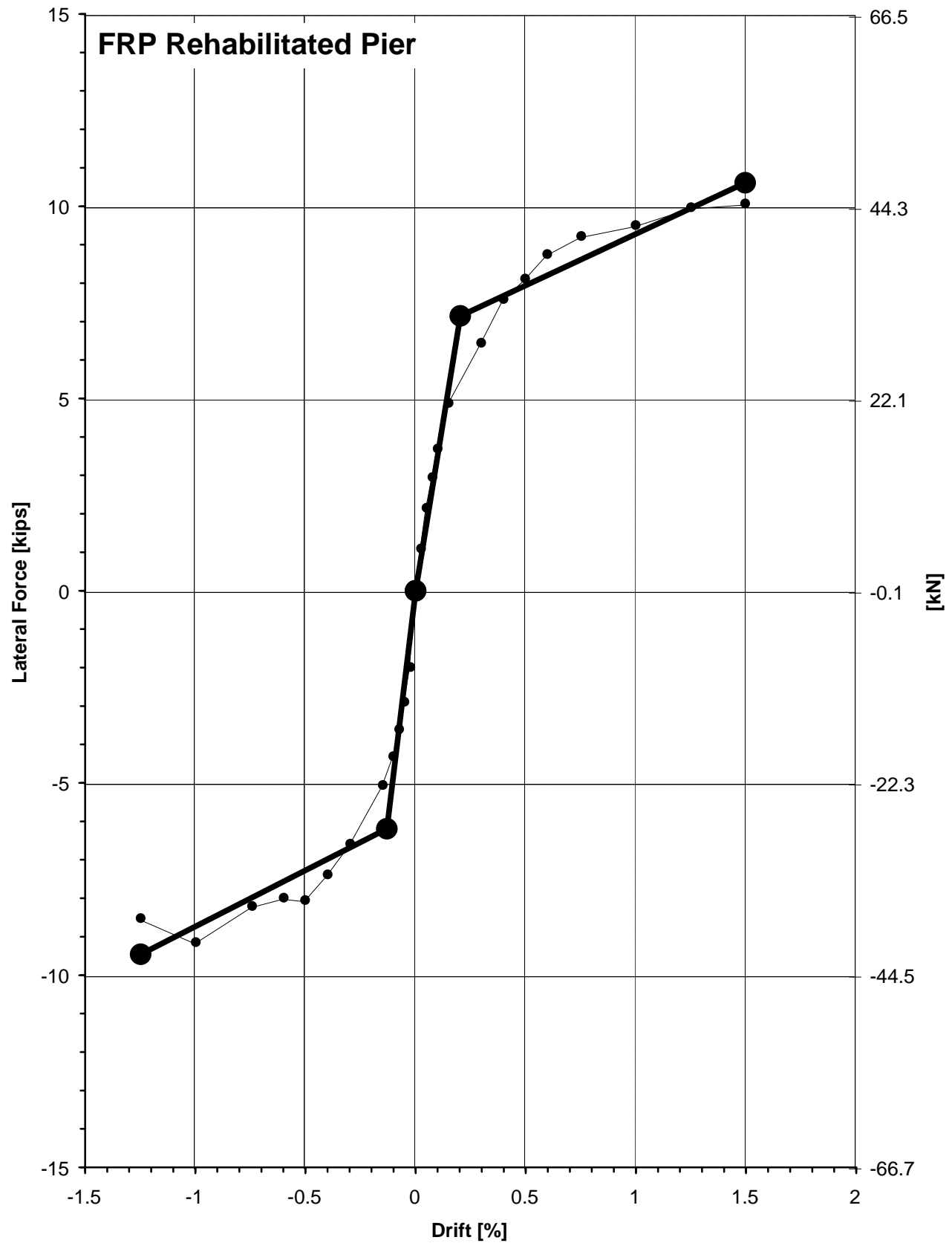


Figure E.3 - Specimen 3F, Multi-Linear Force-Deformation Curve
E.3

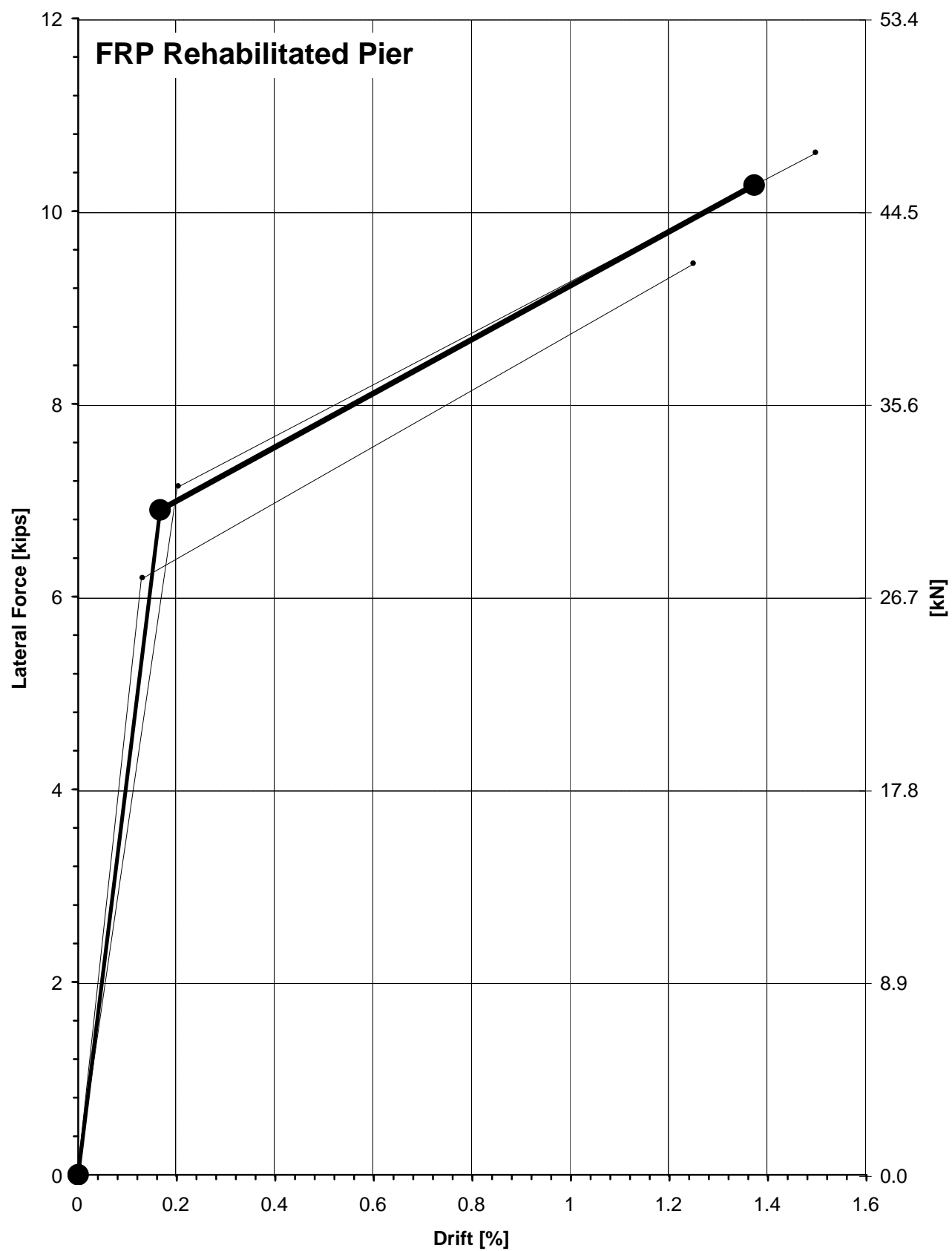


Figure E.4 - Specimen 3F, Composite Force-Deformation Curve
E.4

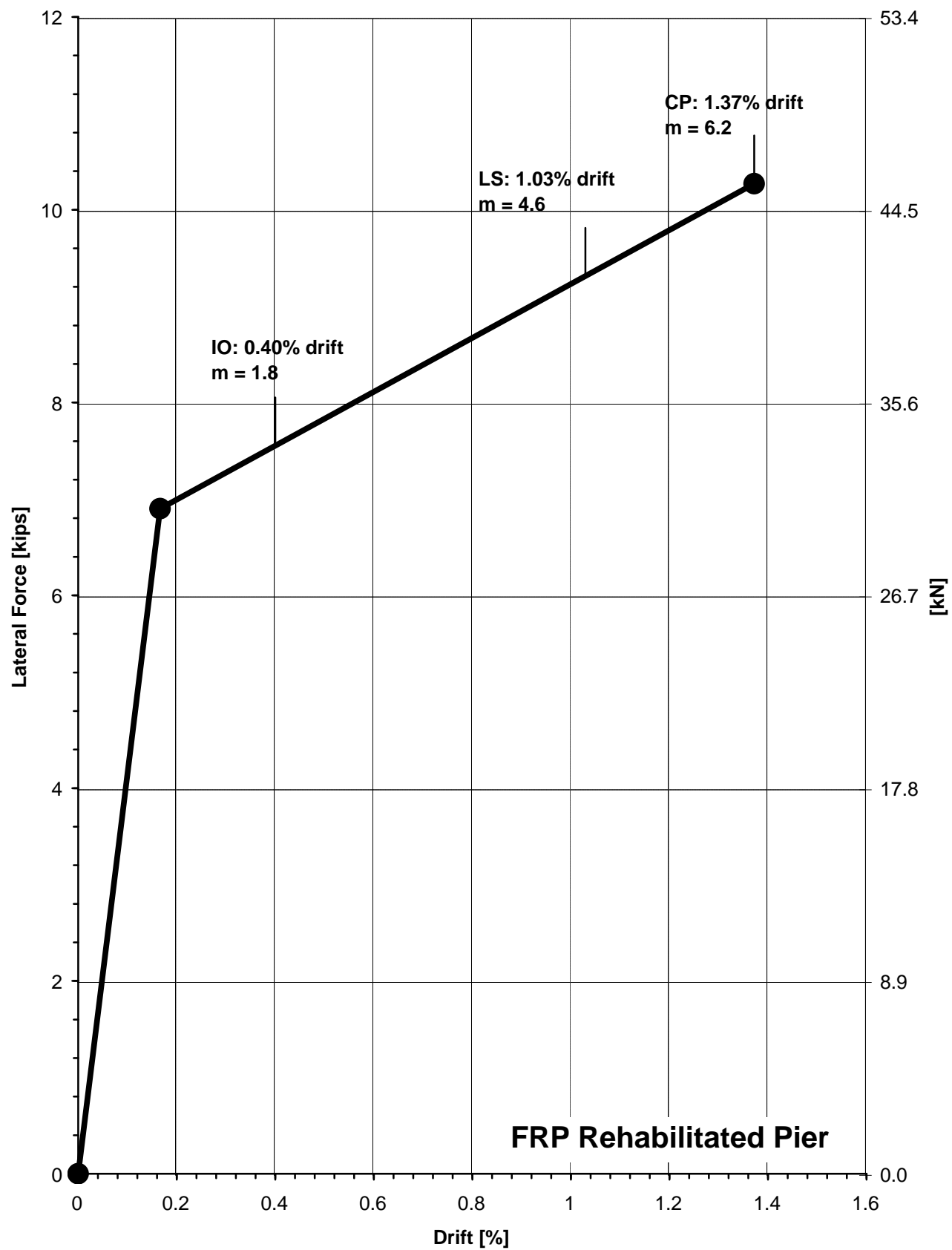


Figure E.5 - Specimen 3F, Performance Level Acceptance Criteria
E.5

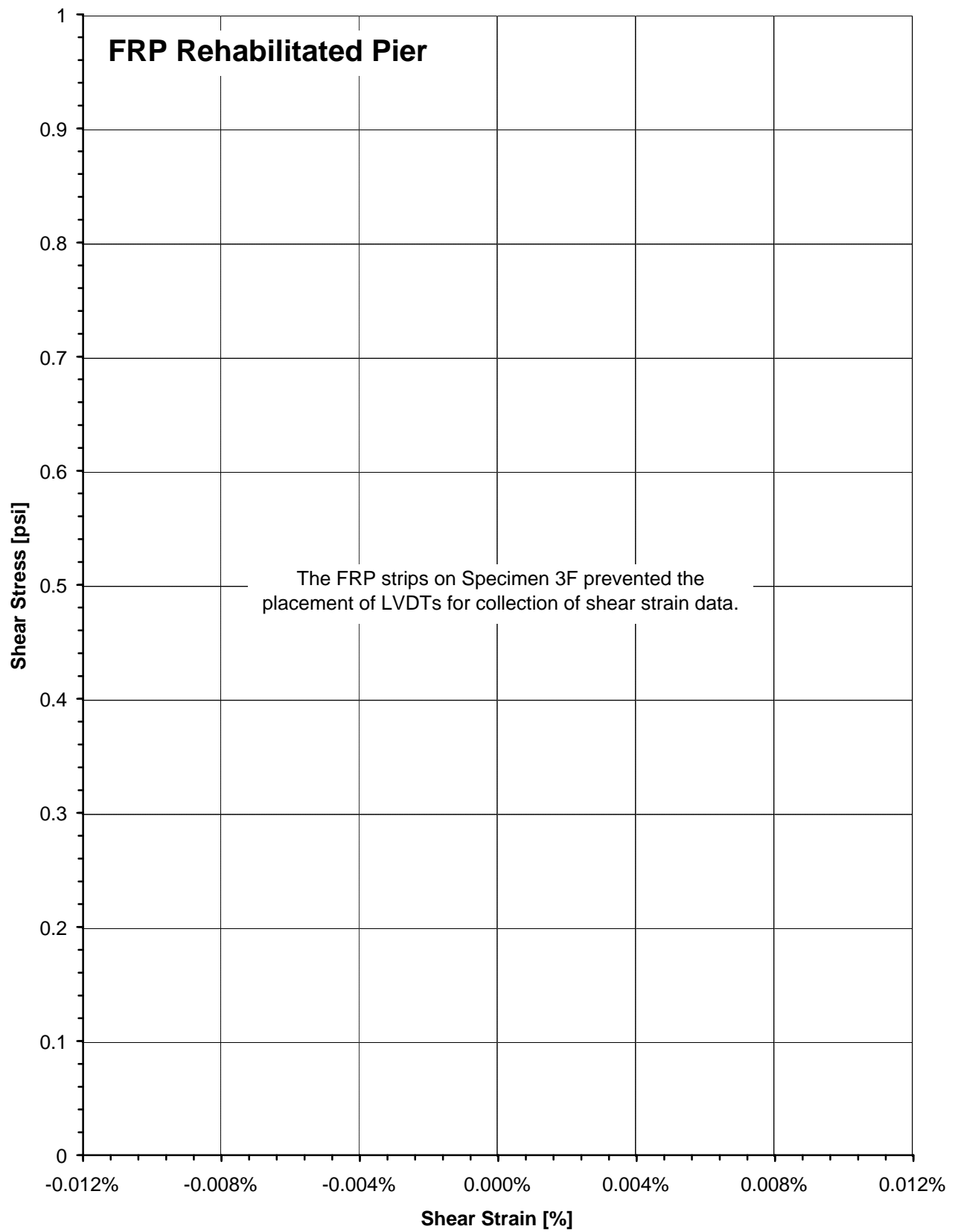


Figure E.6 - Specimen 3F, Shear Stress versus Shear Strain Response
E.6

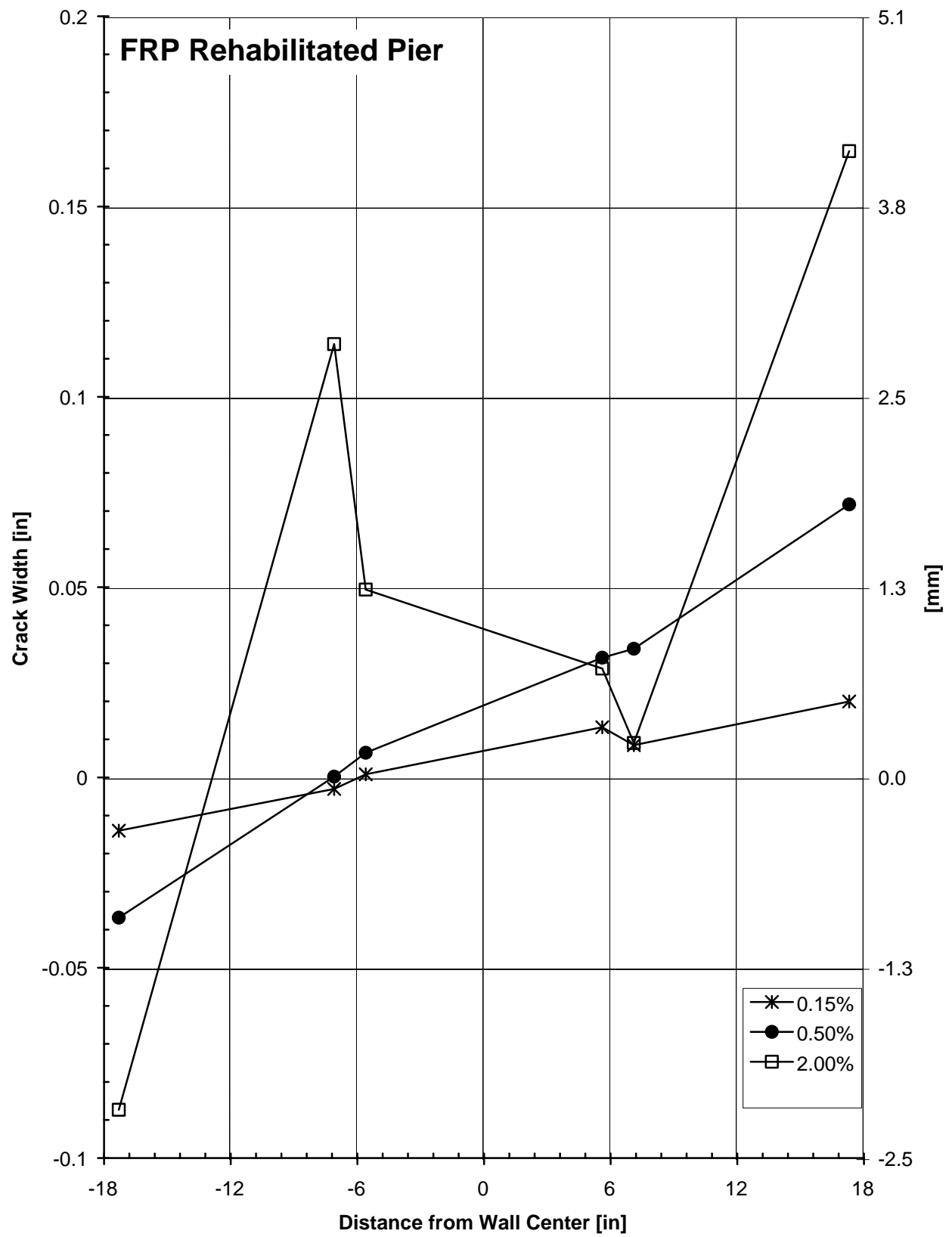


Figure E.7 - Specimen 3F, Crack Width Profile
E.7

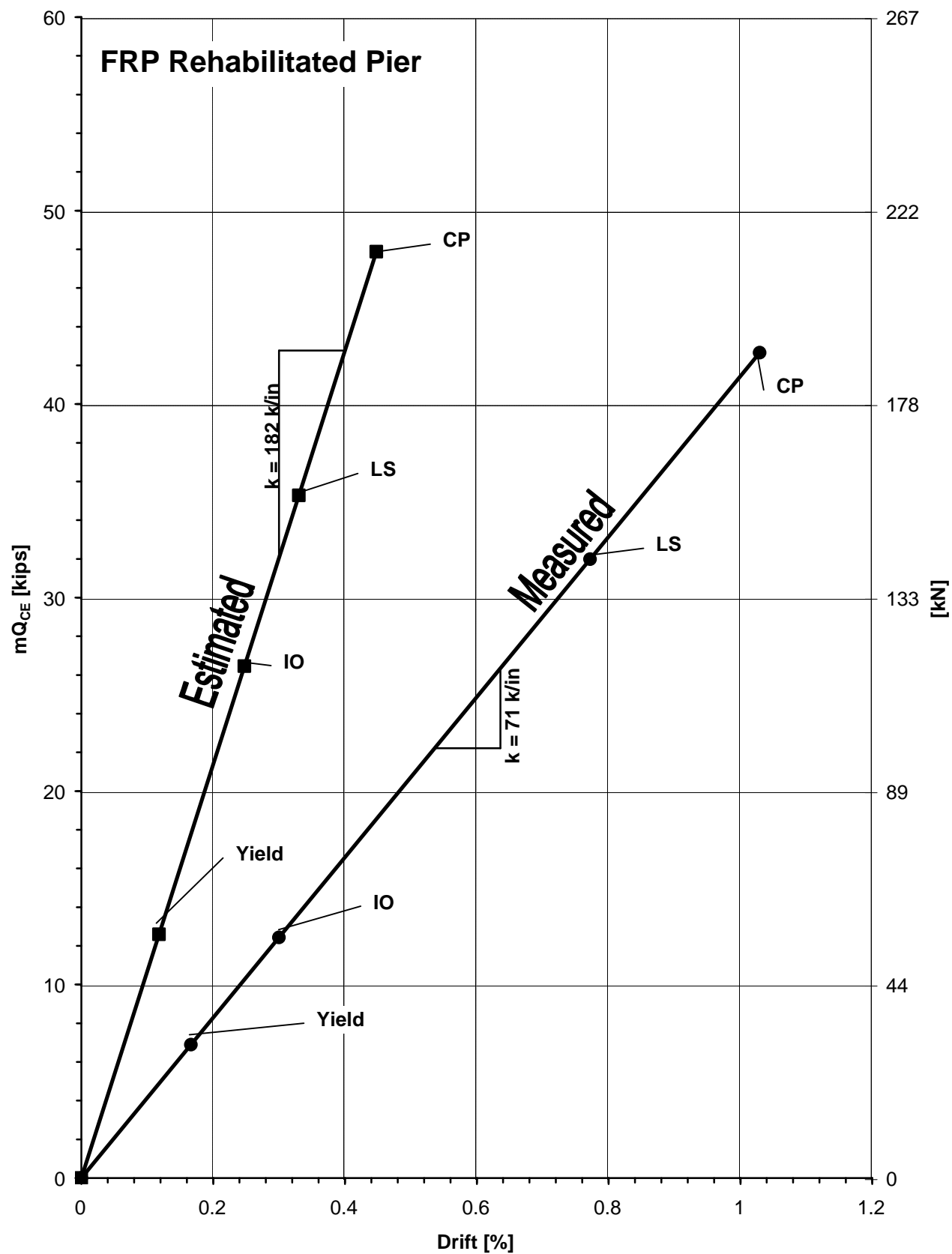


Figure E.8 - Specimen 3F, Comparison of Estimated to Measured LSP Behavior
E.8

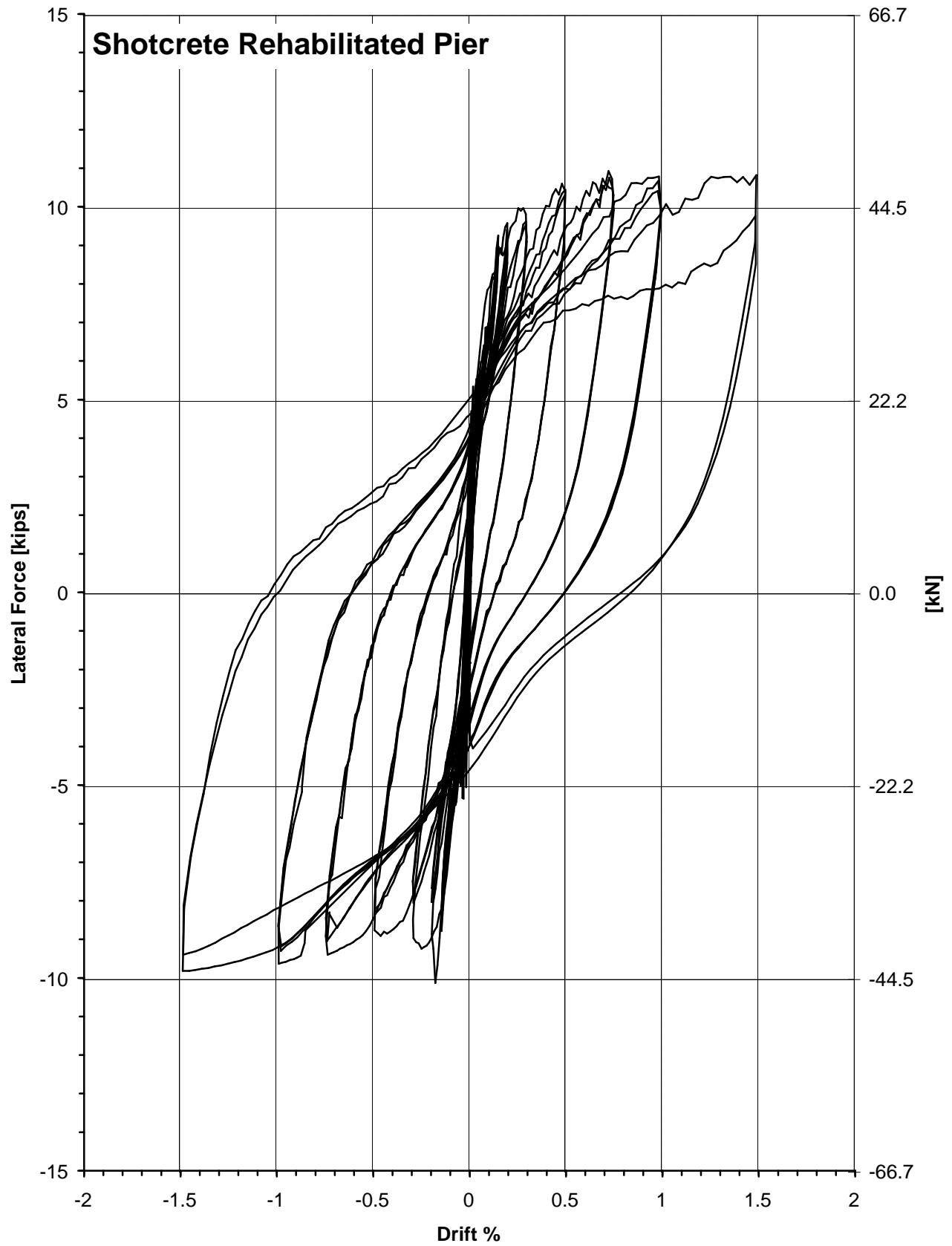


Figure F.1 - Specimen 4F, Hysteretic Response
F.1

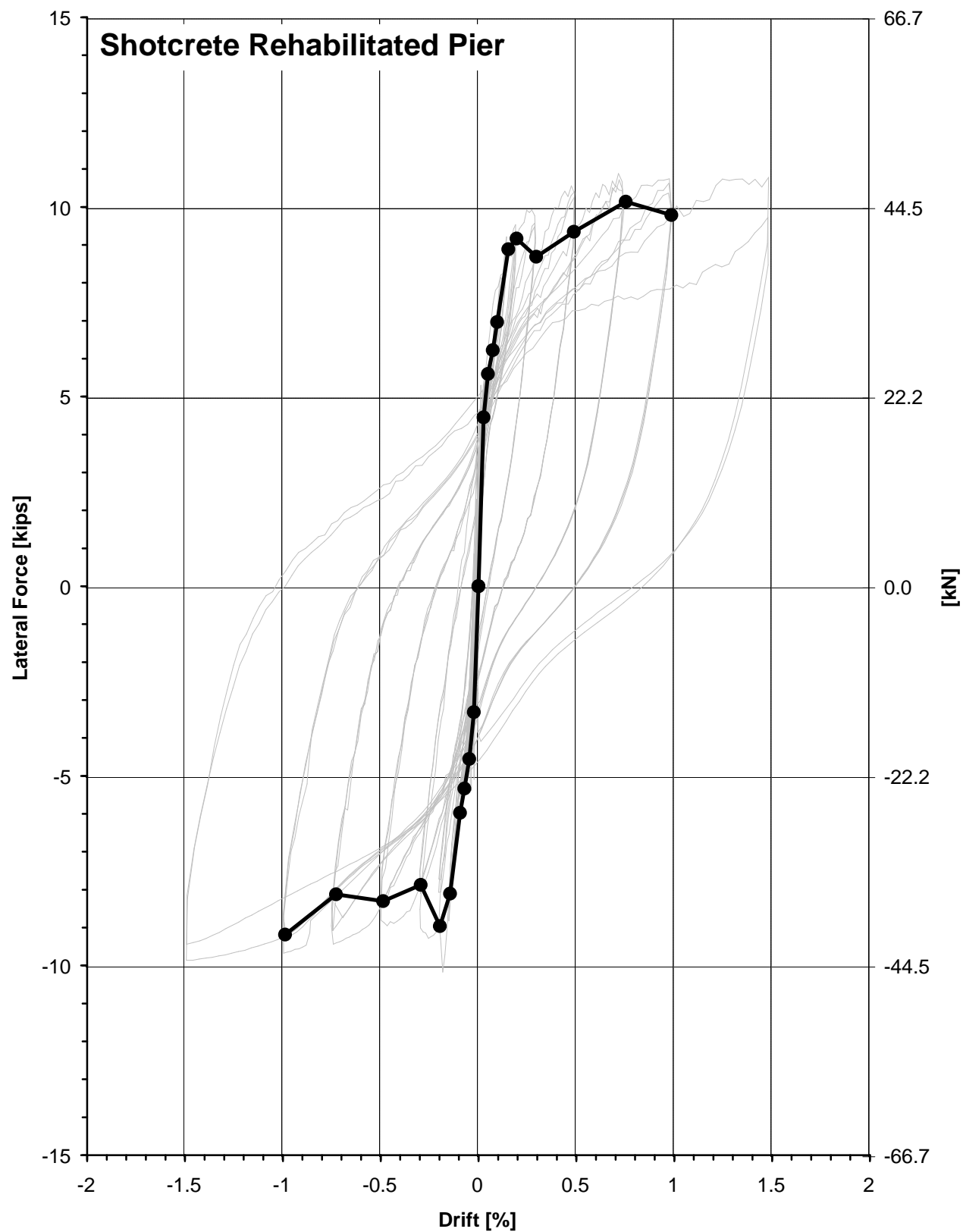


Figure F.2 - Specimen 4F, Backbone Curve
F.2

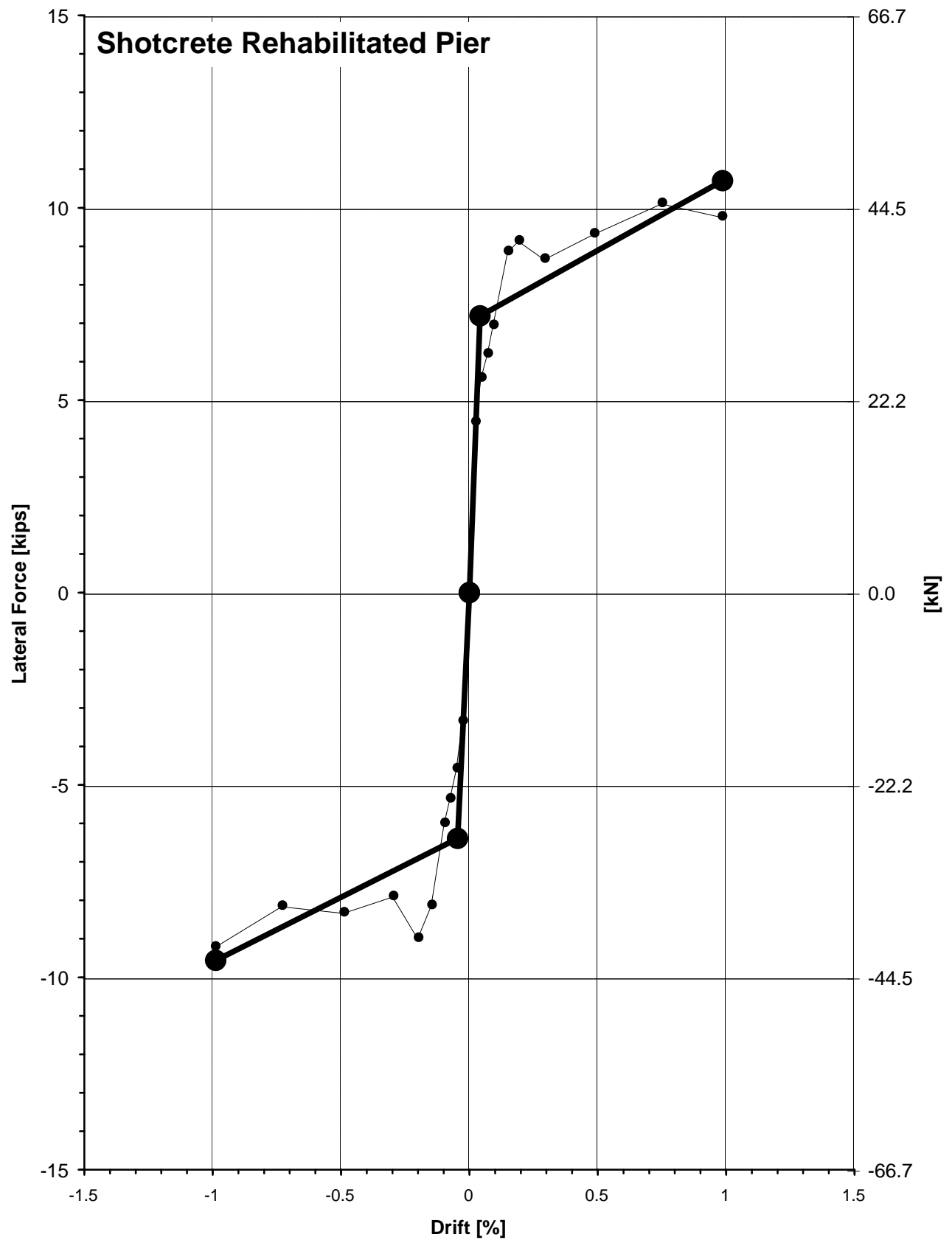


Figure F.3 - Specimen 4F, Multi-Linear Force-Deformation Curve
F.3

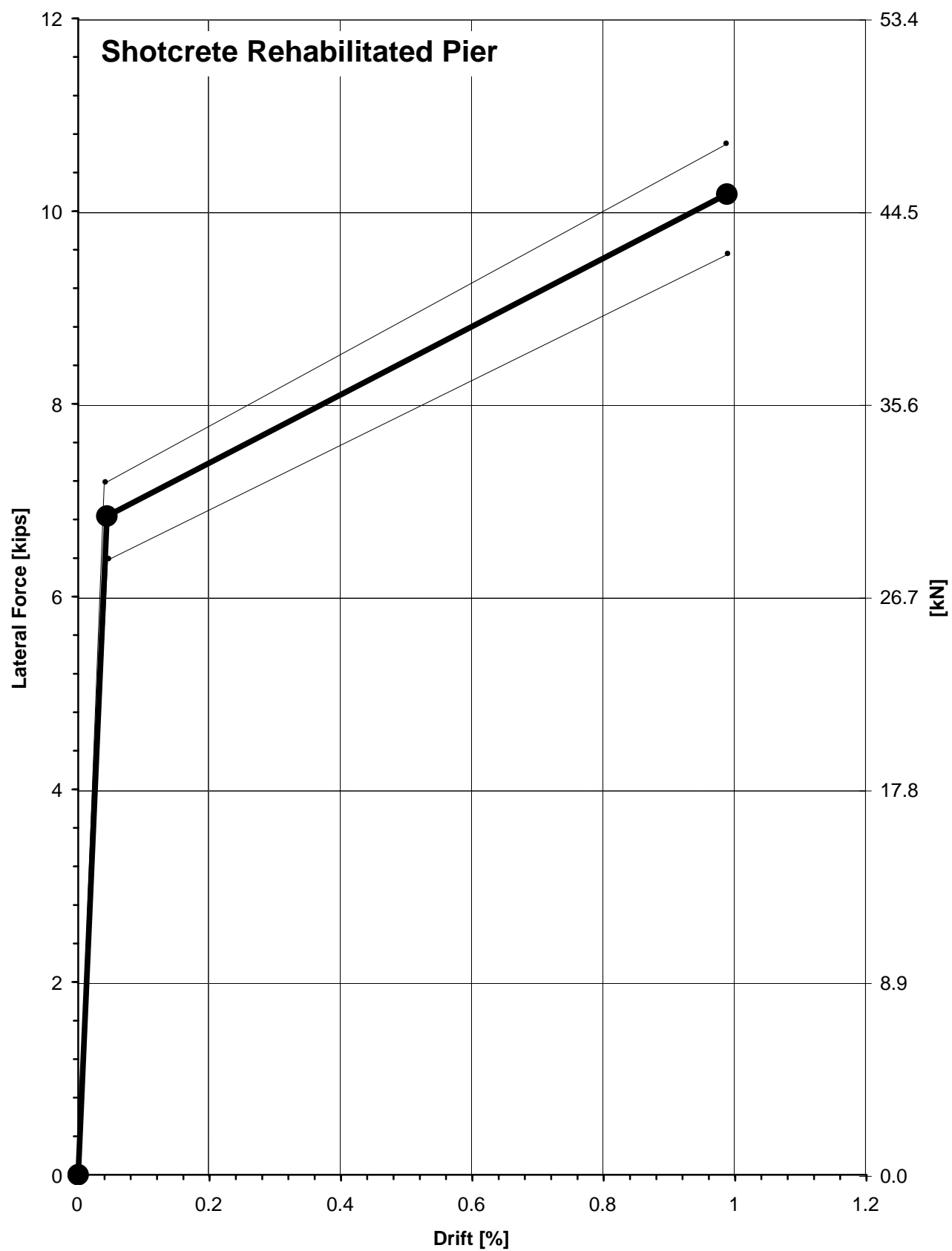


Figure F.4 - Specimen 4F, Composite Force-Deformation Curve
F.4

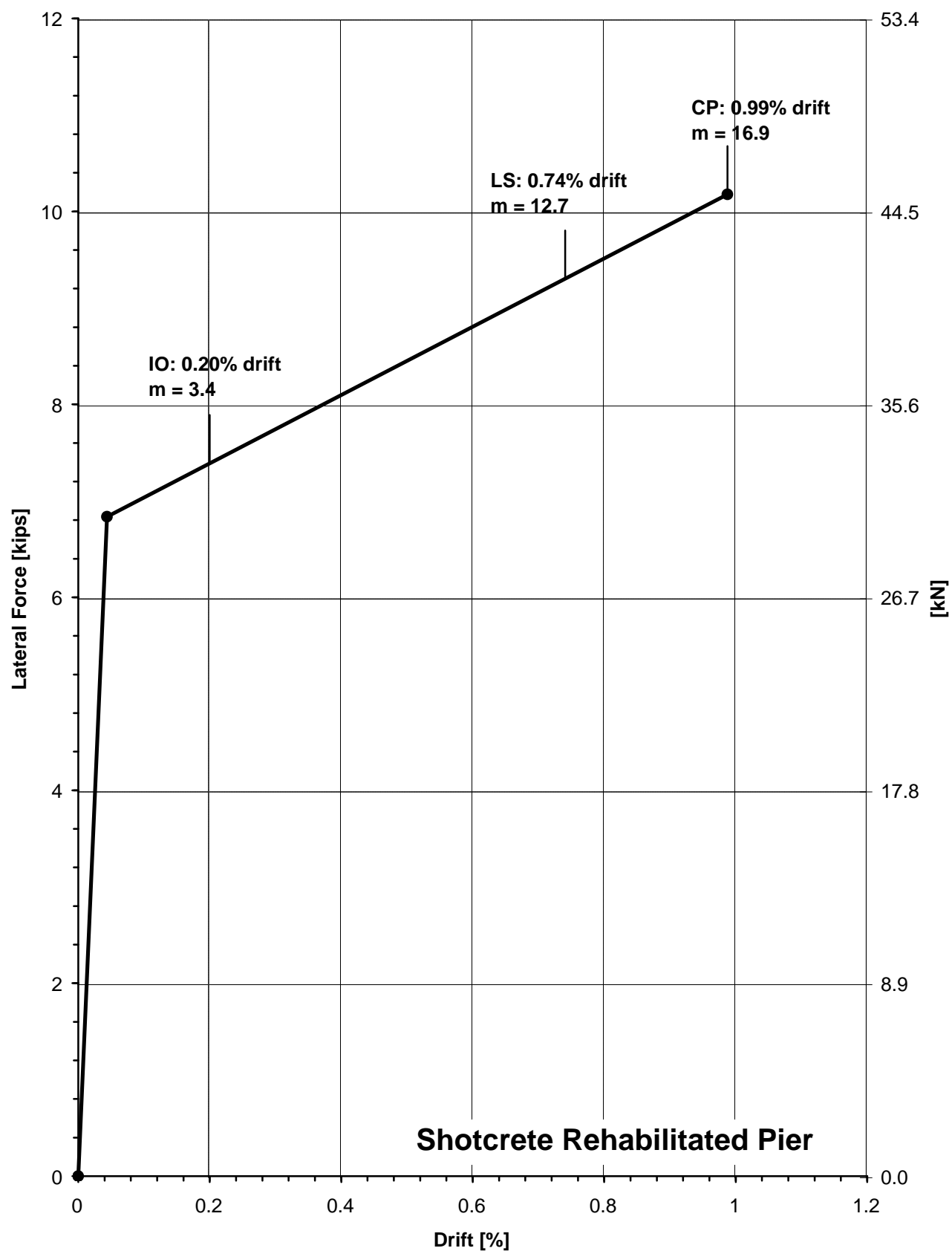


Figure F.5 - Specimen 4F, Performance Level Acceptance Criteria
F.5

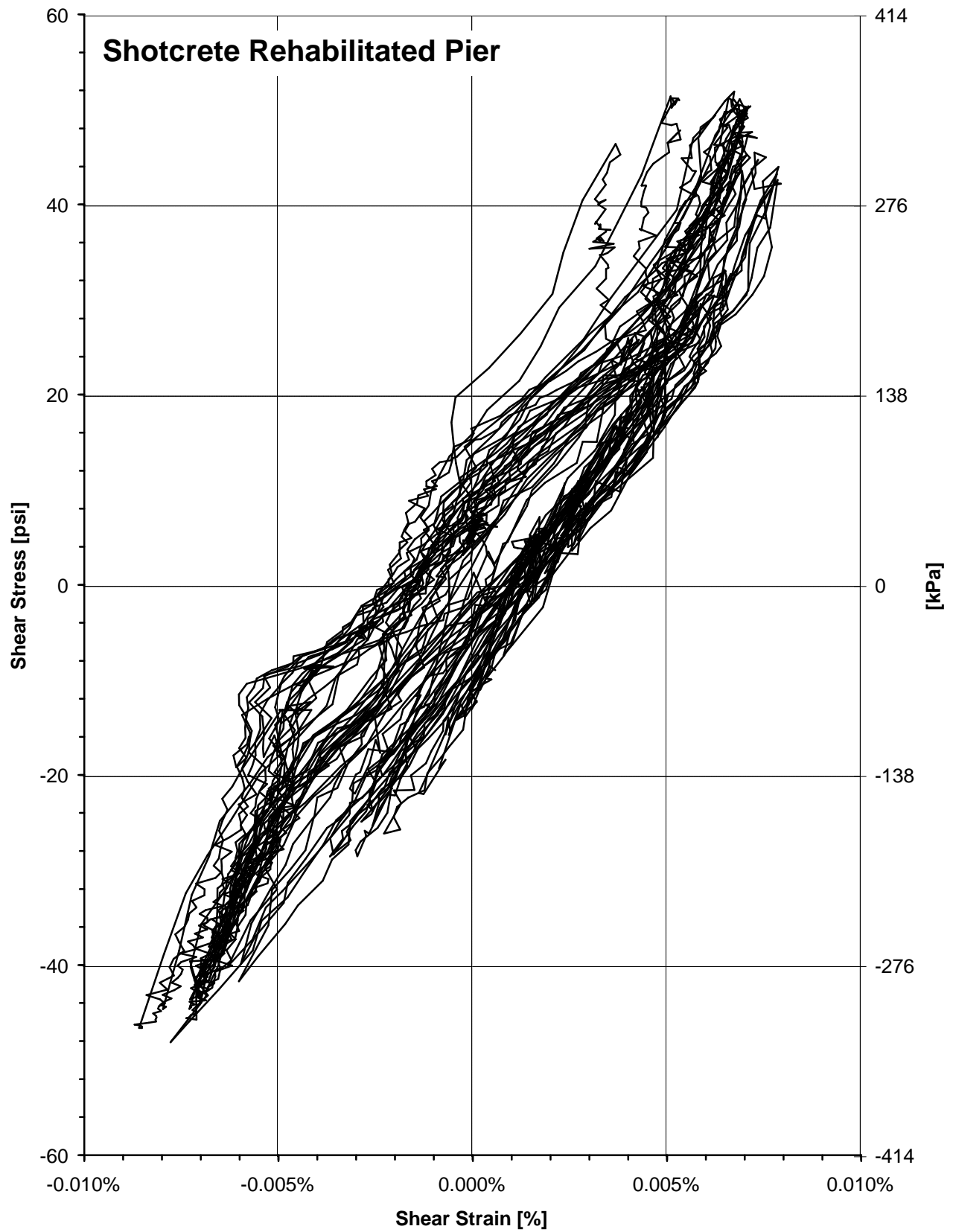


Figure F.6 - Specimen 4F, Shear Stress versus Shear Strain Response
F.6

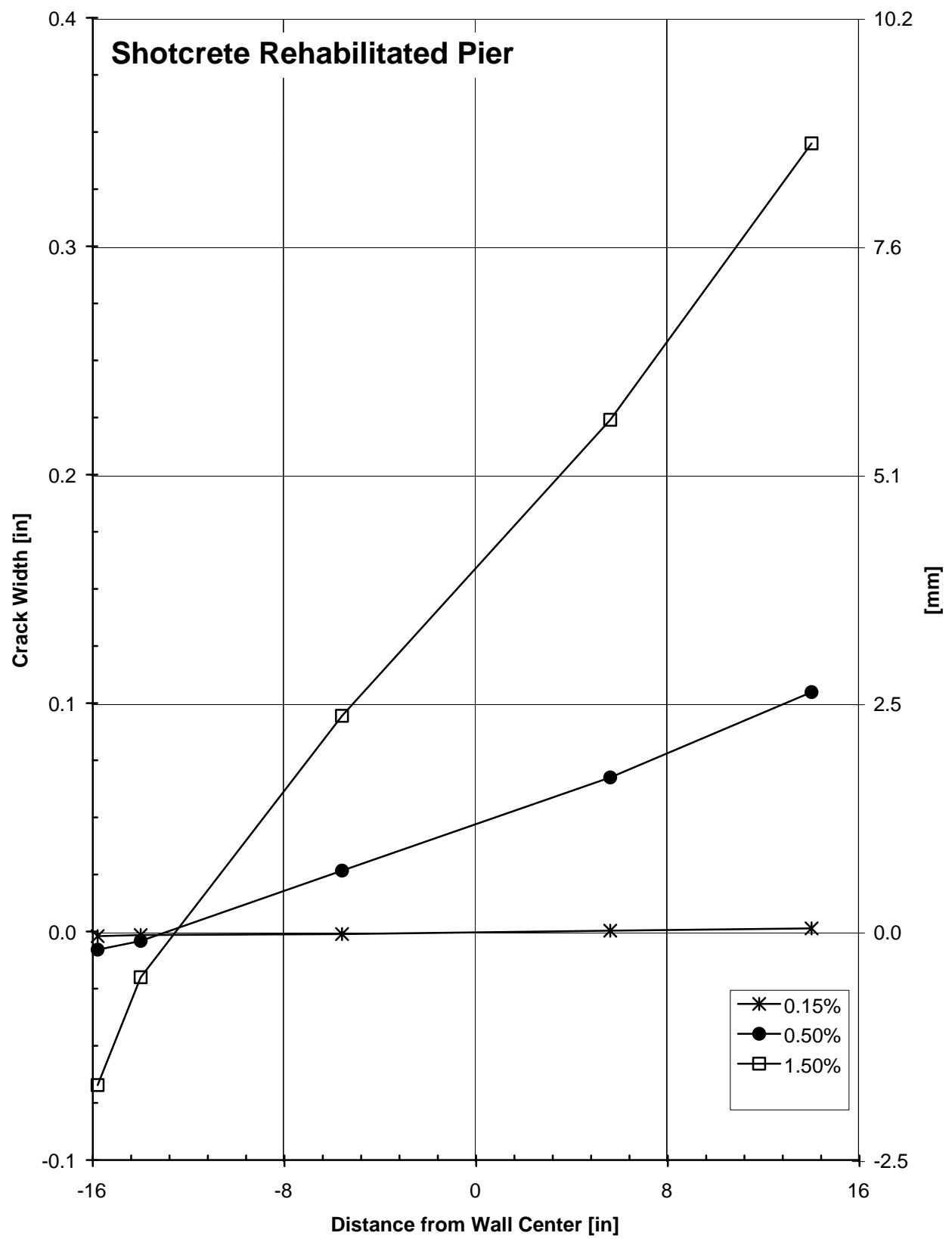


Figure F.7 - Specimen 4F, Crack Width Profile
F.7

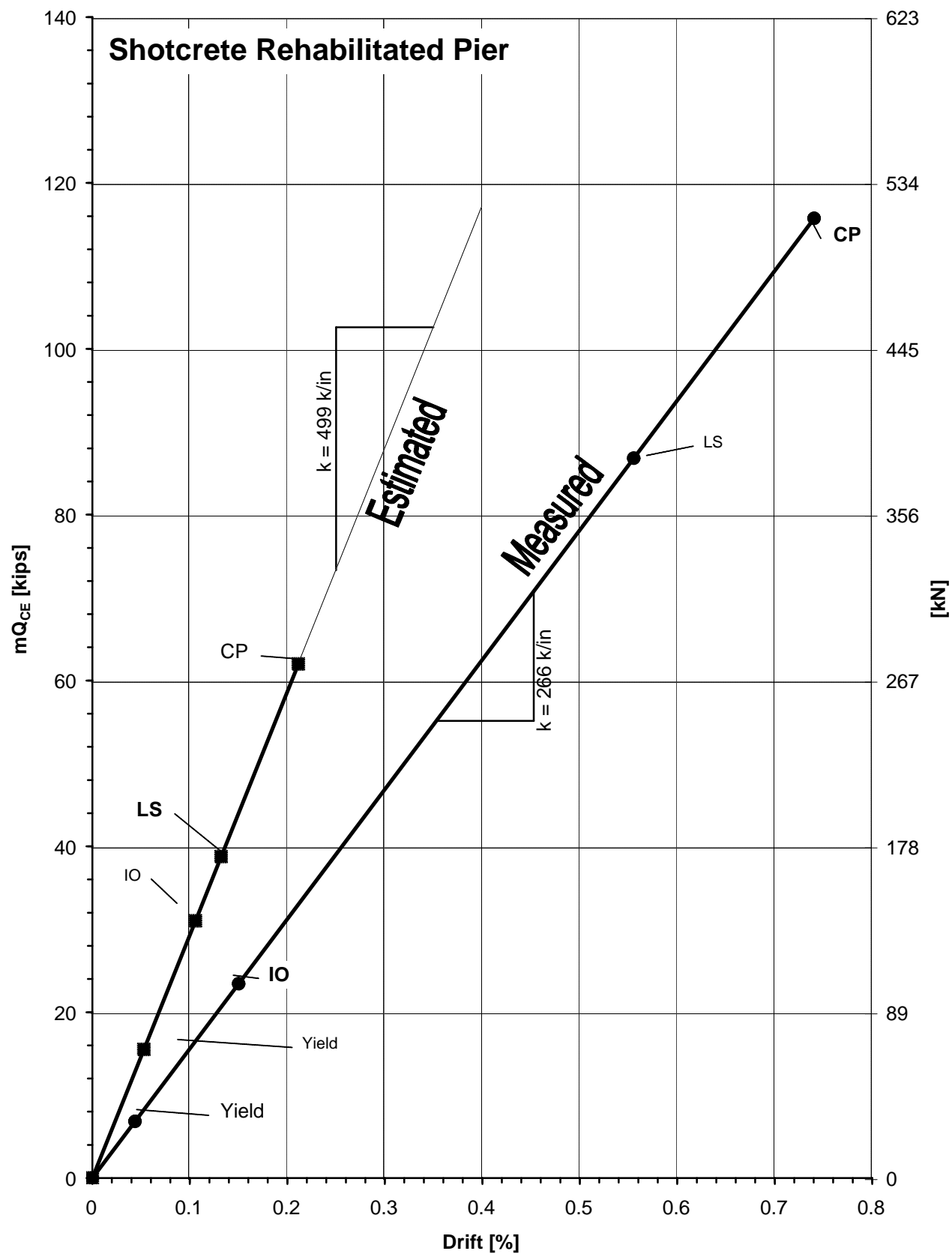


Figure F.8 - Specimen 4F, Comparison of Estimated to Measured LSP Behavior
F.8

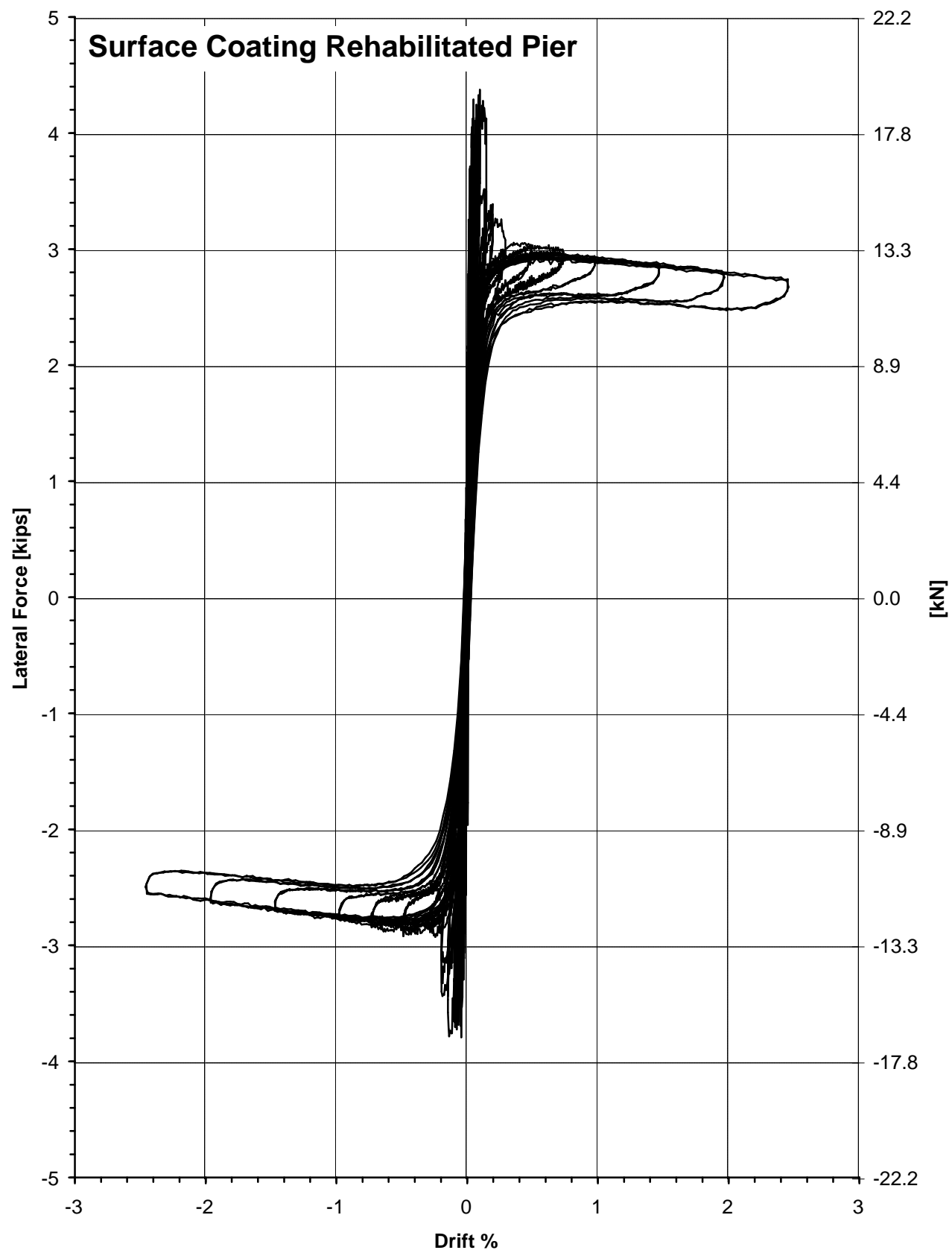


Figure G.1 - Specimen 5F, Hysteretic Response
G.1

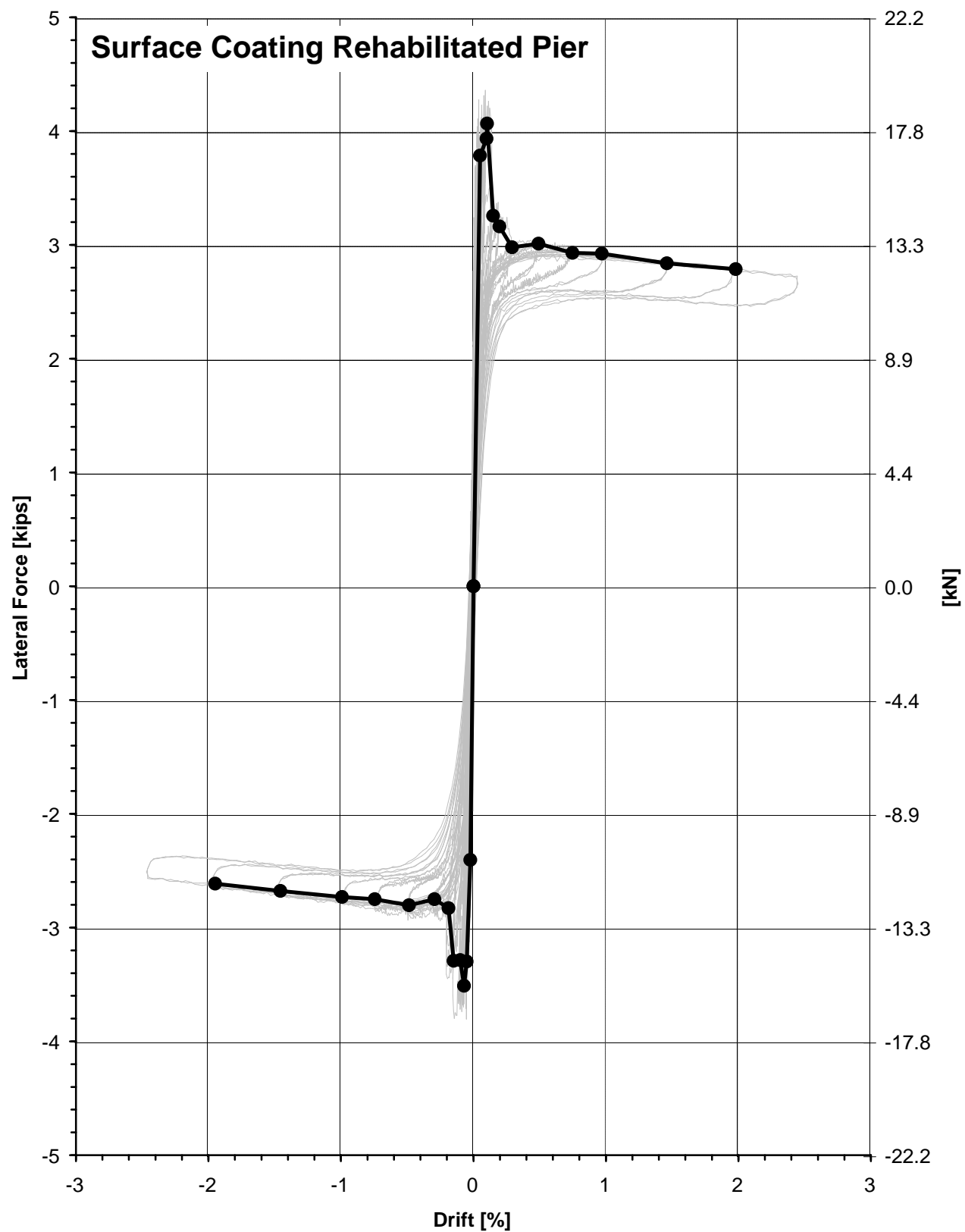


Figure G.2 - Specimen 5F, Backbone Curve
G.2

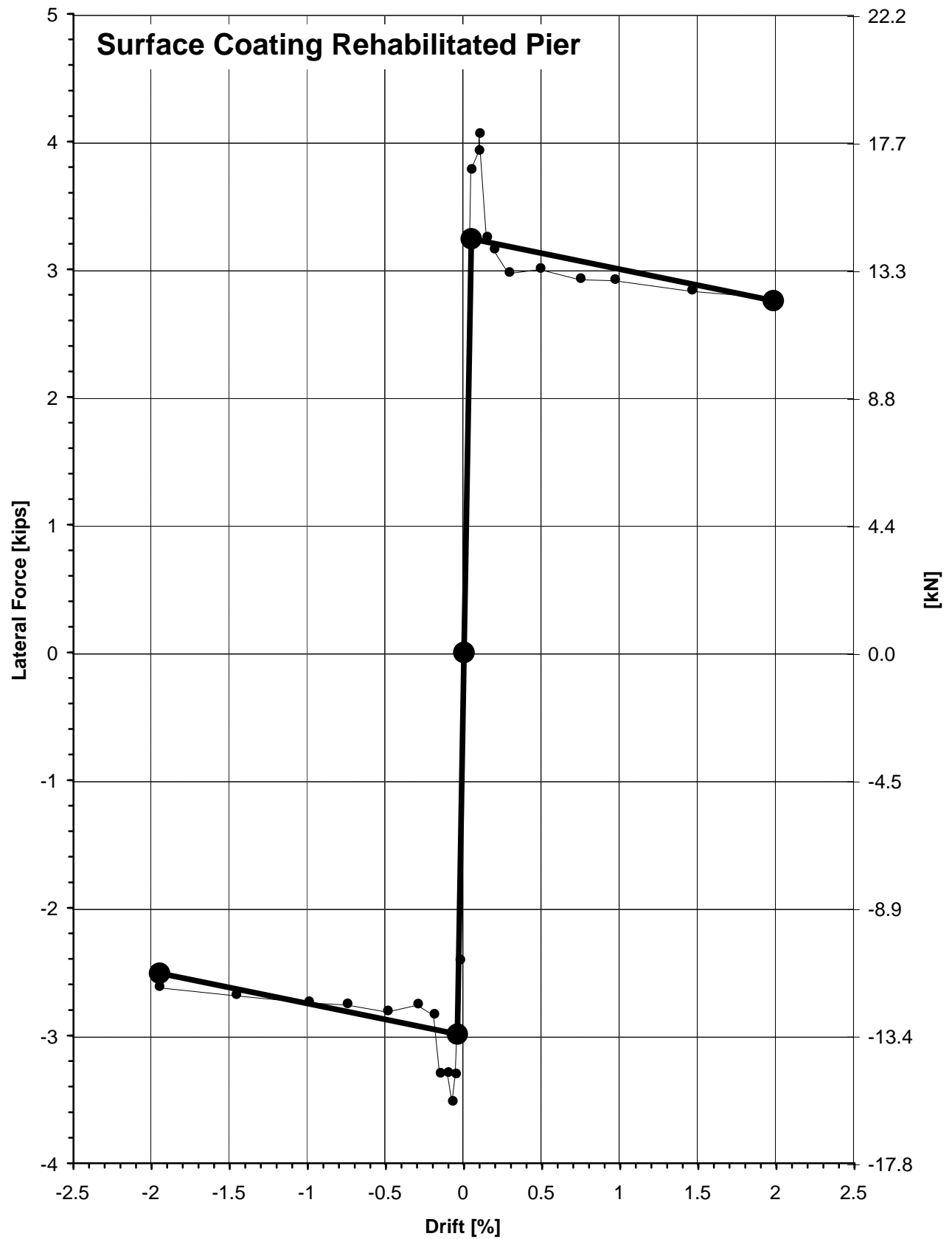


Figure G.3 - Specimen 5F, Multi-Linear Force-Deformation Curve
G.3

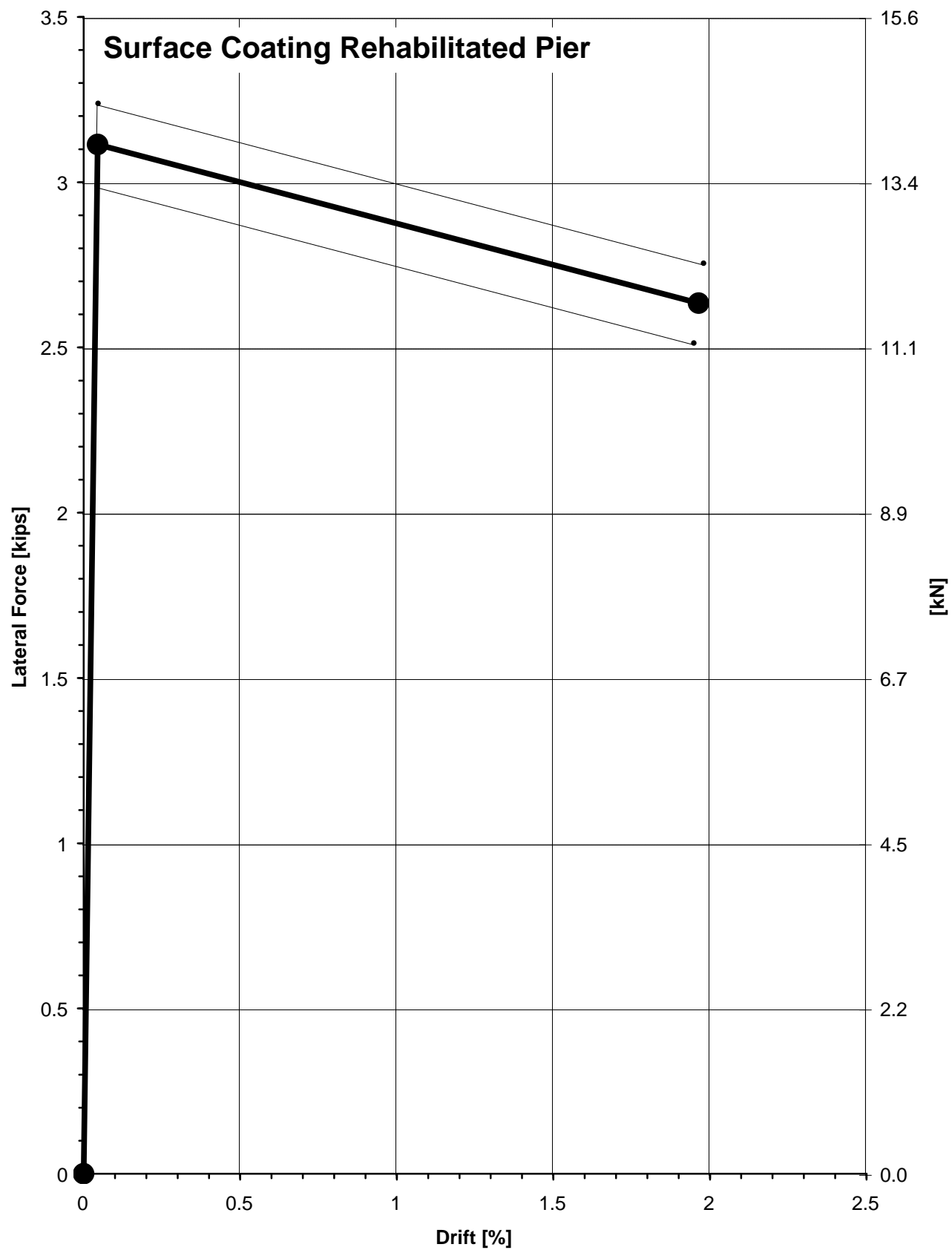


Figure G.4 - Specimen 5F, Composite Force-Deformation Curve
G.4

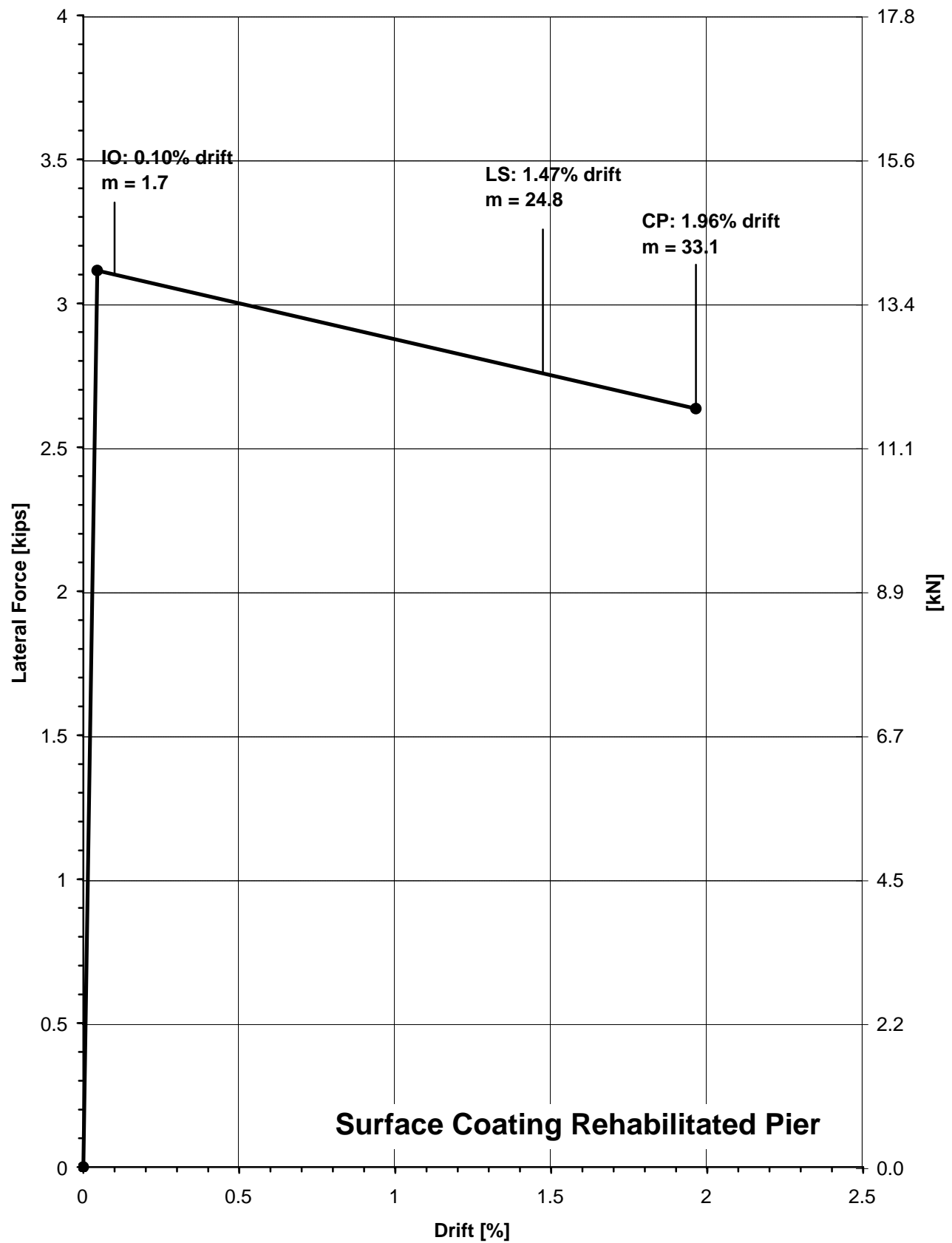


Figure G.5 - Specimen 5F, Performance Level Acceptance Criteria
G.5

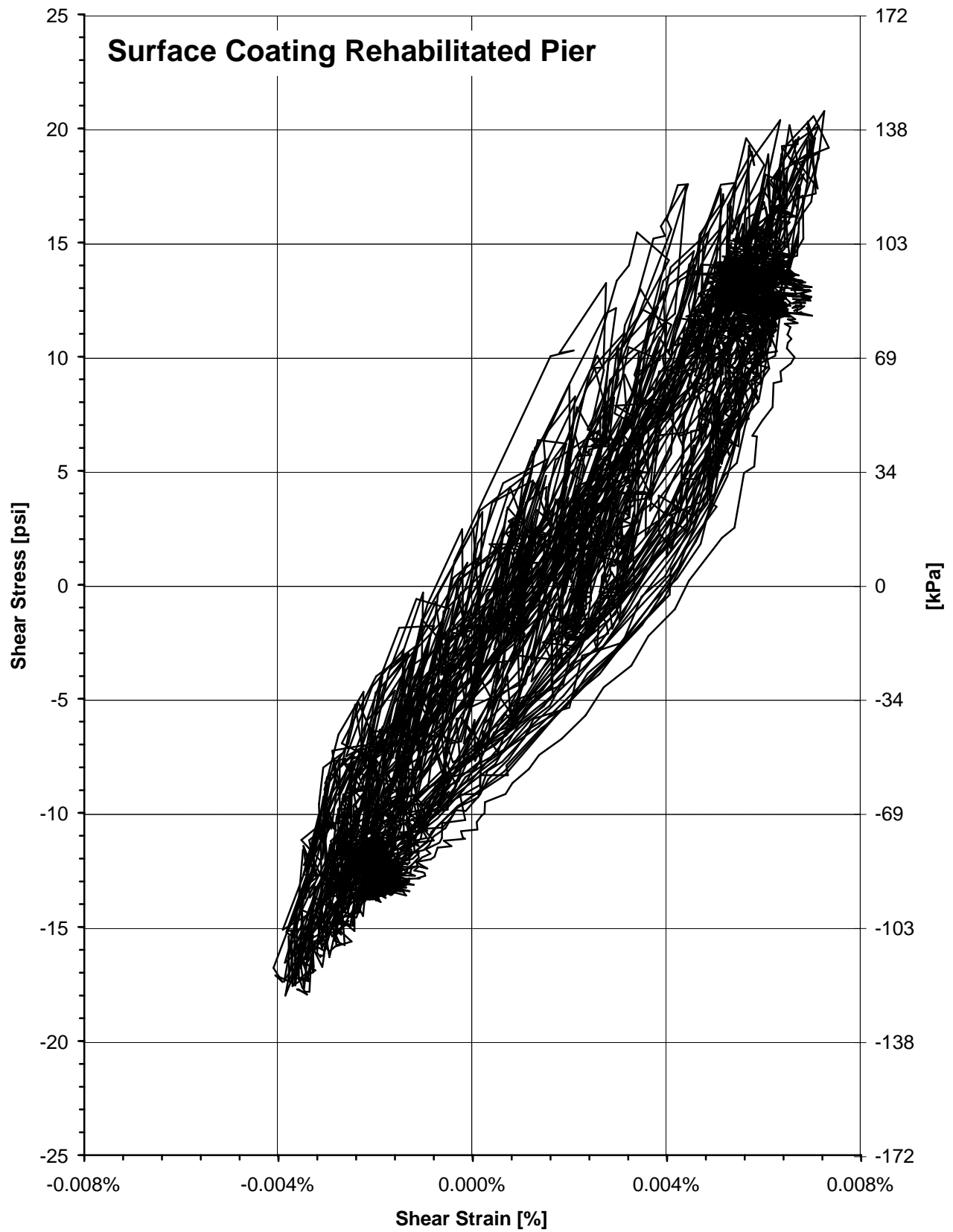


Figure G.6 - Specimen 5F, Shear Stress versus Shear Strain Response
G.6

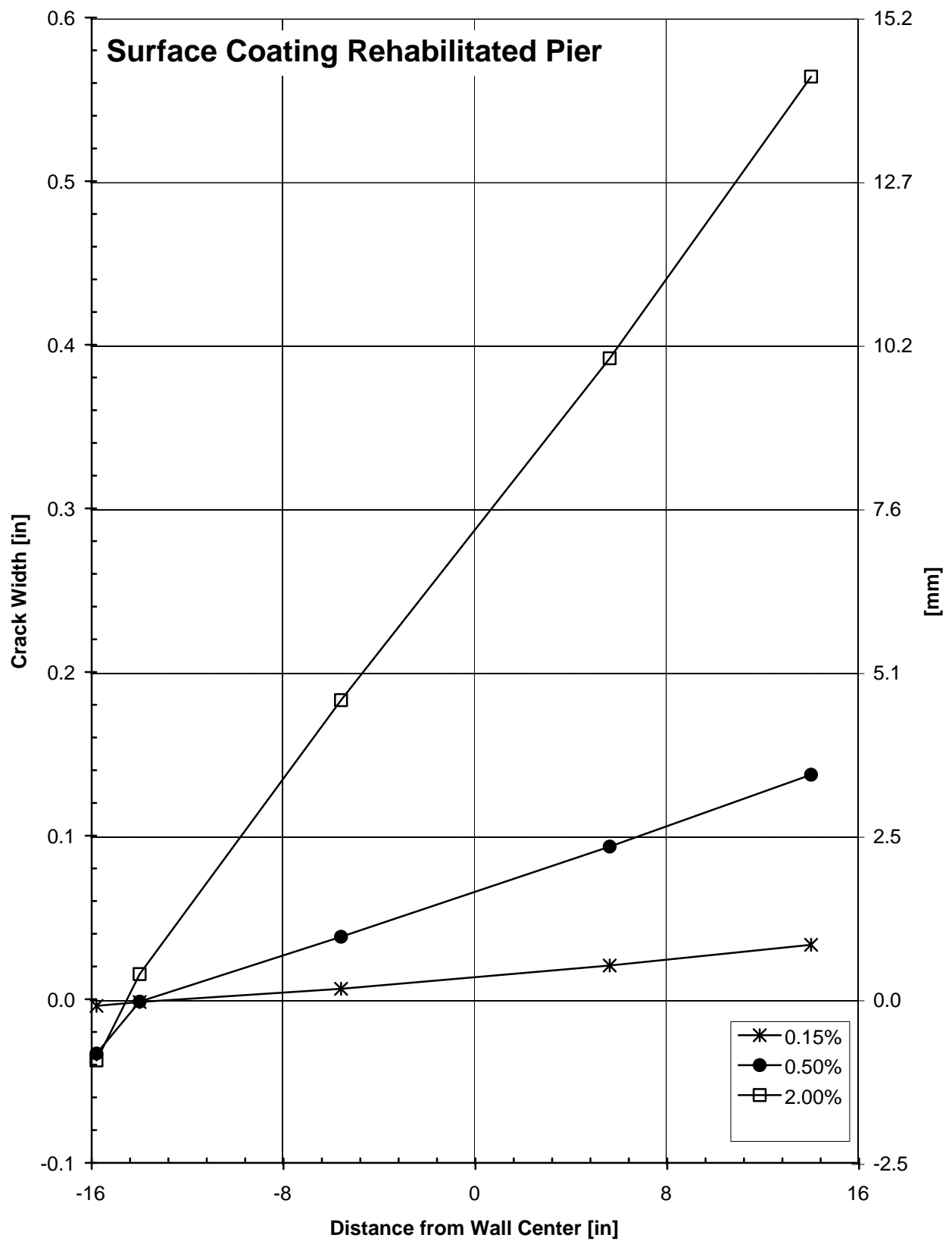


Figure G.7 - Specimen 5F, Crack Width Profile
G.7

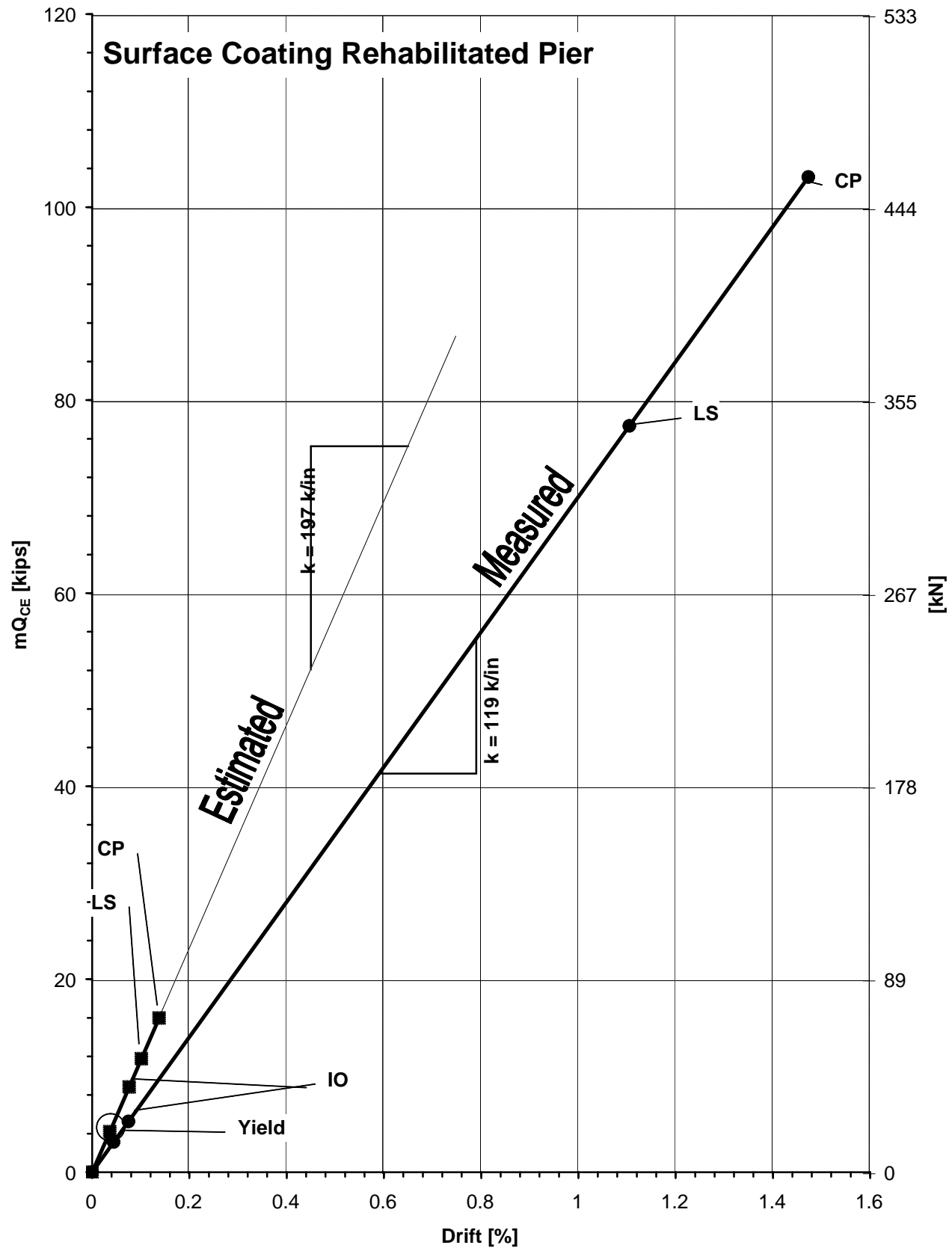


Figure G.8 - Specimen 5F, Comparison of Estimated to Measured LSP Behavior
G.8

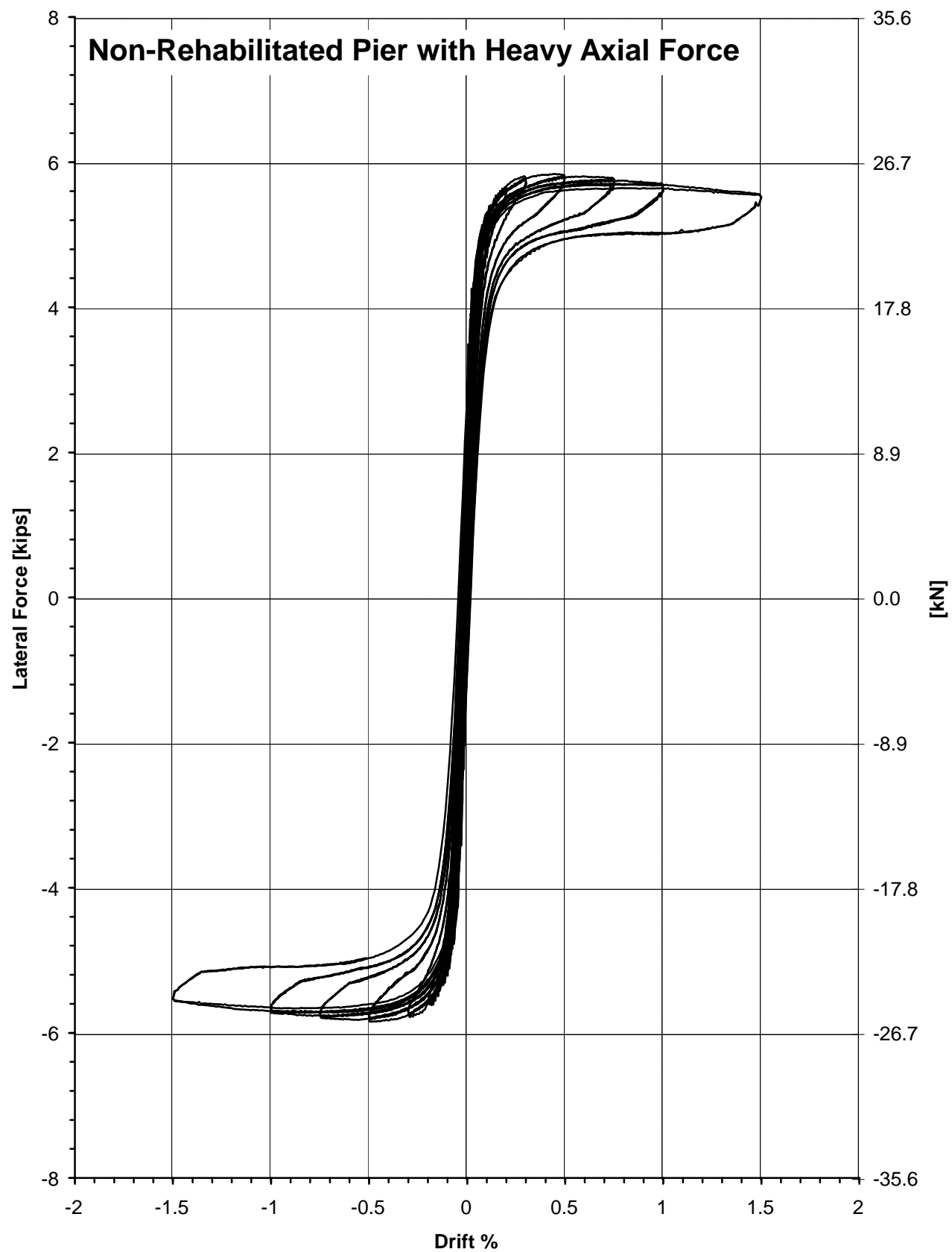


Figure H.1 - Specimen 6F, Hysteretic Response
H.1

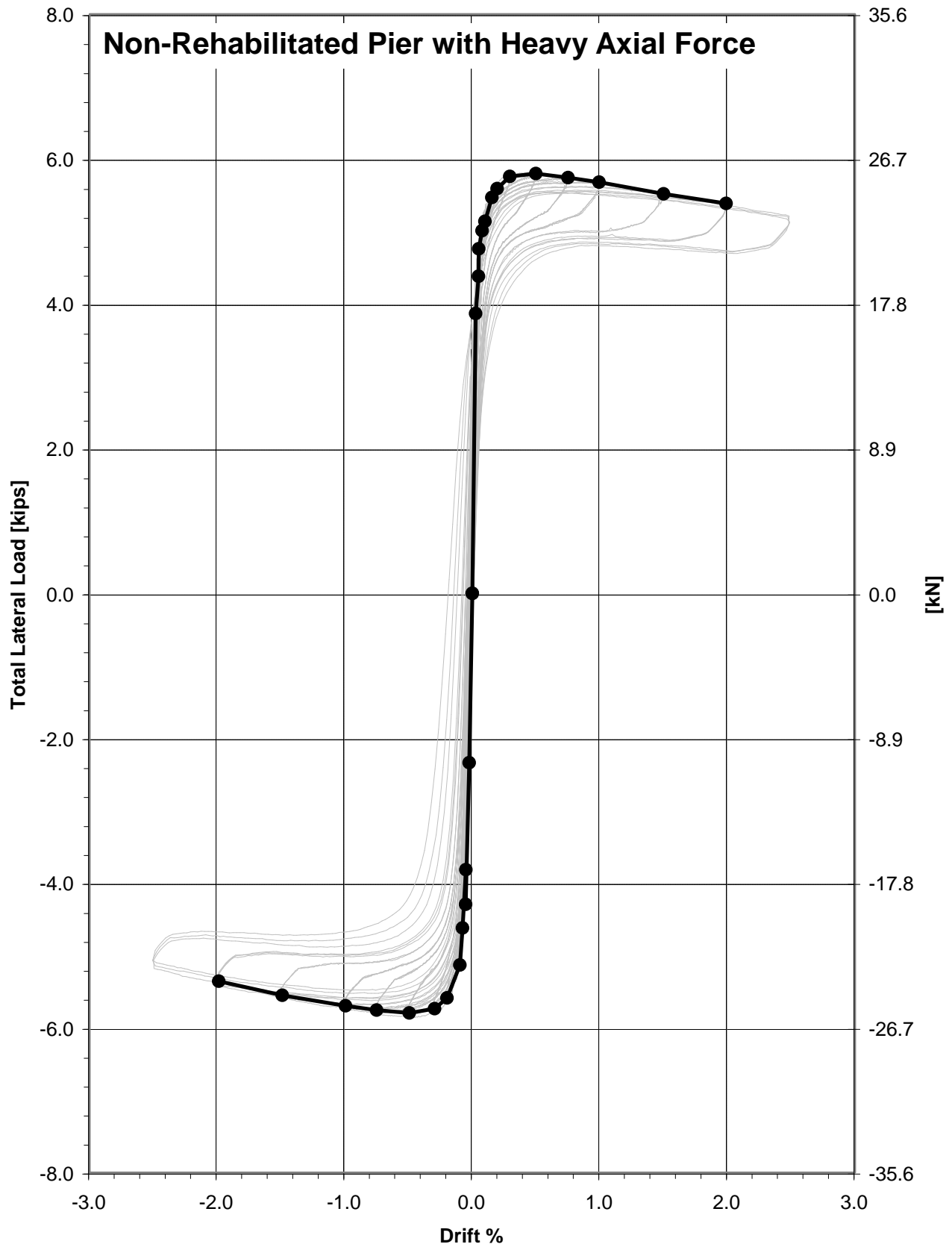


Figure H.2 - Specimen 6F, Backbone Curve
H.2

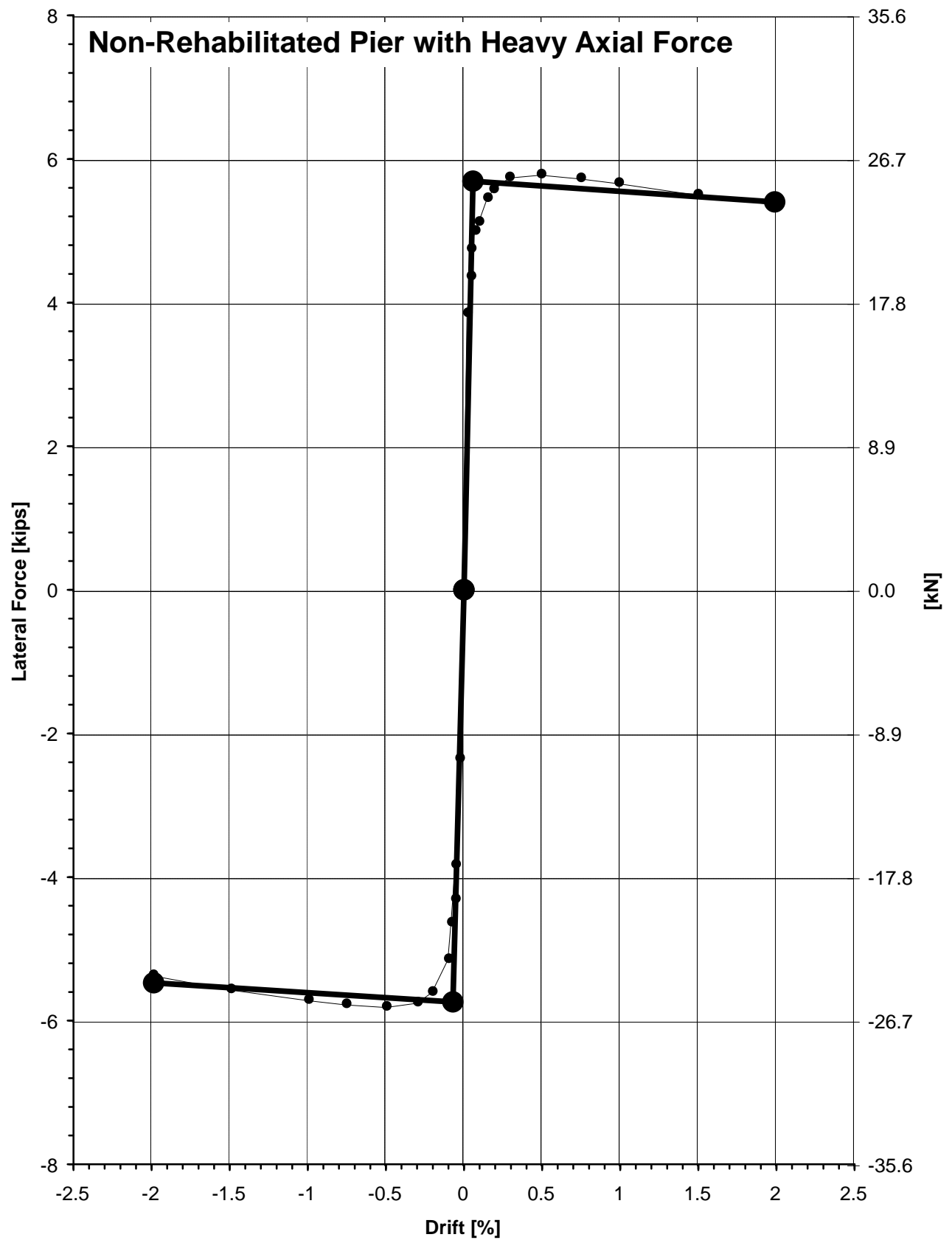


Figure H.3 - Specimen 6F, Multi-Linear Force-Deformation Curve
H.3

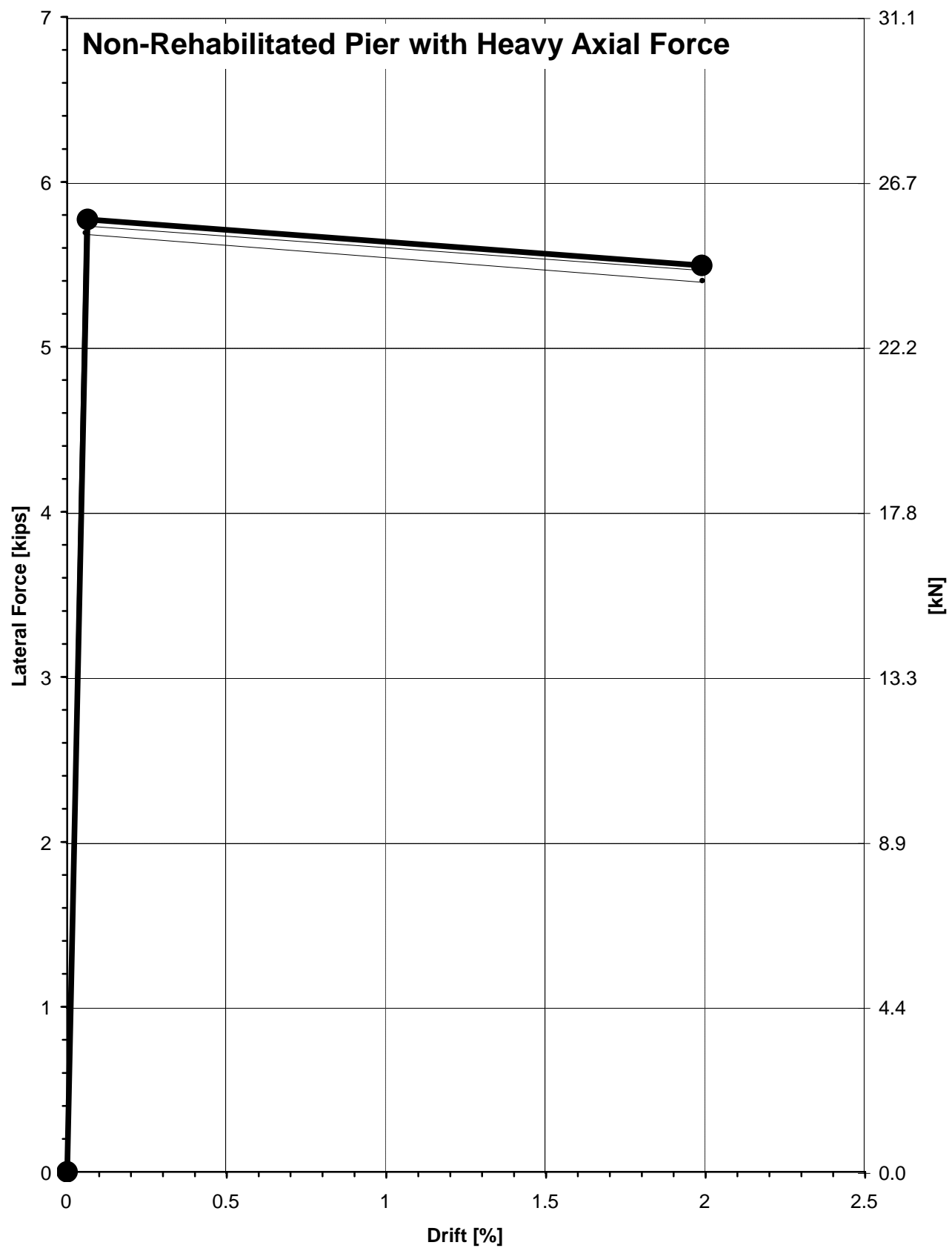


Figure H.4 - Specimen 6F, Composite Force-Deformation Curve
H.4

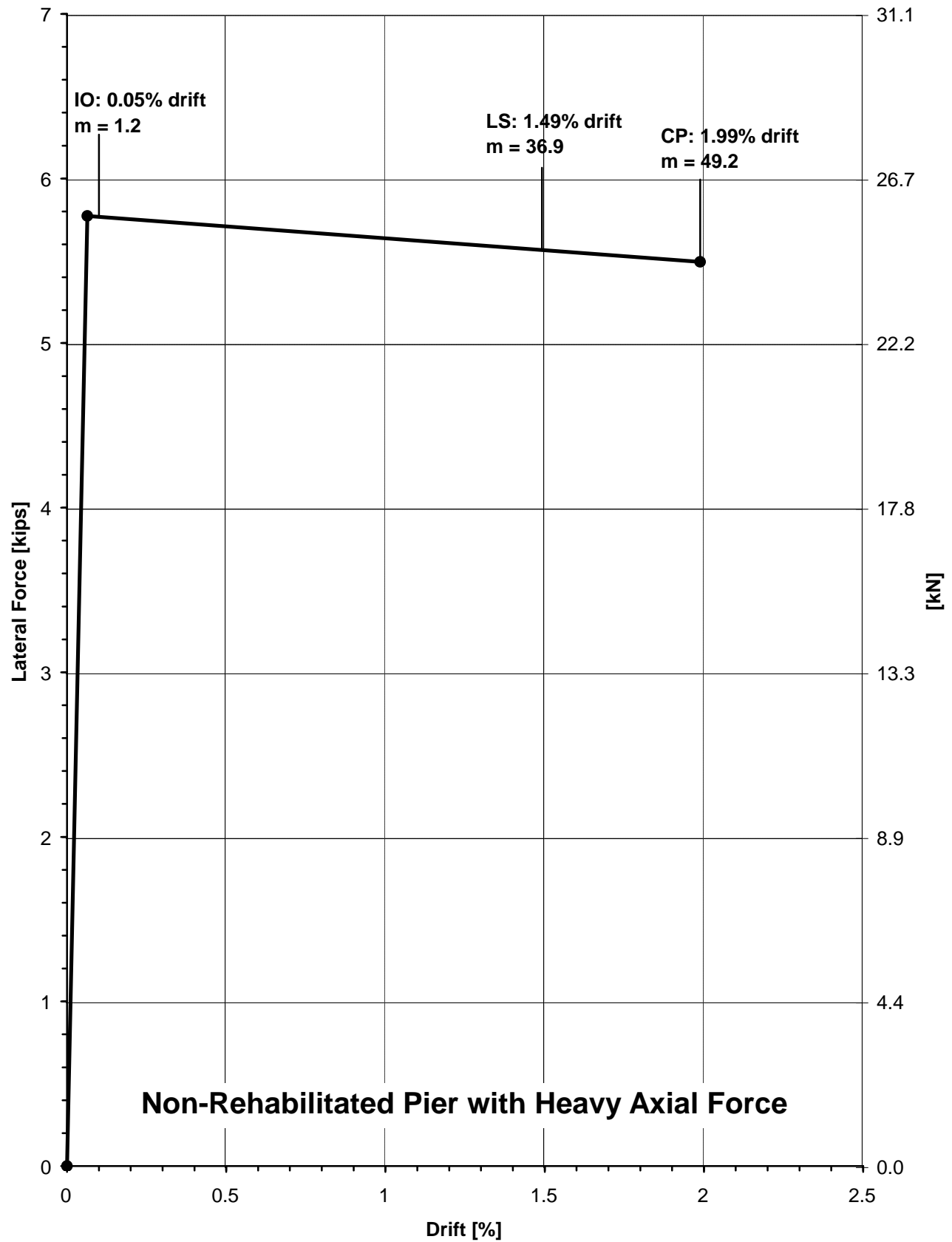


Figure H.5 - Specimen 6F, Performance Level Acceptance Criteria
H.5

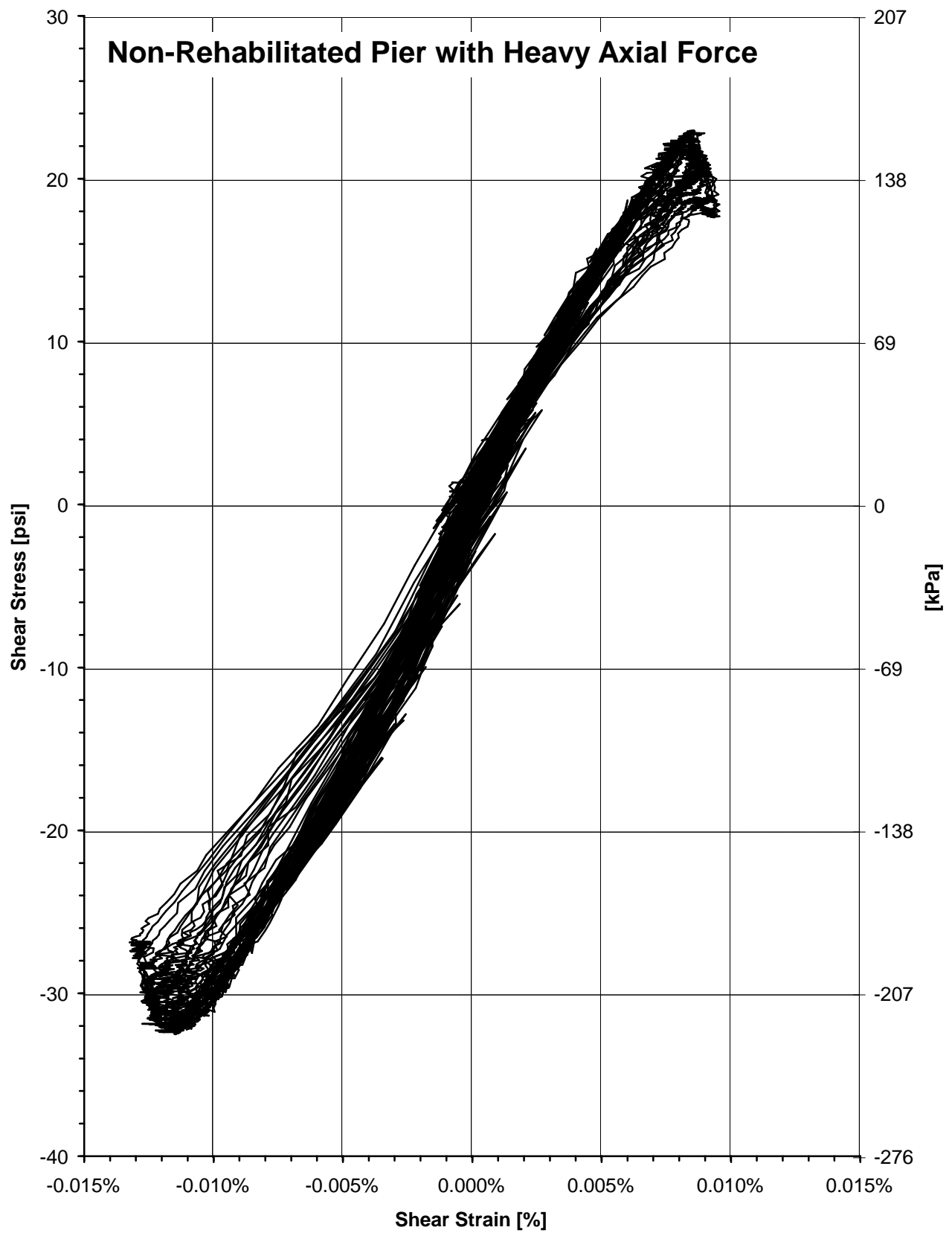


Figure H.6 - Specimen 6F, Shear Stress versus Shear Strain Response
H.6

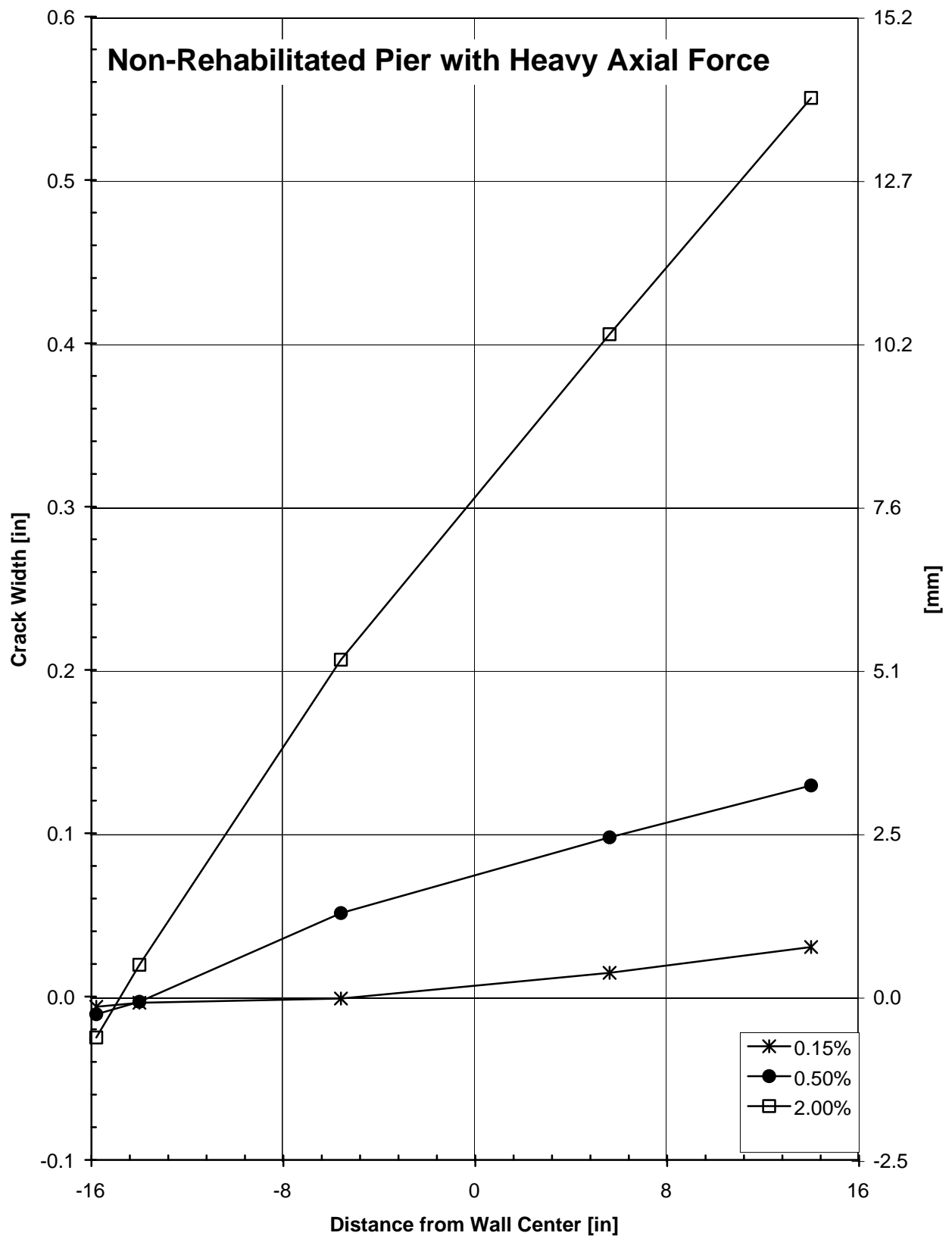


Figure H.7 - Specimen 7F, Crack Width Profile
H.7

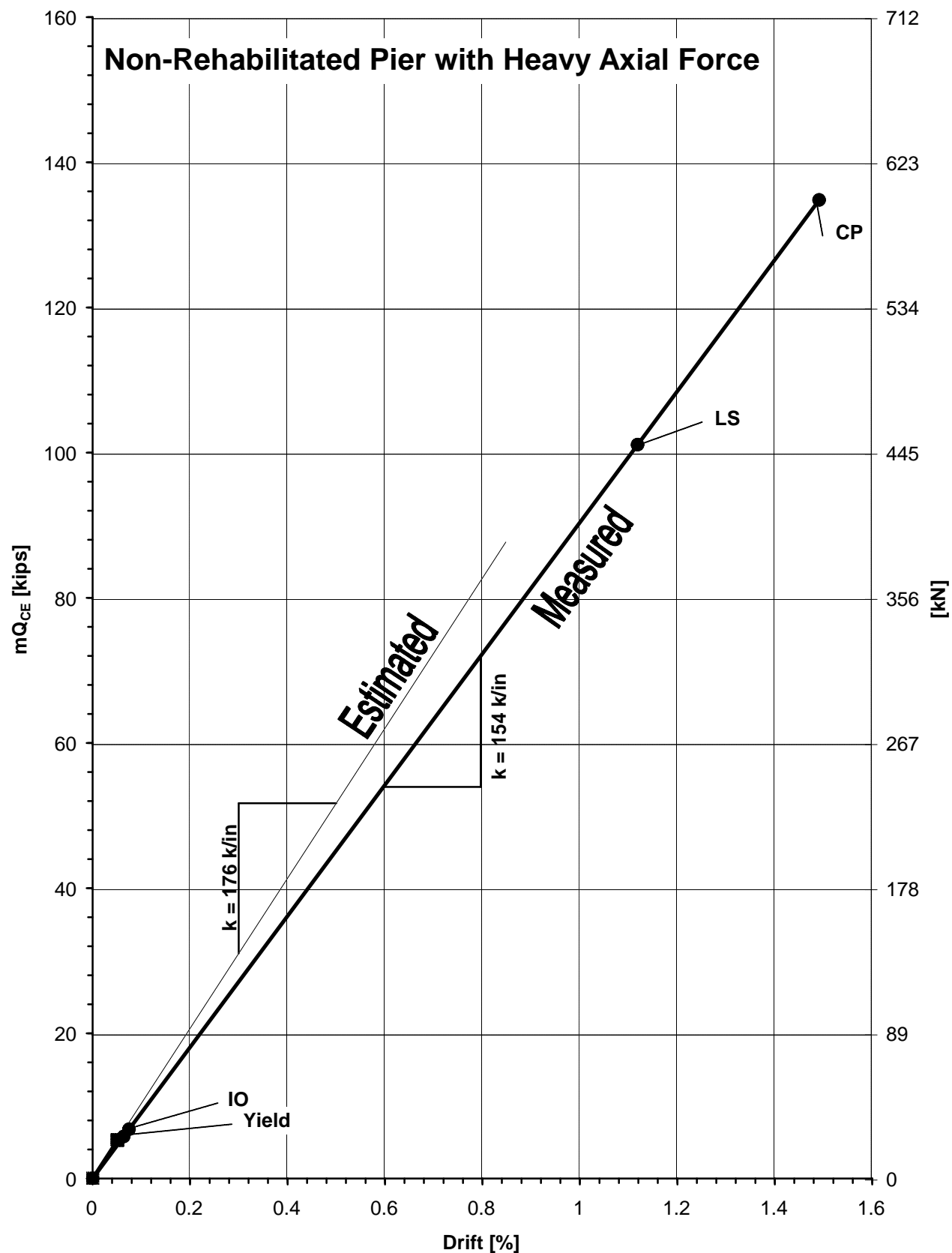


Figure H.8 - Specimen 6F, Comparison of Estimated to Measured LSP Behavior
H.8

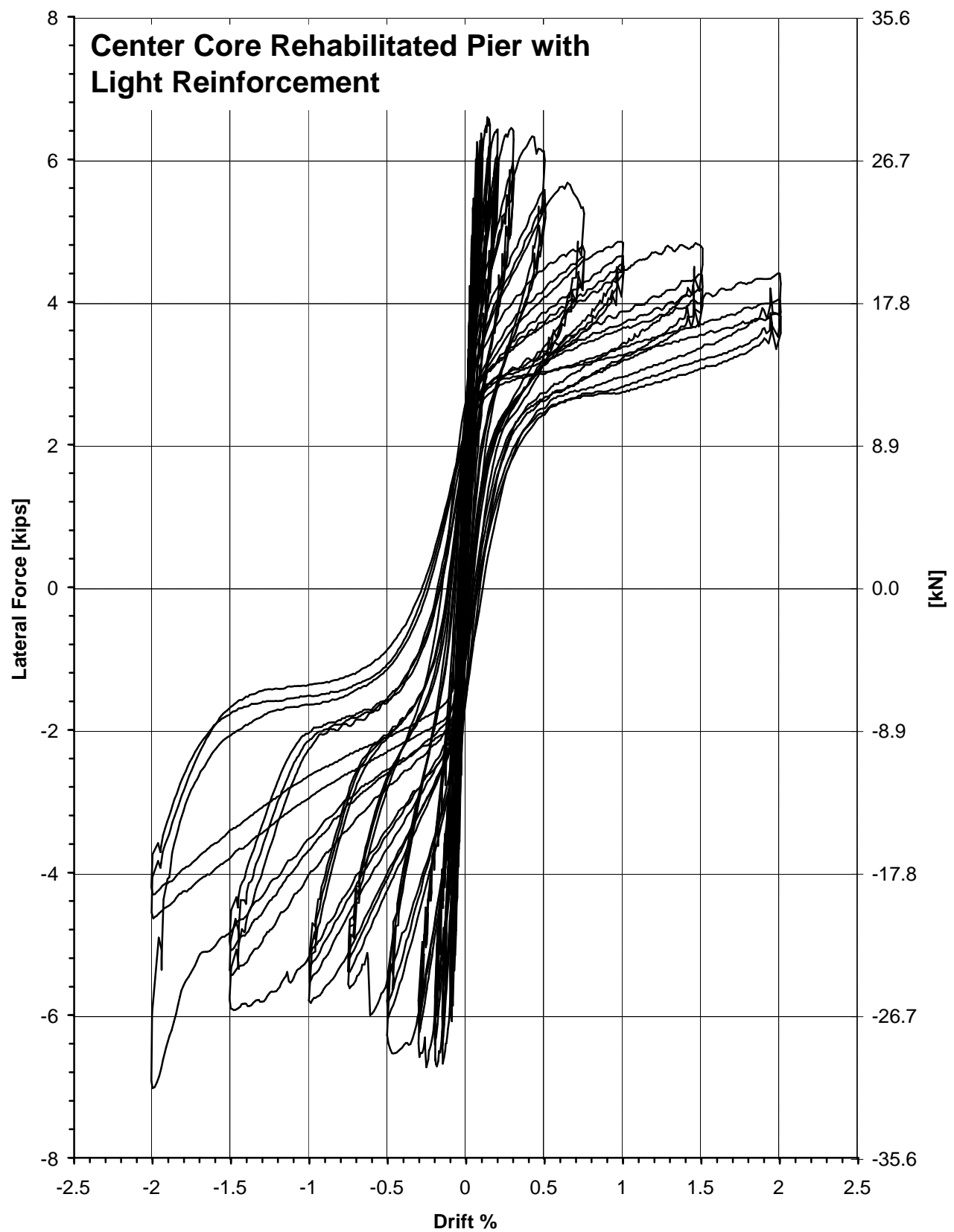


Figure I.1 - Specimen 7F, Hysteretic Response
I.1

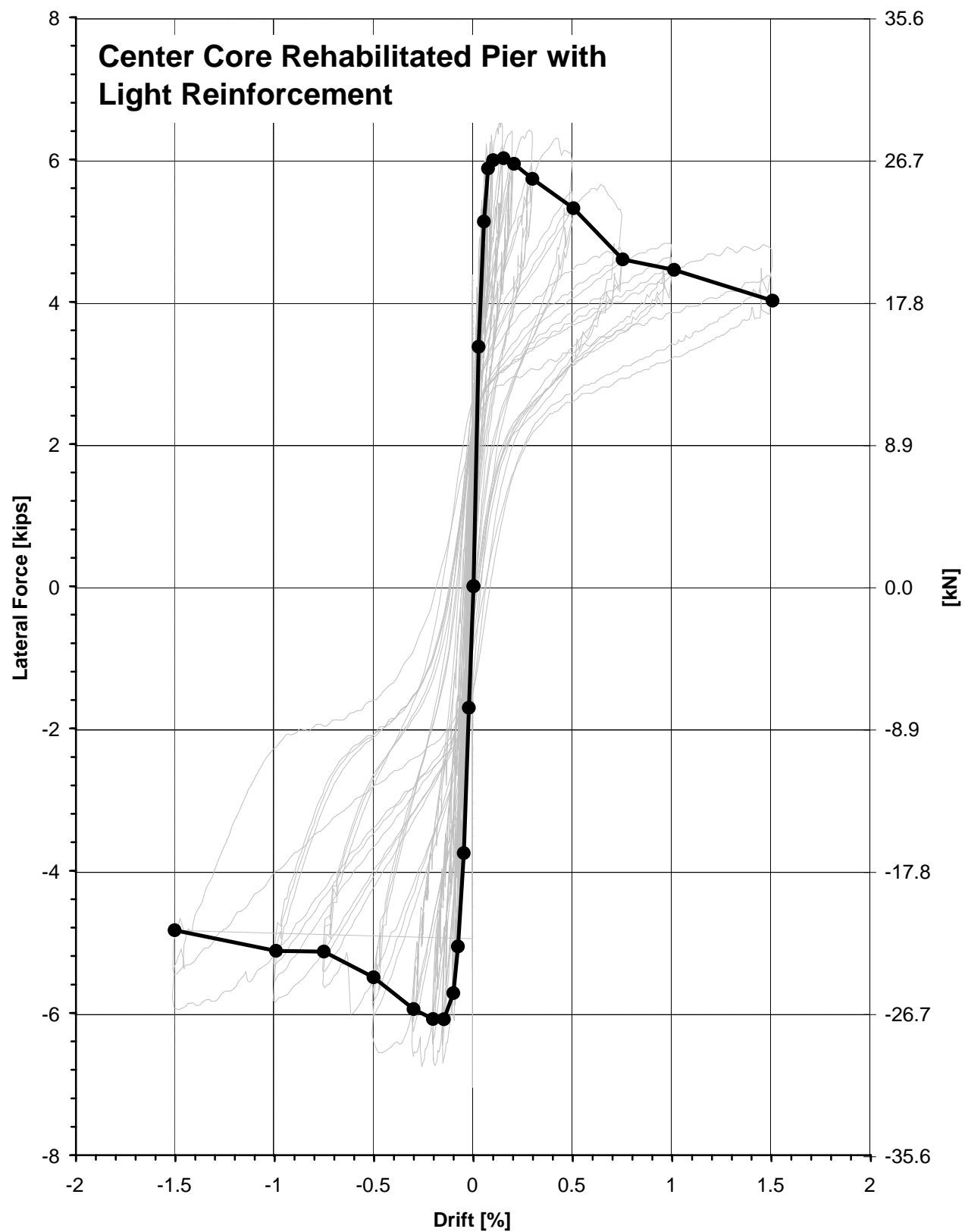


Figure I.2 - Specimen 7F, Backbone Curve
I.2

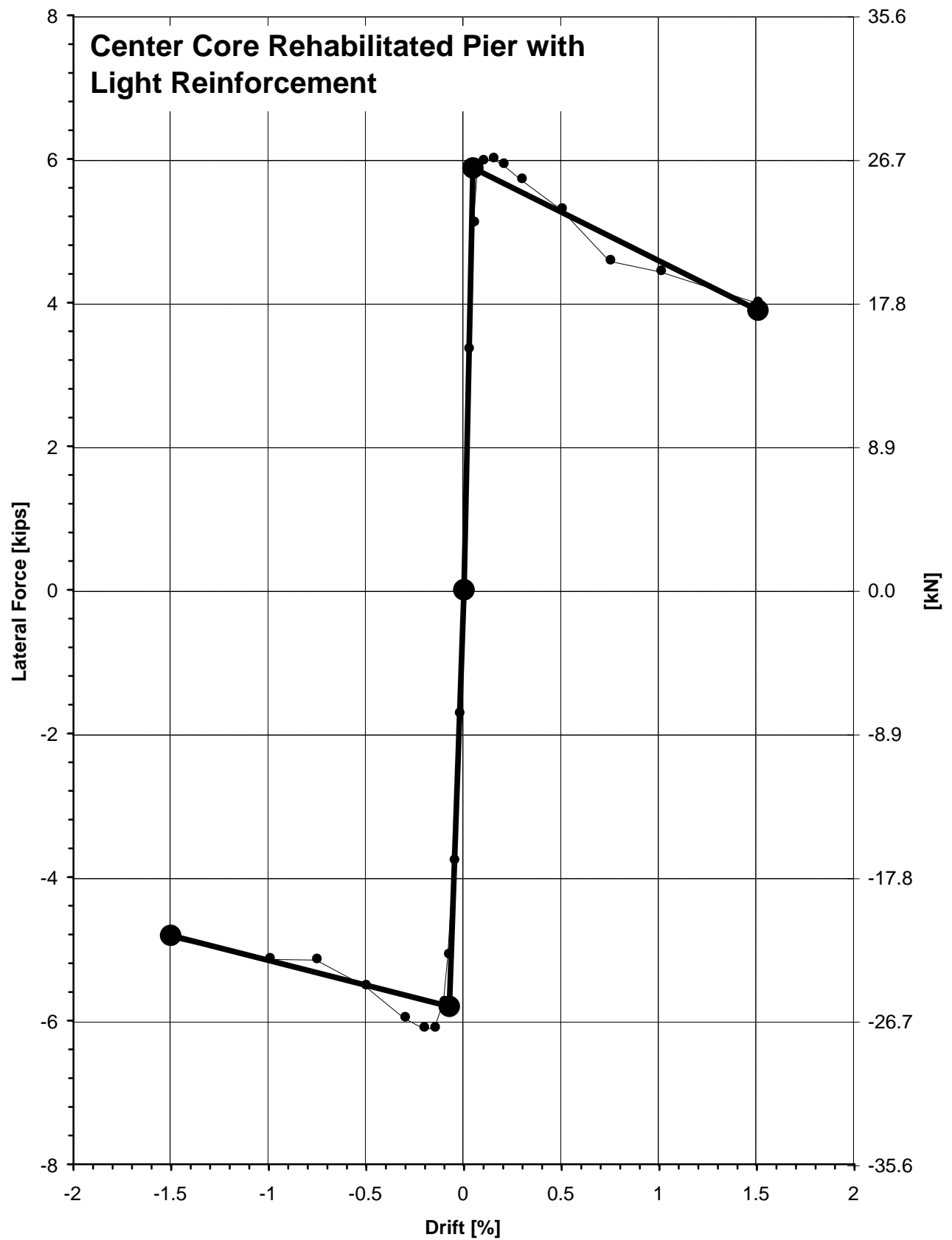


Figure I.3 - Specimen 7F, Multi-Linear Force-Deformation Curve
I.3

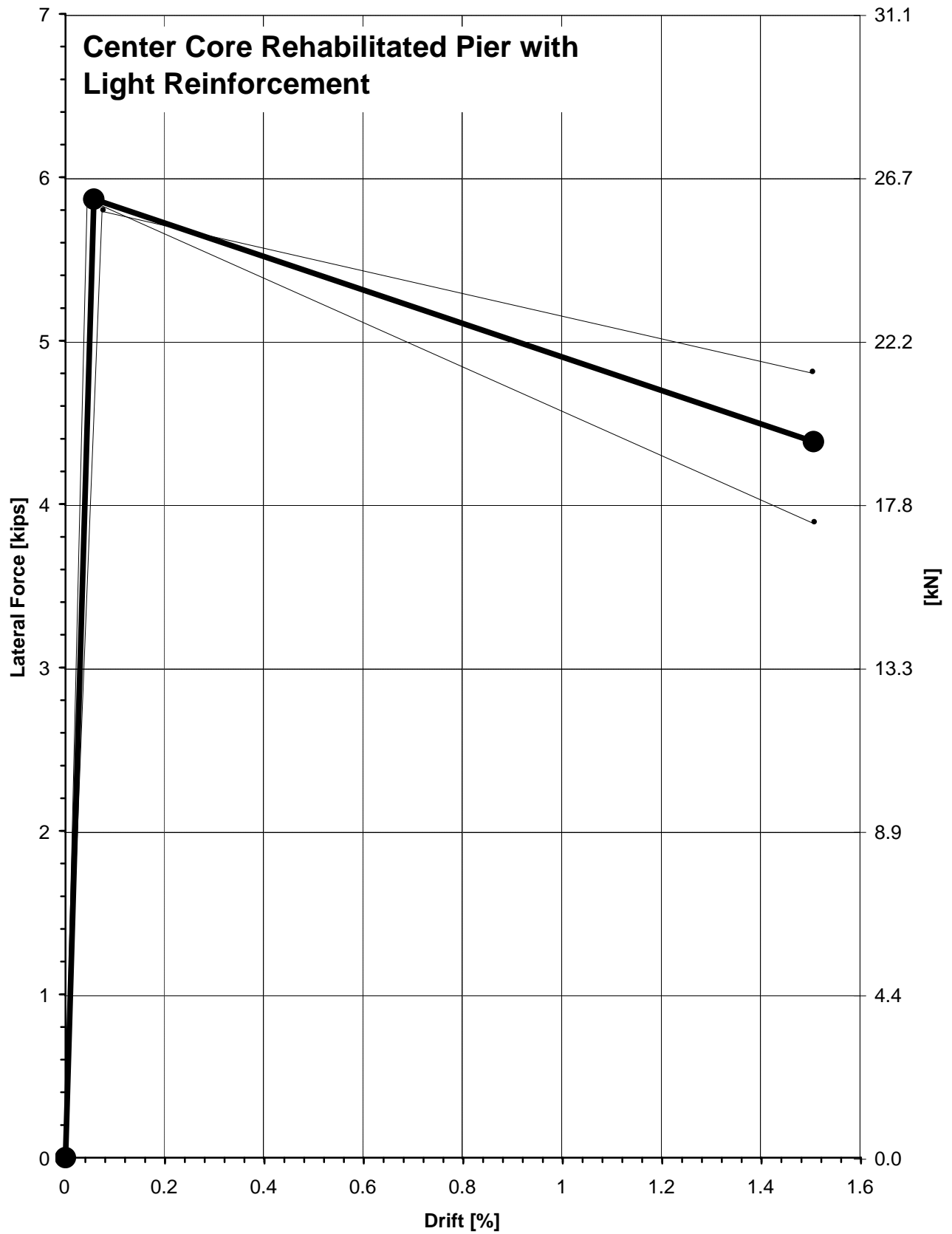


Figure I.4 - Specimen 7F, Composite Force-Deformation Curve
I.4

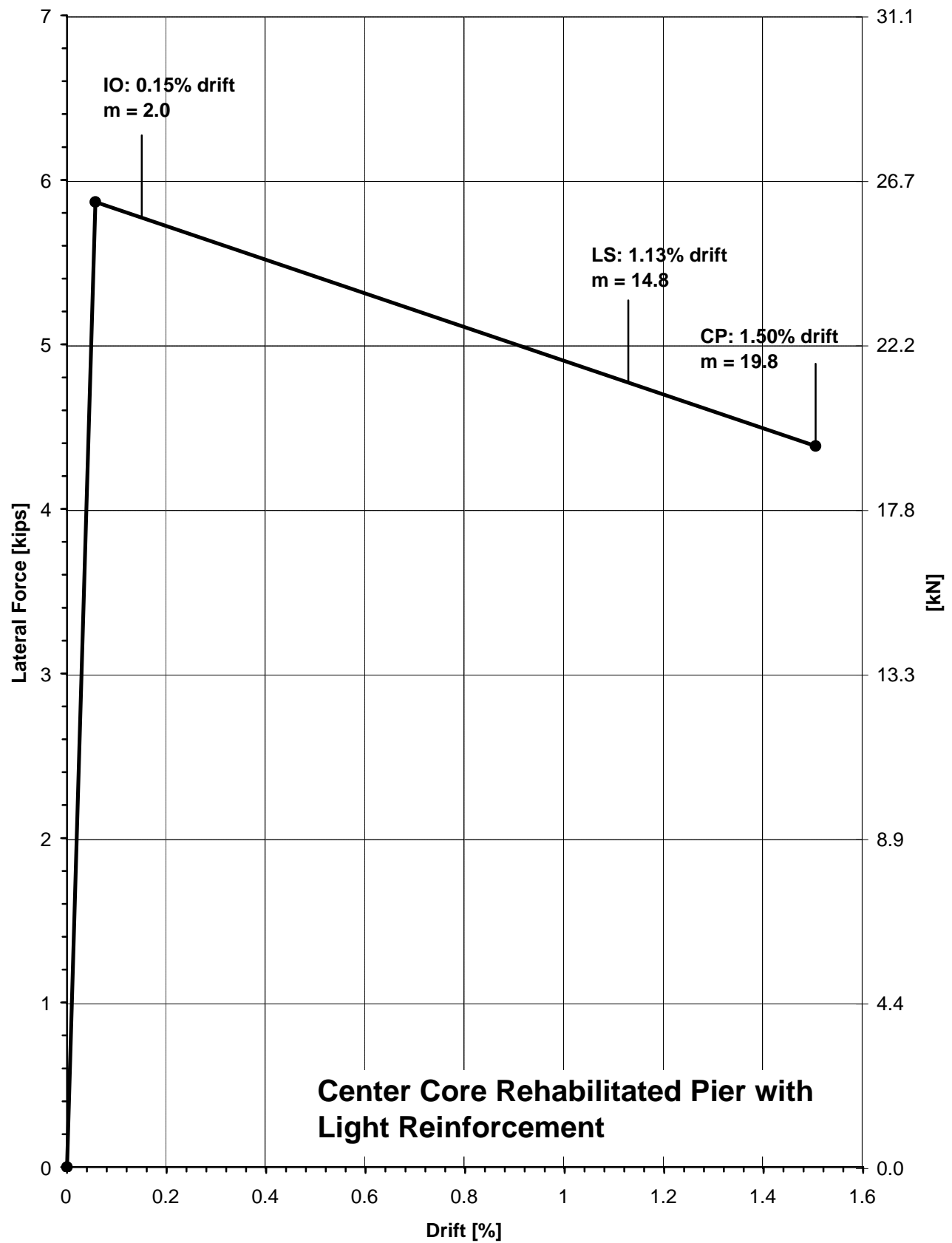


Figure I.5 - Specimen 7F, Performance Level Acceptance Criteria
I.5

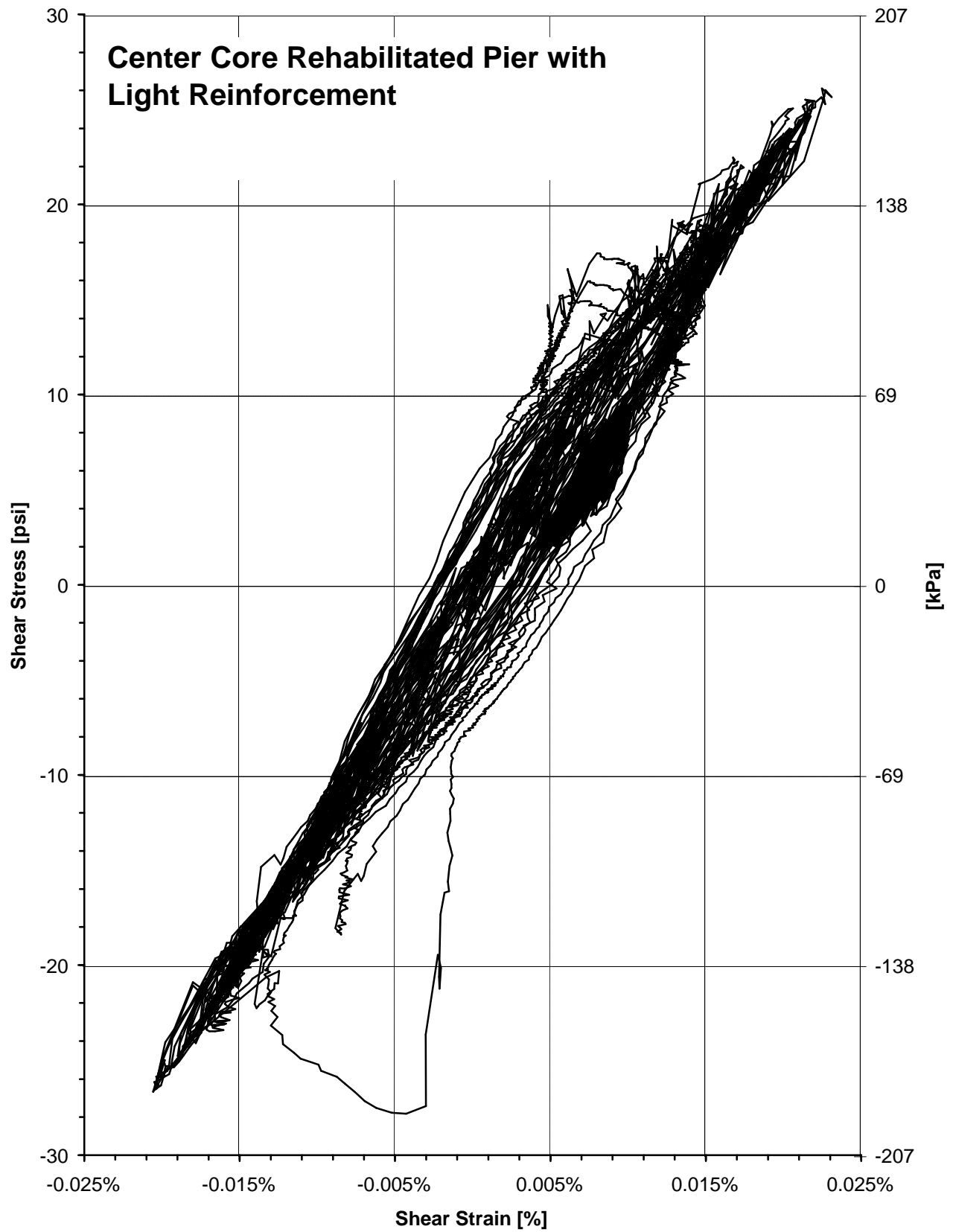


Figure I.6 - Specimen 7F, Shear Stress versus Shear Strain Response
I.6

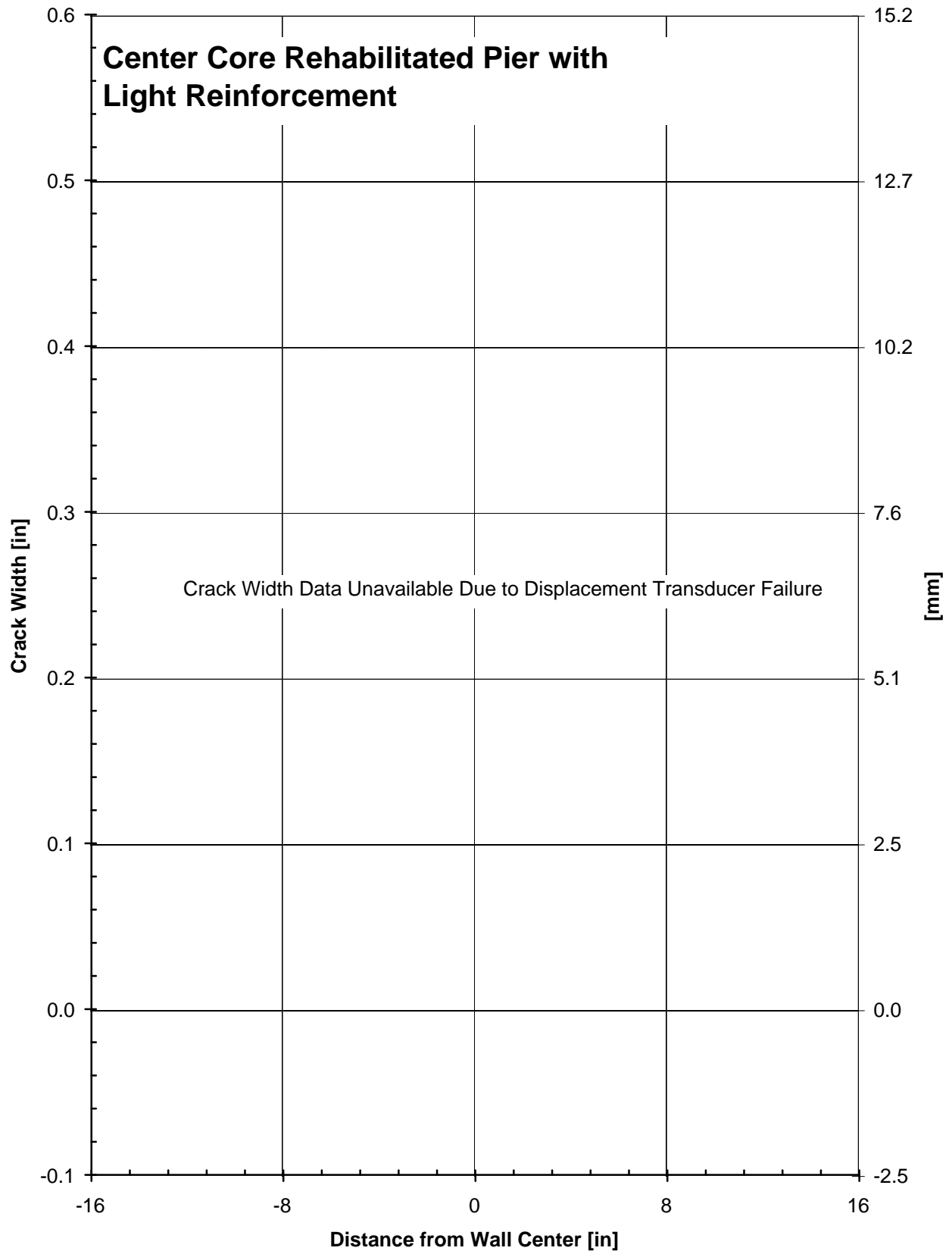


Figure I.7 - Specimen 7F, Crack Width Profile
I.7

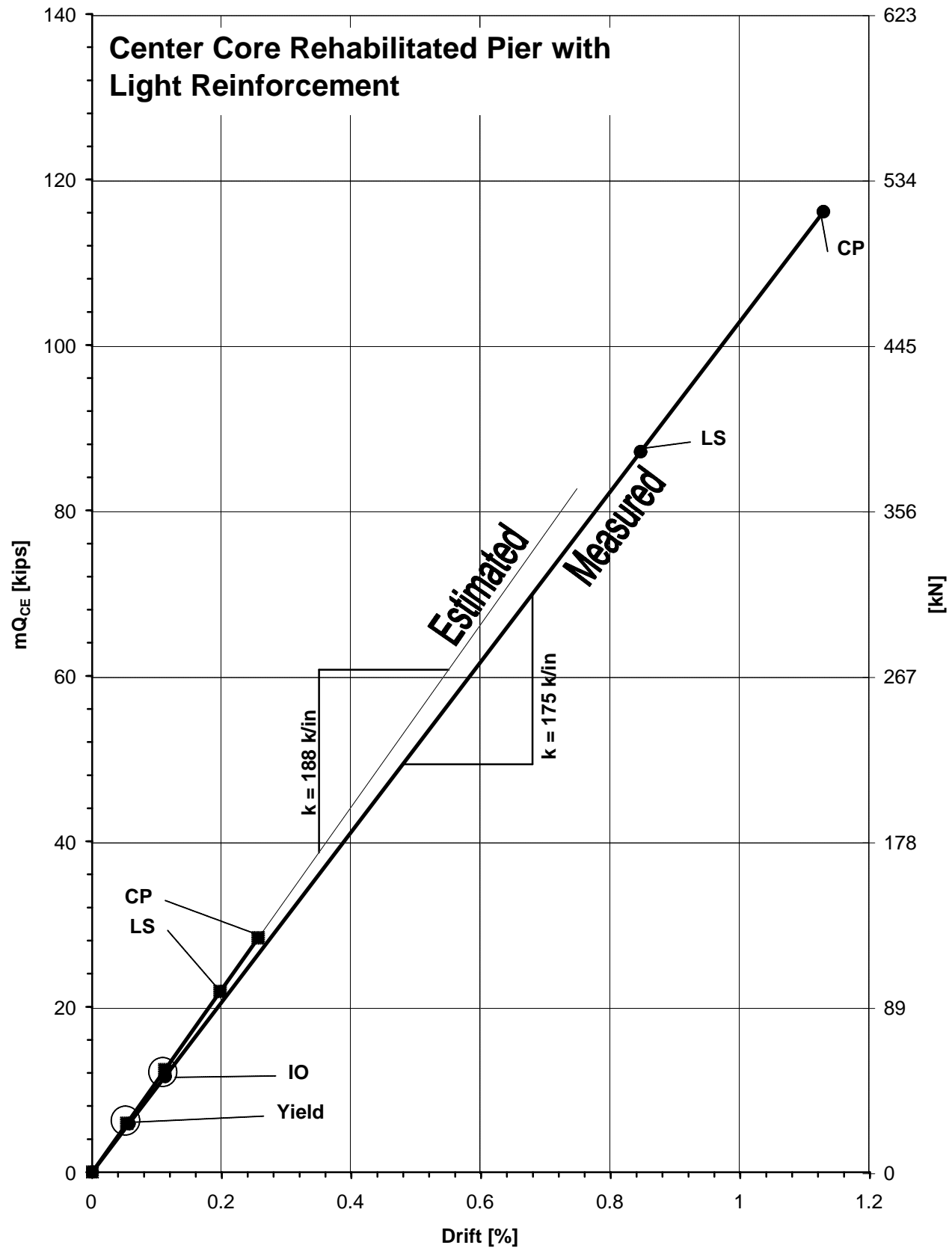


Figure I.8 - Specimen 7F, Comparison of Estimated to Measured LSP Behavior
I.8

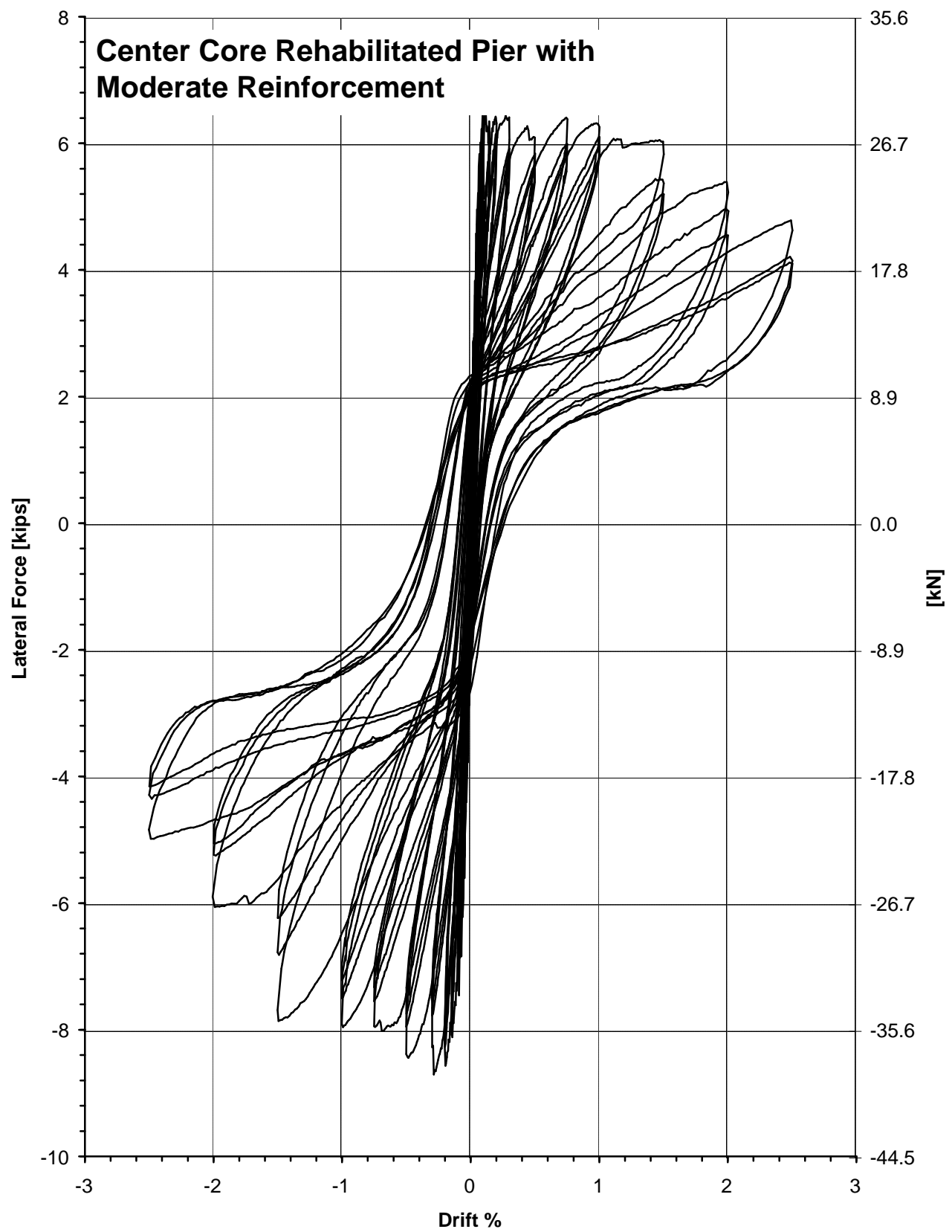


Figure J.1 - Specimen 8F, Hysteretic Response
J.1

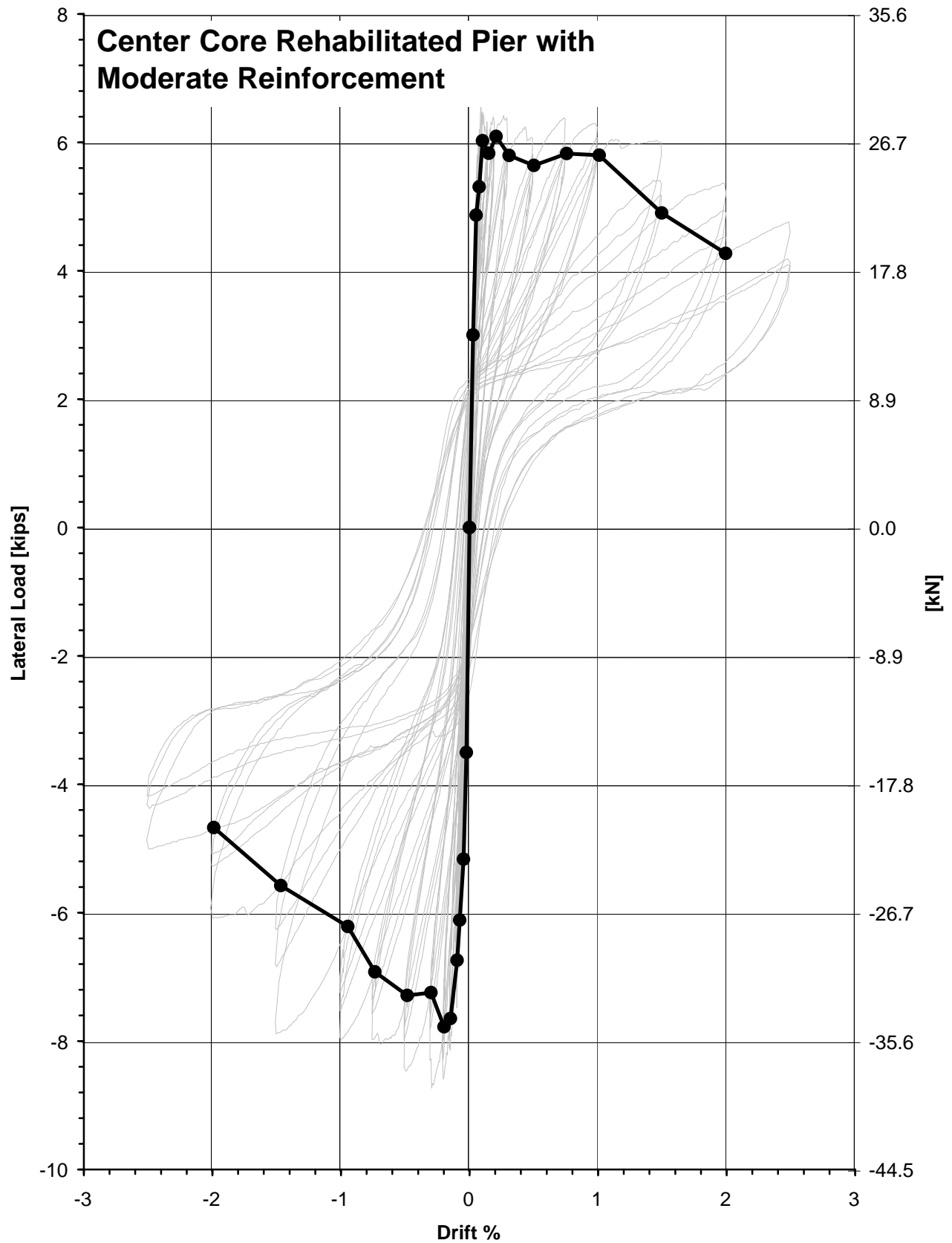


Figure J.2 - Specimen 8F, Backbone Curve
J.2

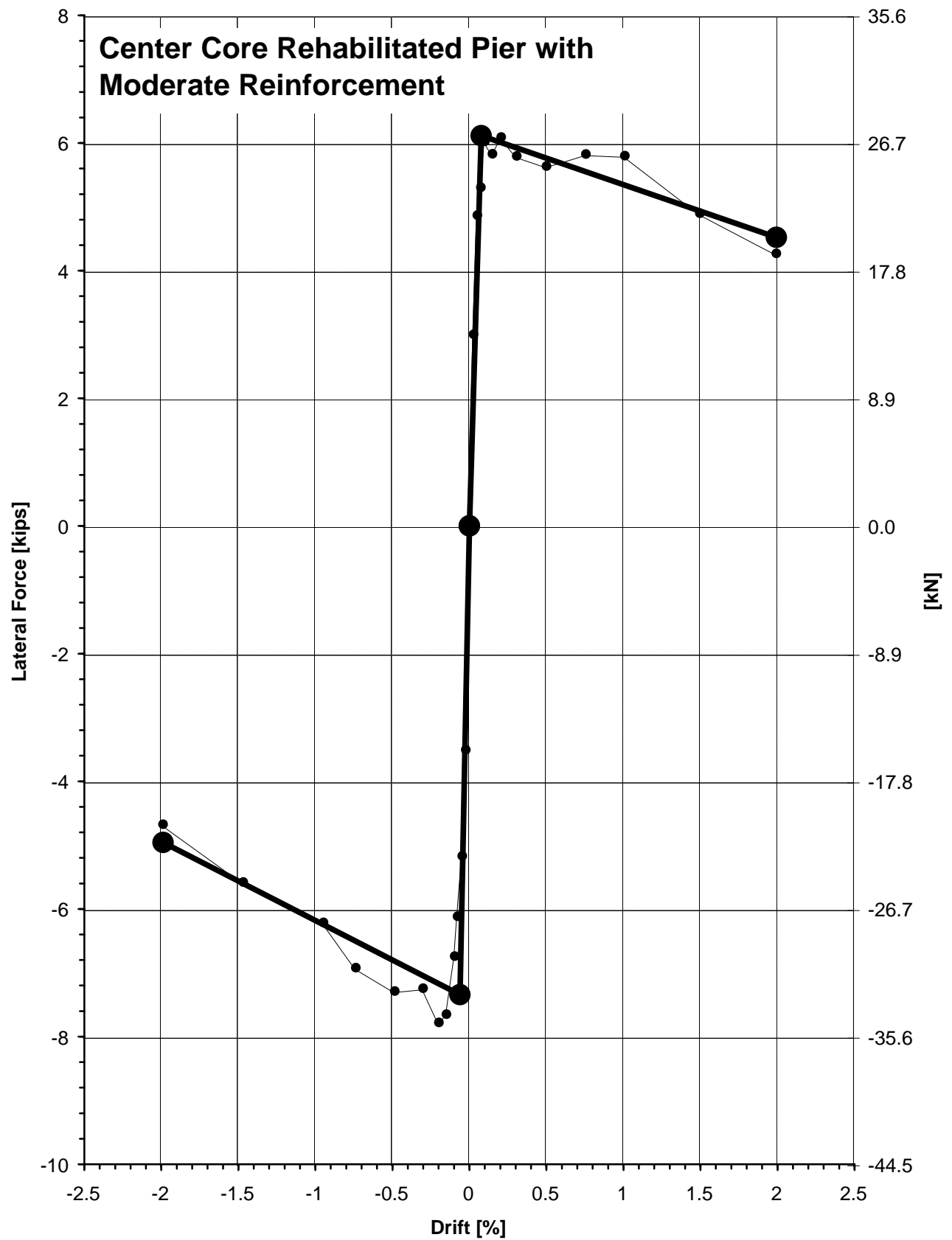


Figure J.3 - Specimen 8F, Multi-Linear Force-Deformation Curve
J.3

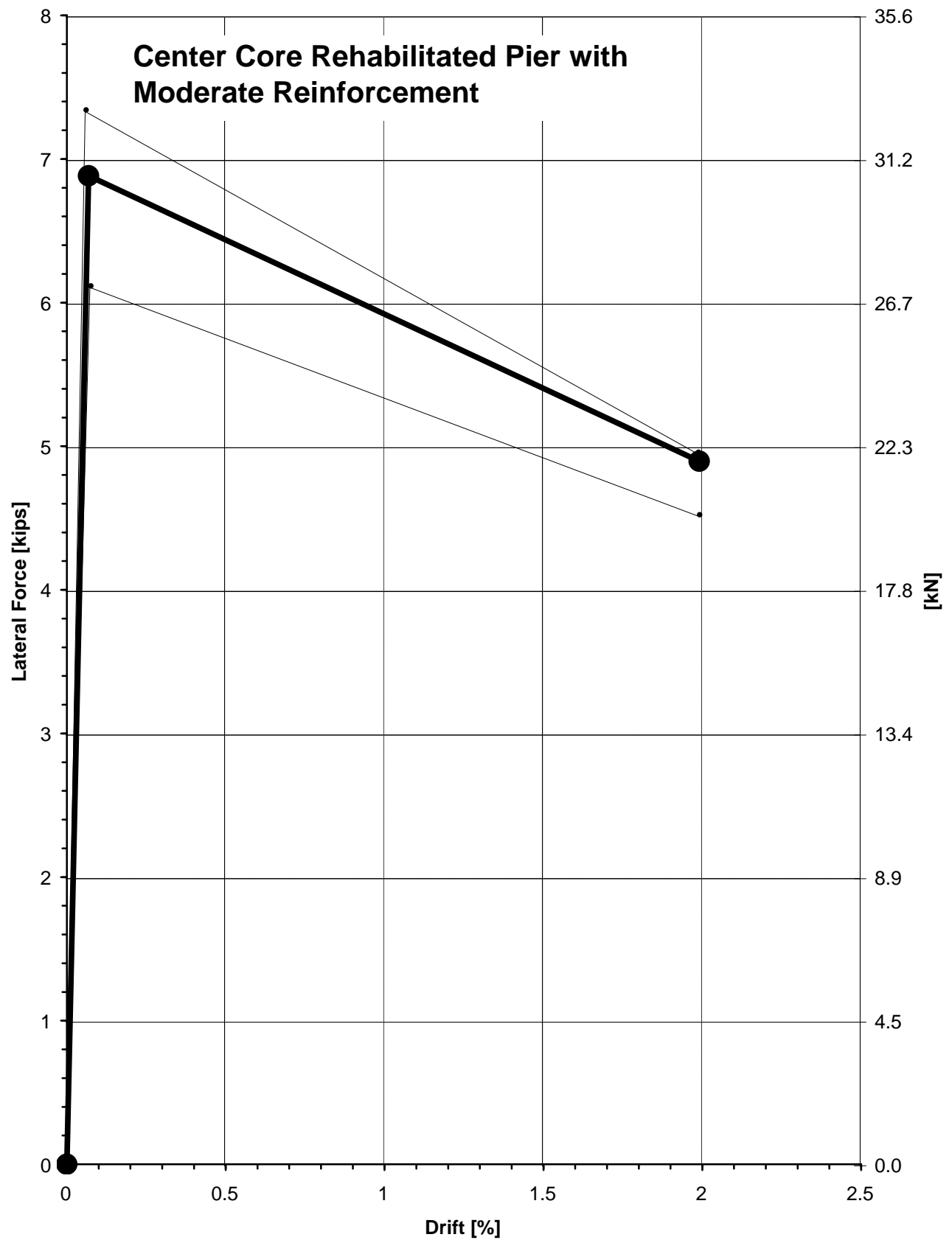


Figure J.4 - Specimen 8F, Composite Force-Deformation Curve
J.4

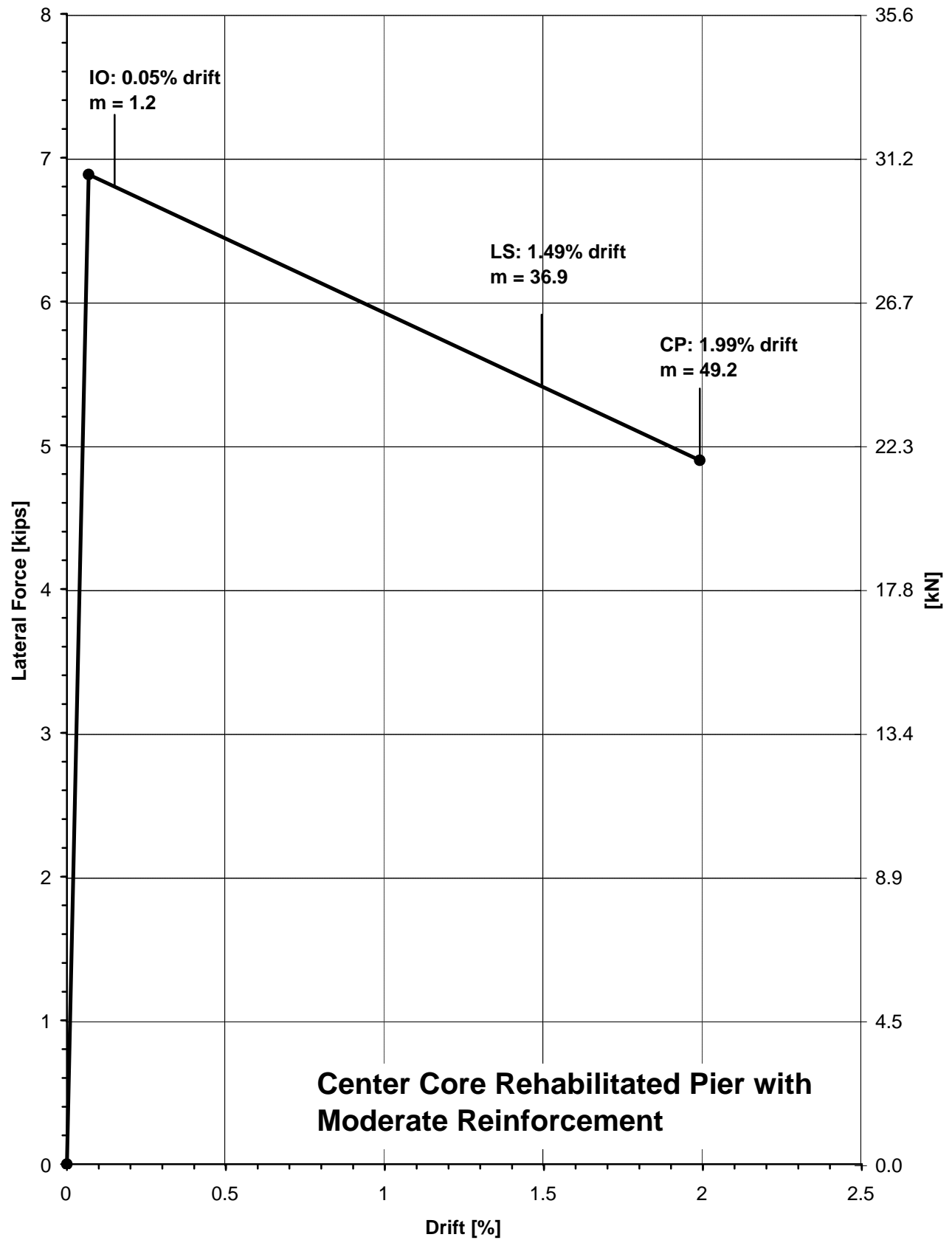


Figure J.5 - Specimen 8F, Performance Level Acceptance Criteria
J.5

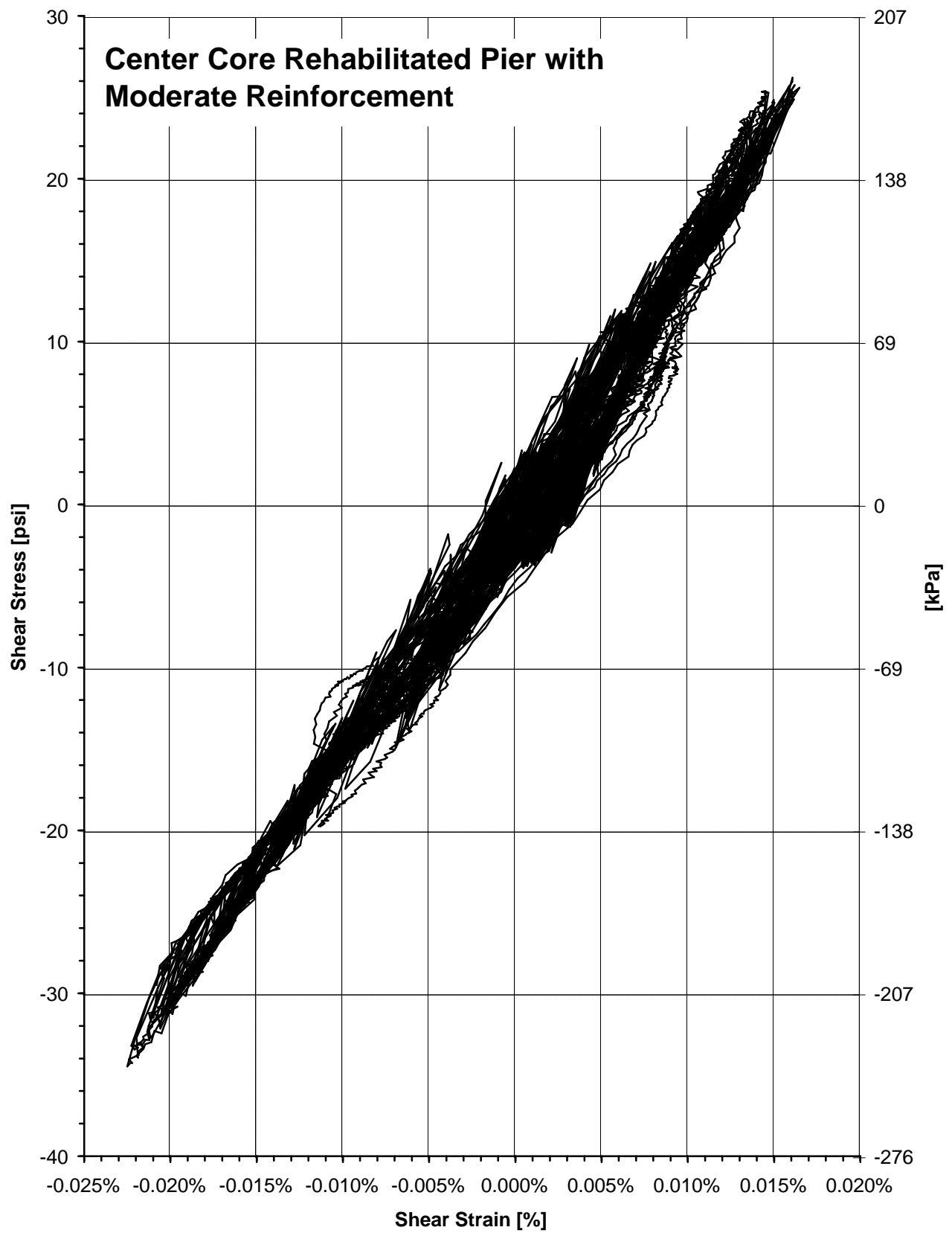


Figure J.6 - Specimen 8F, Shear Stress versus Shear Strain Response
J.6

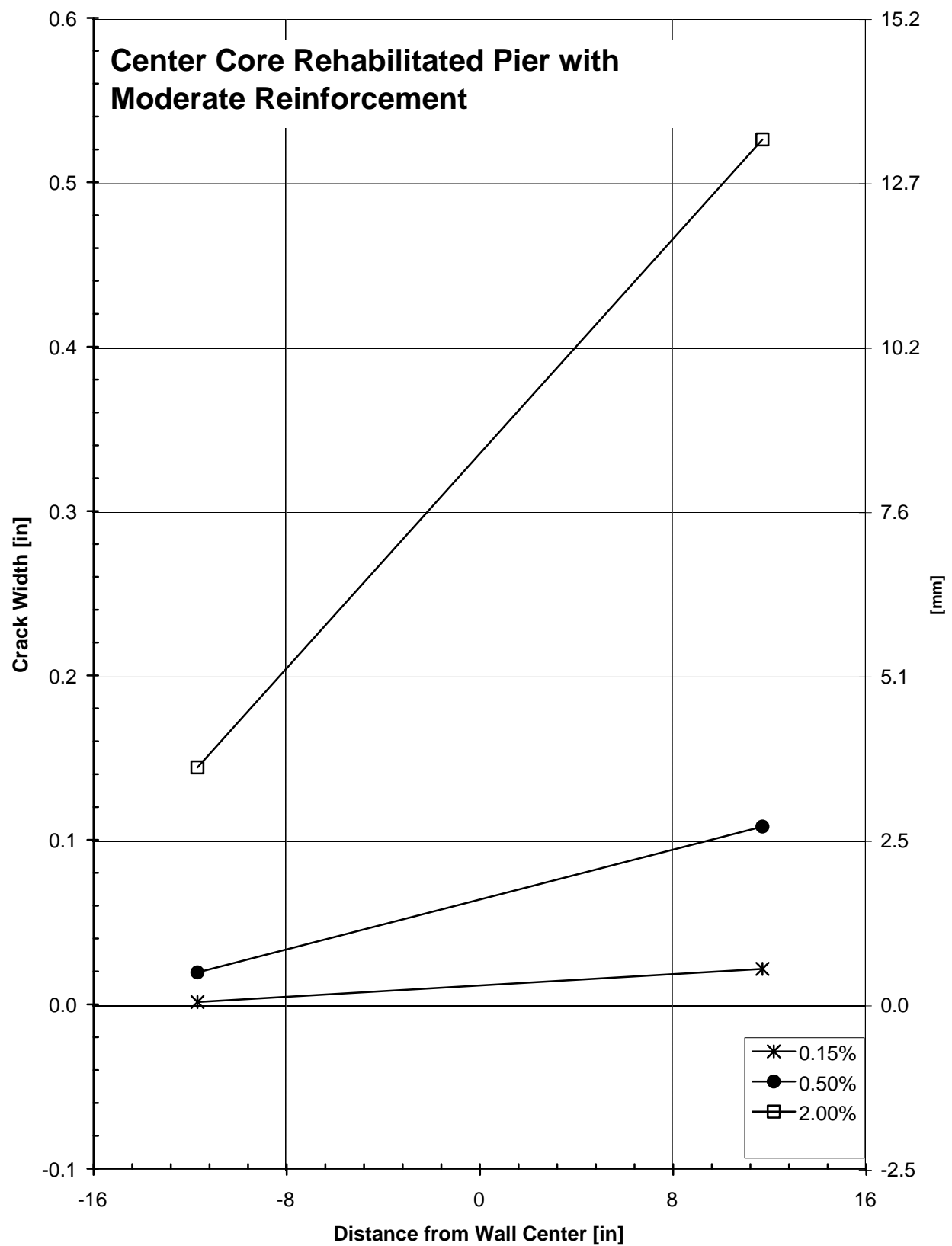


Figure J.7 - Specimen 8F, Crack Width Profile
J.7

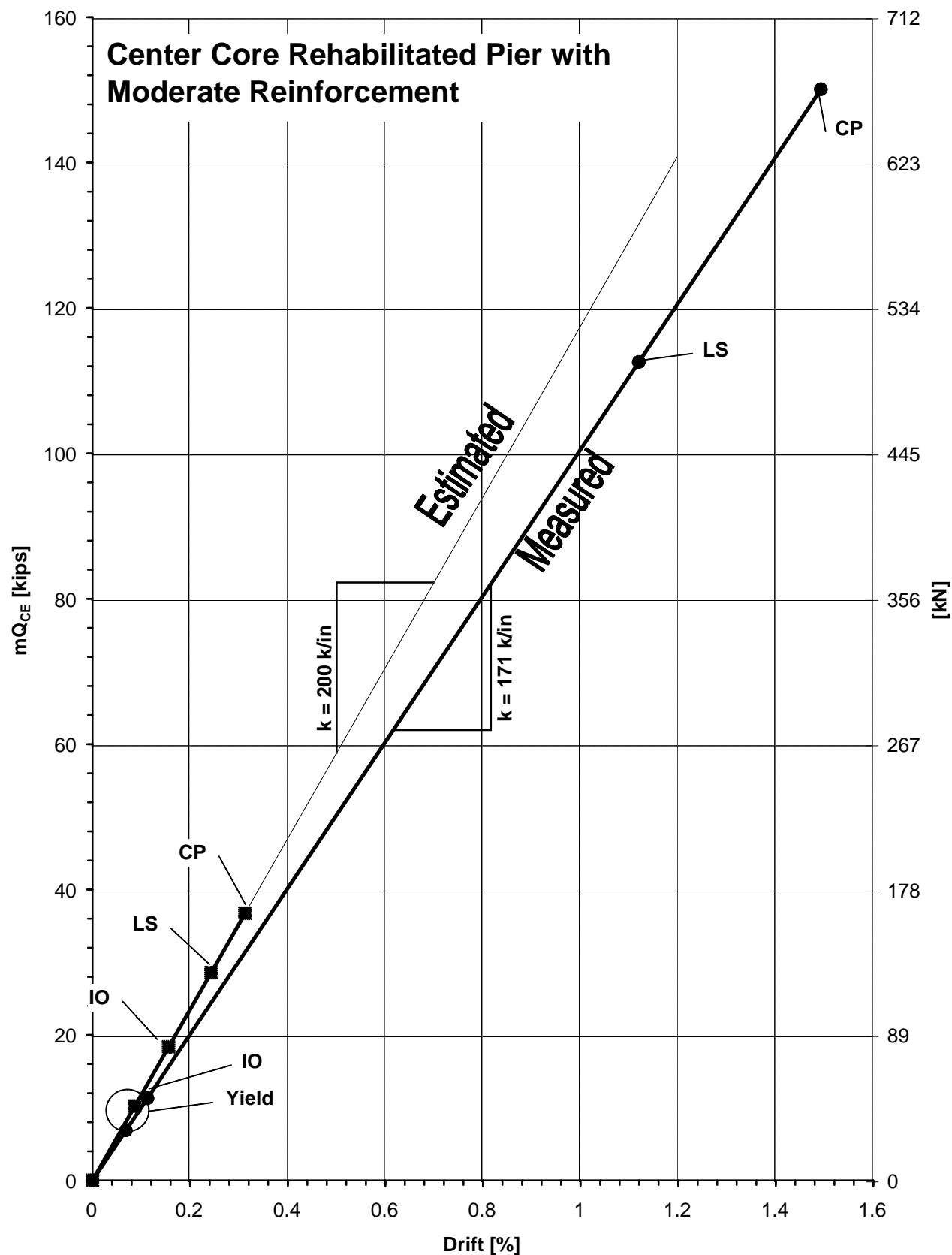


Figure J.8 - Specimen 8F, Comparison of Estimated to Measured LSP Behavior
J.8